Regulation of Ovule Initiation in *Arabidopsis thaliana* by EPIDERMAL PATTERNING FACTOR-LIKE Proteins

A Dissertation Presented for the
Doctor of Philosophy
Degree
The University of Tennessee, Knoxville

Alexander McCoy Overholt
December 2024

ACKNOWLEDGEMENTS

I would like to acknowledge Dr. Elena Shpak for working with me for over seven years and being an excellent mentor. I would also like to acknowledge my committee, Dr. Andreas Nebenfuehr, Dr. Albrecht von Arnim, Dr. Mariano Labrador, and Dr. Joseph Williams for continuous support and insight throughout my studies. Finally, I would like to acknowledge all past and present Shpak lab students, including undergraduates, graduate students, and post-doctoral researchers for assisting in the Shpak lab research.

I would like to acknowledge my grandparents, Gene and Lyn Overholt, who helped facilitate my interest in science at an early age. I would also like to acknowledge my parents, Scott and Teresa Overholt, who have supported me in every way possible, as well as my siblings Ben Overholt, Abby Neiman, and Pierce Overholt who were always there for me. In addition, I would like to acknowledge my cat, Leela, who has kept me company through these years.

I would like to acknowledge Teresa Overholt and Suzanne Stelling for helping paint diagrams for Chapter 1.

We thank Mitsuhiro Aida for sharing with us seeds of *cuc1-5, cuc2-3,* and *cuc3-105* mutants and proCUC3:er-CFP and proCUC2:CUC2-GFP transgenic plants. We thank Andreas Nebenfuehr for sharing pAN456 vector and pBIN-LhGR vector and Zackary Nimchuk for pENT H2BGFP vector. We thank Keiko Torii for seeds of *er-105* with AtML1pro:ER-FLAG.

We thank the National Science Foundation for providing funding with NSF grant IOS-2016756 to Elena D Shpak.

ABSTRACT

Organ initiation and patterning in plants requires coordinated cell-to-cell communication to control cell growth and differentiation. In *Arabidopsis thaliana*, multiple ovules initiate asynchronously along the elongating placentae from stage 9 to stage 10 of floral development. Previous research has established a role for the phytohormone auxin in governing the site of ovule initiation, and for CUP-SHAPED COTYLEDON (CUC) transcription factors in regulation of ovule patterning. ERECTA family receptor-like kinase signaling via the EPIDERMAL PATTERNING FACTOR-LIKE 2 (EPFL2) secretory peptide ligand regulates ovule density and spacing during Arabidopsis fruit development, but the mechanisms underlying this regulation remain unclear. We further investigated the mechanism of ERECTA family signaling during ovule initiation in Arabidopsis. Our experiments established that *EPFL1* and *EPFL2* show distinct, cell-type specific expression throughout the process of ovule initiation. These two ligands positively regulate ovule number in a partially redundant manner without significantly affecting placenta length. To characterize the mechanisms of this regulation, hormone signaling, the expression of genes controlling ovule initiation, and genetic interactions were investigated using the *epfl1 epfl2* mutant. While no clear defects were observed related to auxin, cytokinin, or gibberellins in the *epfl1 epfl2* mutant, a synergistic reduction in ovule initiation was seen when the brassinosteroid related *brassinazole resistant1-1D* mutant or the boundary specific *cup shaped cotyledon3* mutant were crossed with the *epfl1 epfl2* mutant. The expression domain of *DORNROSCHEN* was expanded into boundary tissues in the *epfl1 epfl2* mutant, and this suggests that EPFL1/2 may regulate early differentiation of cells during ovule initiation. In addition, synthetic biology was used to generate an inducible EPFL2 construct with expression is driven by the EPFL2 promoter as a future tool to probe the mechanisms and effects of EPFL2 signaling. Ultimately, this research further characterizes the mechanisms by which EPFL-mediated signaling positively regulates the initiation, spacing and outgrowth of ovules in *Arabidopsis thaliana*.

TABLE OF CONTENTS

Chapter 1 Regulation of Ovule Initiation in *Arabidopsis thaliana* by EPIDERMAL PATTERNING FACTOR-LIKE Proteins 1
Introduction 2
Materials and Methods 20
Results 29
Discussion 57
Chapter 2 Generation of an Inducible EPFL2 Construct Driven by the EPFL2 Promoter 68
Introduction 69
Materials and Methods 70
Results 75
Discussion 80
Chapter 3 Conclusions 84
References 88
Vita 97

LIST OF FIGURES

Figure 1.1. Diagram of ERECTA family signaling pathway 4
Figure 1.2. Diagram of the Arabidopsis gynoecium from stage 8 to stage 10 10
Figure 1.3. Model of gene regulatory networks controlling ovule initiation 19
Figure 1.4. EPFL1 and EPFL2 positively regulate ovule density in a partially redundant manner 30
Figure 1.5. EPFL1, EPFL2, EPFL4, and EPFL6 synergistically regulate gynoecium elongation 32
Figure 1.6. EPFL1 and EPFL2 promote ovule initiation by positively regulating ovule number 34
Figure 1.7. EPFL1/2 regulate ovule density at all stages of ovule initiation 35
Figure 1.8. EPFL1 and EPFL2 promote early ovule growth 37
Figure 1.9. Expression patterns of *EPFL1* and *EPFL2* during early ovule development 39
Figure 1.10. ERf receptors redundantly regulate ovule initiation 41
Figure 1.11. Auxin is able to accumulate into maxima during ovule initiation in the *epfl1 epfl2* mutant 44
Figure 1.12. The efflux transporter of auxin PIN1 is expressed similarly in the wild type and *epfl1 epfl2* mutant 46
Figure 1.13. Inhibition of auxin transport severely reduces ovule density, while exogenous auxin does not affect either placenta length or ovule initiation 48
Figure 1.14. Expression of MP/ARF5 in wild type and *epfl1 epfl2* 49
Figure 1.15. Exogenous cytokinins promote placenta elongation while exogenous gibberellins inhibit ovule density 50
Figure 1.16. The *bzr1-1D* mutation inhibits ovule initiation in the *epfl1 epfl2* background 52
Figure 1.17. EPFL1 EPFL2 and CUC2,3 regulate ovule initiation and growth synergistically 54
Figure 1.18. Expression of EPFL2 and CUC2 is not altered in *cuc2 cuc3* and *epfl1 epfl2* mutants, respectively 56
Figure 1.19. Expanded expression of *DRN* in *epfl1 epfl2* compared to the wild type 58
Figure 1.20. Expression of DRN and CUC3 in wild type and *epfl1 epfl2* mutants 59
Figure 2.1. The structure of T-DNA insert in the pAMO113 vector 71
Figure 2.2. Induction of EPFL2 in the SAM boundary leads to decreased expression of *CLV3*, *MCT1* and *MCT2* 77
Figure 2.3. Induction of H2B-GFP/EPFL2 in the *epfl1 epfl2* mutant containing DRN and CUC3 reporters during ovule initiation 79

Chapter 1

Regulation of Ovule Initiation in *Arabidopsis thaliana* by EPIDERMAL PATTERNING FACTOR-LIKE Proteins

Introduction

ERECTA Family Signaling During Plant Development and Ovule Initiation

Plants are sessile organisms that form complex arrangements of above ground organs, and the formation of these organs requires cell-to-cell communication to coordinate cell division, cell expansion, and cell differentiation. One primary mechanism for intercellular communication during plant development occurs through the receptor-like kinase (RK) family of proteins. Small molecules and peptides can act as ligands for specific RK complexes that induce signal transduction through the kinase domains. RK family consists of over 600 proteins in *Arabidopsis thaliana*, and at least 400 of these are predicted to be localized to the plasma membrane where they interact with other receptors or perceive extracellular signals. Over 200 of these RKs are leucine-rich repeat receptor-like kinases (LRR-RLK), and several of these LRR-RLKs are critical regulators of plant architecture, cell differentiation, and response to the environment. The mechanisms of signaling through these different LRR-RLKs are diverse, and their downstream targets vary greatly (Shiu and Bleecker, 2001; Wang et al., 2008; Furumizu and Aalen, 2023).

Arabidopsis thaliana has three ERECTA family (ERf) receptors consisting of ERECTA (ER), ERECTA-LIKE1 (ERL1), and ERL2 (Shpak et al., 2004). These receptors regulate stomata differentiation, plant architecture, meristem maintenance, and reproductive development (Torii et al., 1996; Shpak et al., 2004; Shpak et al., 2005; Chen et al., 2013; Uchida et al., 2013). Research has suggested that ERfs function predominantly via phosphorylation and activation of a mitogen-activated protein kinase (MAPK) cascade

consisting of YODA (MKKK), MKK4/5/7/9, and MPK3/6 (Bergmann et al., 2004; Wang et al., 2007; Jewaria et al., 2013; Lampard et al., 2014; Putarjunan et al., 2019) (Fig. 1.1). ERfs are known to respond to a family of EPIDERMAL PATTERNING FACTOR/ EPIDERMAL PATTERNING FACTOR-LIKE (EPF/EPFL) secretory protein ligands, and there are 11 *EPF/EPFL* genes in *Arabidopsis thaliana*. These proteins are secreted into the extracellular space where they are processed via proteases to generate a mature peptide that is roughly 45 to 70 amino acids in length (Shimada et al., 2011). The mature peptide then interacts with the LRR domains of ERf proteins and other coreceptors to alter the signaling activity of the receptor complex. EPF1 and EPF2 are two of the most thoroughly studied ERf ligands due to their agonistic activity during ERf mediated repression of stomata differentiation, and these ligands bind to ERfs in the presence of interacting LRR coreceptor TMM and LRR-RLKs coreceptor from the *SERK* family (Hara et al., 2007; Lee et al., 2012; Jewaria et al., 2013; Meng et al., 2015). Conversely, EPFL9 shows antagonistic activity during stomatal development by binding the ERf complex but not activating the kinase cascade (Hunt et al., 2010; Ohki et al., 2011; Shimada et al., 2011; Lee et al., 2015). *EPFL1*, *EPFL2*, *EPFL4*, and *EPFL6* have been found to regulate other developmental processes such as plant height and architecture, shoot apical meristem maintenance, leaf tooth formation, and ovule development (Abrash et al., 2011; Tameshige et al., 2016; Kosentka et al., 2019; Kawamoto et al., 2020). All four of these ligands are able to act agonistically by repressing stomata differentiation when ectopically expressed or applied to the abaxial epidermis of cotyledons (Abrash et al., 2011). While these ligands act

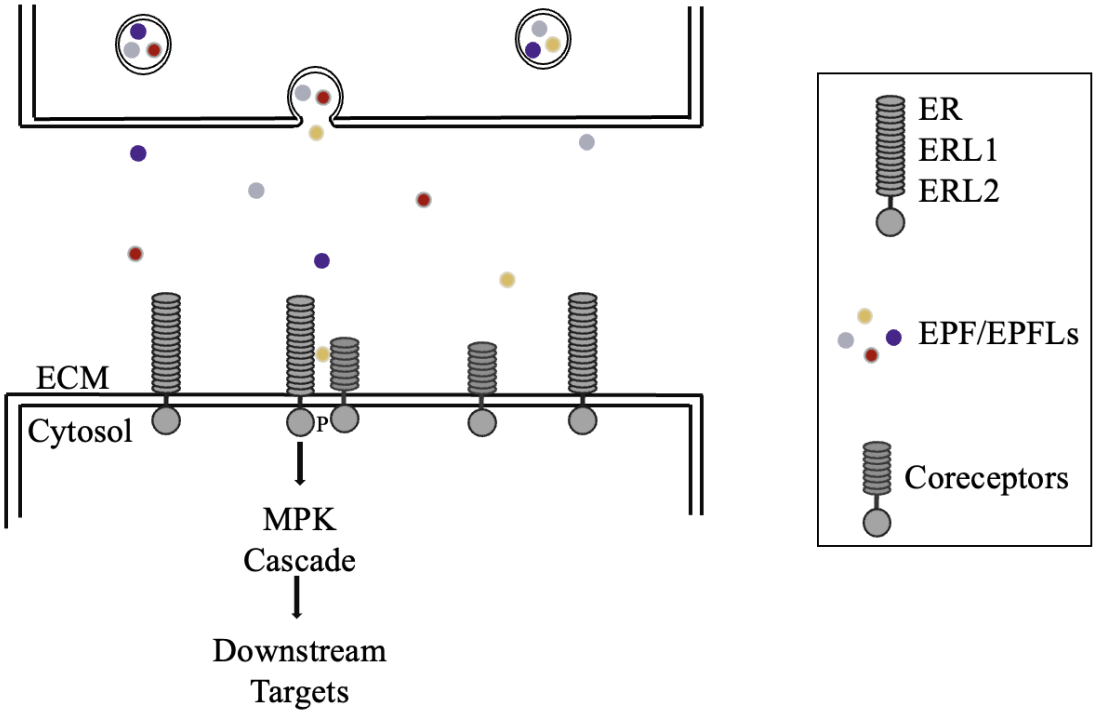

Figure 1.1. Diagram of ERECTA family signaling pathway

This diagram displays a simplistic overview of ERf signaling. EPFL peptides are secreted into the extracellular matrix where they may bind the extracellular domain of ERf receptors. This leads to the recruitment of coreceptors such as SERKs. This activates the intracellular kinase domains and leads to activation of the MAP KINASE (MPK) cascade. Ultimately, this leads to the phosphorylation of downstream targets.

somewhat redundantly to control certain traits such as fertility and shoot apical meristem width, these four ligands show unique expression patterns and control certain traits non-redundantly. For instance, *EPFL2* has been implicated in leaf tooth development, ovule initiation, and cotyledon development, while *EPFL4* and *EPFL6* are known to control pedicel length and plant height (Abrash et al., 2011; Tameshige et al., 2016; Kosentka et al., 2019; Kawamoto et al., 2020; Fujihara et al., 2021). Understanding the roles of individual *EPFL* genes will allow for a better understanding of ERf/EPFL signaling in many developmental contexts.

The ERf signaling pathway first appeared in bryophytes, while this pathway is absent in algae species. *Physcomitrium patens*, a model organism for studying early bryophytes, possesses 6 ERf receptors and 10 EPF/EPFL peptides (Caine et al., 2016). One of these peptides is homologous to EPF1, the negative regulator of stomata development in Arabidopsis, while the other 9 peptides are in the EPFL4/5/6 clade. *PpEPF1* was shown to be capable of regulating stomata density at the base of the sporophyte, and this highlights the conservation of some ERf signaling pathways (Caine et al., 2016). During the evolution of vascular plants, the EPFL1/2/3 clade arose. *Selaginella moellendorffii*, the model organism for early evolution of vascular plants, possesses 10 ligands from the EPFL1/2/3 clade, 4 ligands from the EPFL4/5/6 clade, and 4 ligands in the stomata regulating clades (Caine et al., 2016). An expression atlas of *S. moellendorffii* shows that several of the EPFL1/2/3 clade peptides are expressed in apical and basal meristematic tissue as well as leaf primordia (Ferrari et al., 2020). The significance of the evolution of the EPFL1/2/3 clade, and its functional distinction from the EPFL4/5/6 clade is unclear. In general, all

land plants possess ERf signaling pathways, but whether the functions of EPFL1/2/3 and EPFL4/5/6 clades are conserved is unclear. Unraveling the signaling cascades and downstream targets of EPFL1/2 signaling in *Arabidopsis thaliana* may lead to a stronger understanding of potentially conserved signaling pathways.

A publication by Kawamoto et al. in 2020 first characterized the role of *EPFL2* and ERf receptors in the regulation of ovule number and density in *Arabidopsis thaliana* (Kawamoto et al., 2020). This publication utilized a Genome Wide Association Study to identify *EPFL2* as a regulator of ovule number. Microscopic analysis revealed that *epfl2-2* mutants produce significantly fewer ovules per length of the fruit relative to wild type fruits. In addition to the decreased density, the *epfl2-2* mutant displays aberrant spacing between ovules with occasional fusion of ovule primordia. The use of a fluorescent reporter driven by the *EPFL2* promoter showed expression in a few boundary cells between ovule primordia, and this boundary expression is only seen along the apical-basal axis rather than surrounding the entire ovule. To further quantify the phenotype seen in the *epfl2-2* mutant, the authors used a reporter for the AP2-like transcription factor DORNROSCHEN (DRN). This reporter is expressed in the founder cells of forming ovule primordia during early stages of their initiation. The authors noted a significant deviation in the number of cells between each *DRN* expression peak in the *epfl2-2* mutant relative to wild type. In addition, the authors analyzed the expression patterns and phenotypes of ERf receptors. All 3 receptors showed expression in ovule primordia, although the analysis did not include stage 9 of carpel development when ovules are initiated. In addition, certain combinations of double mutants for the receptors generated reduced ovule density, such as the *erl1 erl2*

double mutant (Kawamoto et al., 2020). This suggests that *ERL1* and *ERL2* play a role in promoting ovule density, but the *er erl1 erl2* triple mutant was not examined, so it is possible that all three receptors play some role. In conclusion, the authors were able to identify *EPFL2* as a novel positive regulator of ovule initiation in *Arabidopsis thaliana*, but the mechanism by which EPFL2 regulates ovule density, and the potential role of other EPFL1/2/3 clade ligands was not investigated.

Flower Development and Ovule Initiation

Flowers are the structures generated by angiosperms to facilitate sexual reproduction, and they initiate from inflorescence meristems during the reproductive phase. Flower structures are diverse, including differences in the number and arrangement of the various floral organs. In the model organism *Arabidopsis thaliana*, flowers are composed of four whorls of organs: four sepals in the outermost whorl, four petals in the second whorl, six stamens in the third whorl, and two fused carpels in the innermost whorl (Smyth et al., 1990). The stamens are the male reproductive organs that generate pollen containing the male gamete, while the two fused carpels make up the gynoecium, which contains ovules that house the female gametophytes (Smyth et al., 1990). The patterning of floral organ identity in the various whorls is primarily controlled by the presence of MADS-box transcription factors (Bowman et al., 1989; Bowman et al., 1991), while the spacing and number of organs may be regulated by other factors such as phytohormones (Benkova et al., 2003). Early flower development in Arabidopsis is classically separated into 12 distinct stages. The first sign of organogenesis within the floral meristem is the emergence of sepal

primordia at stage 3. After sepals begin to develop, petals and stamens initiate at stage 5, and they are completely encased by the sepals by stage 6. At this same time, the gynoecium initiates and appears as an open-ended tube composed of the two fused carpel primordia. From stages 6 to 11, the floral organs continue to differentiate, develop, and expand in a coordinated manner until stage 12 when the flower bud opens and the stamens are able to pollinate the gynoecium (Smyth et al., 1990).

The plant kingdom shows a large degree of morphological diversity in many different structures. One particularly diverse structure in plants is the carpel and gynoecium (collection of all carpels), and these structures first arose in angiosperms as a significant evolutionary innovation of land plants (Becker, 2020). The ancestral carpel is thought to have been ascidiate (bottle-shaped) and lacking post-genital fusions of the carpel margin meristems (Becker, 2020). In addition, this ancestral flower contained multiple free carpels, and each carpel contained a single ovule (Becker, 2020). Angiosperms have evolved into multiple clades over time, with the largest being the core eudicots, composed of roughly 230,000 species (Ferrándiz, 2010). The ancestral core eudiocot is thought to have contained two fused carpels like *Arabidopsis thaliana* (found in the Rosid clade of eudicots), but Arabidopsis carpels are post-genitally divided by a false septum where carpel walls are connected to the silique by replum tissue (Ferrándiz, 2010). Other eudicots have utilized other carpel morphologies, such as congenital separation of carpel valves seen in model Asterids. In general, gynoecium morphology is highly diverse, and *Arabidopsis thaliana* possesses a highly derived gynoecium that contains several significant morphological

differences from many other species even within the core eudicots including differences in carpel number, ovule number, placenta arrangement, and septum fusion (Becker, 2020).

Plants require tightly coordinated regulation of lateral organ primordia initiation during organogenesis to achieve proper morphology. Lateral shoot organs initiate in the peripheral regions of meristematic tissues throughout development, and these organs include leaves, flowers, and various floral organs. The spatiotemporal control of lateral organ initiation determines the number and placement of organs throughout plant development, and this process is known to be regulated by phytohormones, signaling pathways, and transcription factors (Benkova et al., 2003). Several of these main regulatory genes are conserved in plants, but the spatiotemporal modulation of these pathways may explain morphological differences amongst genera (Sluis and Hake, 2015).

In many plant species, the placenta tissue is capable of initiating multiple ovules per fruit (Cucinotta et al., 2014). In *Arabidopsis thaliana*, the gynoecium is composed of two fused carpels containing two carpel margin meristems that are flanked by placenta tissue in the peripheral regions where ovule primordia initiate (Smyth et al., 1990; Robinson-Beers et al., 1992; Cucinotta et al., 2014; Yu et al., 2020). The process of ovule initiation occurs asynchronously from stages 9 through 11 of flower development in *Arabidopsis*, where ovule primordia continuously initiate from newly generated placenta tissue in spaces between previously formed ovules as the gynoecium elongates (Yu et al., 2020; Hu et al., 2022) (Fig. 1.2). At stage 8, the placenta tissue is flat with no visible protrusions of ovule primordia. To further dissect the processes occurring during ovule initation, the stage 9 has been broken into three separate stages 9a, 9b, and 9c. Stage 9a is

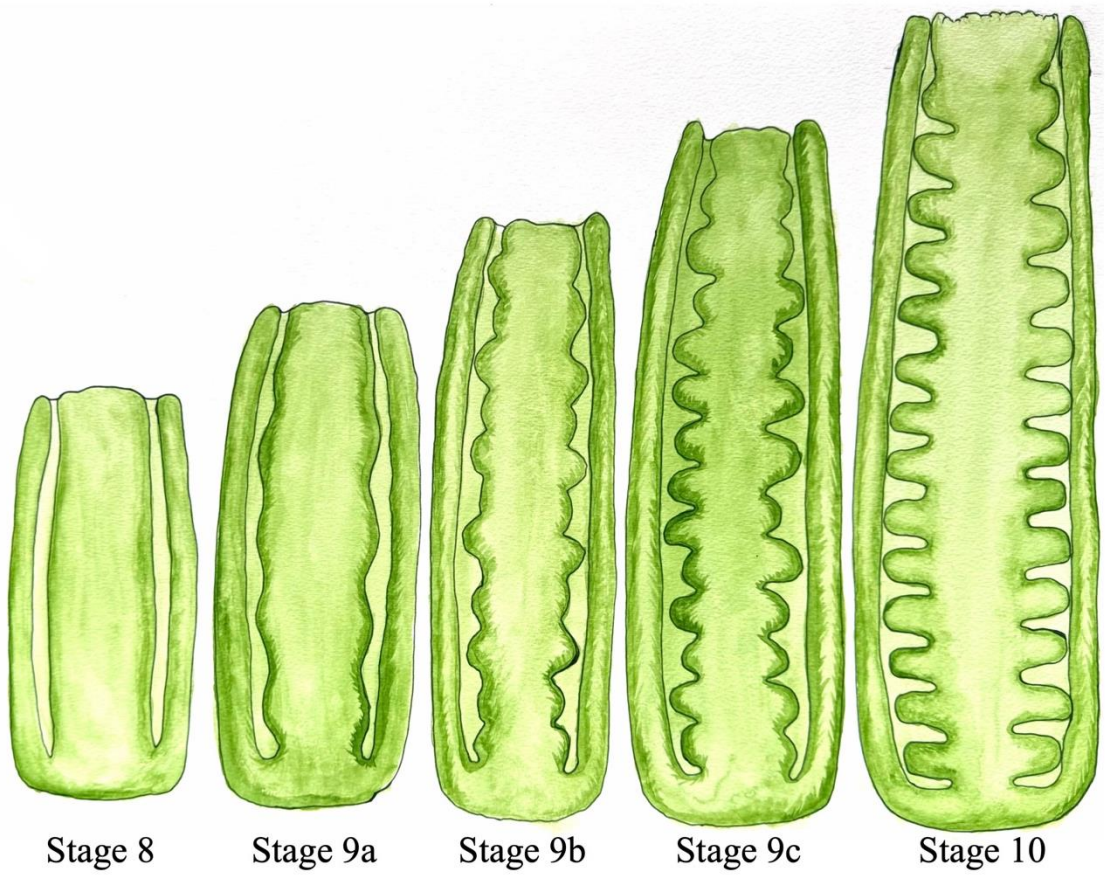

Figure 1.2. Diagram of the Arabidopsis gynoecium from stage 8 to stage 10
This diagram shows longitudinal cross sections of the Arabidopsis gynoecium from stage 8 to stage 10. This diagram highlights the asynchrony of ovule initiation as the placenta elongates throughout stage 9.

when the first few ovules begin to initiate. Stage 9b is when the first round of subsequent ovules begins to initiate in the spaces between the initial primordia. During stage 9c the third round of ovule primordia initiate in newly generated spaces along the placenta (Fig. 1.2). At stage 10 the majority of ovule primordia have initiated and begun to undergo differentiation (Yu et al., 2020). While total ovule number is ultimately regulated by the available amount of placenta tissue, the spacing of these ovule primordia along the placenta also affects the ovule number and seed yield.

Ovule primordia initiate from the placenta via periclinal divisions in the L2, or subepidermal, layer of cells (Schneitz et al., 1995). Ovule primordia appear as dome-shaped protrusions from the placenta tissue at stage 1-I of ovule development, and the stage of ovule development is not related to the stage of floral development. Stage 1-II of ovule development occurs when ovule primordia elongate and begin to express WUSCHEL at the apex of the ovule (Schneitz et al., 1995; Vijayan et al., 2021). During stage 2 of ovule development, a proximal distal axis becomes apparent with proximal funiculus, central chalaza, and distal nucellus (Vijayan et al., 2021). A subepidermal cell in the nucellus enlarges to become the megaspore mother cell, which will undergo meiosis in stage 2-V and cell degeneration in stage 3-I to leave a single functional female gametophyte (Schneitz et al., 1995). The inner and outer integuments initiate from somatic epidermal cells adjacent to the chalazal region during stages 2-II and 2-III, respectively, and these integuments continue to elongate throughout stages 2 and 3 of ovule development to surround the nucellus and developing embryo sac (Schneitz et al., 1995). Research suggests that the early outgrowth of ovule primordia is driven by tissue-specific growth in internal tissues

at the base of the ovules during stages 1-I through 1-II, whereas growth is more evenly distributed between cell layers during stages 2-I and 2-II (Vijayan et al., 2021). Ultimately, this detailed characterization of ovule development in Arabidopsis generates a reference when analyzing developmental mutants.

Regulation of Ovule Initiation

Organogenesis in plants requires tightly coordinated control of cell proliferation and differentiation, and intercellular communication is critical for regulation of these processes. During ovule primordia initiation, several phytohormones have been shown to play important roles in regulating either placenta length, ovule number, and/or ovule density. The phytohormone auxin is known to be essential for the initiation of ovule primordium, but other phytohormones such as brassinosteroids (BR), cytokinin (CK), and gibberellins (GA) also contribute to overall ovule number. While each hormone contributes independently to determine ovule number, some of these hormone pathways exhibit crosstalk.

The initiation of ovule primordia in Arabidopsis has similarities to the initiation of lateral organ primordia, such as leaves and flowers, by shoot apical meristems (Cucinotta et al., 2014). Lateral organ primordia initiation involves the concentration of auxin into peaks within the peripheral zone of the shoot apical meristem via polar auxin transport (Kuhlemeier and Reinhardt, 2001; Benkova et al., 2003). The patterning of these auxin maxima determines the spacing of lateral organ primordia as they emerge from the dome-shaped meristem (Kuhlemeier and Reinhardt, 2001; Heisler et al., 2005). In addition to

regulating the initiation and spacing of lateral organ primordia, auxin is also involved in controlling ovule primordia initiation along the placenta, as well as controlling overall gynoecium development. Mutants with defective auxin biosynthesis, transport, or signaling display defective placenta development and reduced or abolished ovule initiation (Yu et al., 2020).

One major pathway for production of indole-3-acetic acid (IAA), the most common active endogenous auxin found in plants, is catalyzed by flavin monooxygenases of the YUCCA gene family that use indole-3-pyruvic acid as a substrate (Zhao et al., 2001; Cao et al., 2019). The *yuc1 yuc4* mutants display severe defects in gynoecium development and fail to make ovule primordia (Cheng et al., 2006). While auxin biosynthesis is critical for overall auxin availability, research suggests that polar auxin transport is also necessary for ovule initiation. PINFORMED 1 (PIN1) is the primary polar auxin efflux transporter regulating ovule initiation in Arabidopsis. The *pin1-1* mutant makes few gynoecia that lack ovules along the placenta, and this suggests that PIN1 is essential for ovule initiation (Okada et al., 1991). PIN1 is expressed throughout L1 of the placenta at stage 8 of flower development before ovules initiate, but expression is upregulated at sites of ovule initiation during stage 9a when ovules begin to initiate (Galbiati et al., 2013; Yu et al., 2020; Yu et al., 2022). During ovule initiation, PIN1 localization on the plasma membrane is reoriented in certain L1 cells to concentrate auxin into a peak (Yu et al., 2020). After an ovule is initiated and developing, PIN1 localization in cells near the base of ovule primordia is reoriented to direct auxin back to the placenta so that additional ovules can be initiated in the regions between previously formed ovules (Yu et al., 2020; Yu et al., 2022).

PINFORMED 3 (PIN3) has been shown to have similar roles as PIN1 during late ovule initiation, with *pin3* mutants having reduced ovule initiation during late stages (Hu et al., 2022). Inhibition of auxin efflux via N-1-naphthylphthalamic acid (NPA) treatment during ovule initiation reduces or abolishes ovule initiation (Nemhauser et al., 2000; Larsson et al., 2014; Yu et al., 2020). The transcriptional responses to auxin are regulated by AUXIN RESPPONSE FACTOR (ARF) proteins and INDOLE-3-ACETIC ACID INDUCIBLE (Aux/IAA) proteins. Canonically, Aux/IAA proteins are bound to ARF transcription factors in the absence of auxin, whereby they repress the auxin response. In the presence of auxin, Aux/IAA proteins are polyubiquitinated and degraded, and this relieves the inhibition of ARFs allowing them to activate the auxin response (Guilfoyle et al., 1998; Lavy and Estelle, 2016). ARF5/MONOPTEROS (MP) is known to regulate organ initiation, and the weak allele *mpS319* fails to make a proper carpel margin meristem, placenta, or ovule primordia (Hardtke and Berleth, 1998; Alonso et al., 2003; Galbiati et al., 2013; Cucinotta et al., 2021). MP has been shown to regulate expression of genes such as *AINTEGUMENTA* (*ANT*), *CUP-SHAPED COTYLEDON1* (*CUC1)*, and *CUC2* (Galbiati et al., 2013). In addition, ARF3/ETTIN (ETT) is known to regulate gynoecium development in an apical-basal fashion, and the *ett* mutants have aberrant development of the ovary leading to reduced ovule number (Sessions et al., 1997; Nemhauser et al., 2000). The Aux/IAA protein IAA3, also known as SHORT HYPOCOTYL 2 (SHY2) functions to repress the auxin response in the absence of auxin perception during gynoecium development (Guilfoyle et al., 1998; Tian et al., 2002). A gain of function *shy2-2* mutation that prevents degradation of SHY2 in the presence of auxin leads to overall reduced

gynoecium size (Li et al., 2020a). While auxin is clearly critical for ovule initiation, this phytohormone also regulates many other developmental processes that precede ovule initiation. This factor, along with genetic redundancy, has made genetic analysis of the role of auxin-related genes during ovule initiation somewhat difficult.

Cytokinin is a phytohormone that is involved in regulating cell proliferation and differentiation (Skoog and Miller, 1957). CYTOKININ OXIDASE (CKX) proteins are responsible for the degradation of cytokinin, and the *ckx3 ckx5* double mutant has increased levels of endogenous cytokinin in flowers (Werner et al., 2003; Bartrina et al., 2011). The increase in cytokinin leads to a significant increase in the length of the placenta and the number of ovules relative to wild type (Ashikari et al., 2005; Bartrina et al., 2011). In addition, treatment of inflorescences with the synthetic cytokinin 6-benzylamino purine (BAP) causes a significant increase in overall ovule number (Galbiati et al., 2013). This suggests that increased cytokinin leads to increased placenta length and a subsequent increase in ovule number. Loss of cytokinin histidine kinase receptors or type-B ARABIDOPSIS RESPONSE REGULATOR transcription factors, that are positive regulators of the cytokinin response, leads to significantly reduced gynoecium size and ovule number, further supporting the role of cytokinin in promoting placenta elongation and ovule number (Higuchi et al., 2004; Bencivenga et al., 2012). While this data suggests that cytokinin promotes ovule number primarily by increasing placenta length, cytokinin may also play roles in regulating ovule density. UDP-GLUCOSYL TRANSFERASE enzymes UGT85A3 and UGT73C1 are capable of reversibly inactivating zeatin-type cytokinins through O-glucosylation (Hou et al., 2004). The *ugt85a3* mutant has increased

ovule number without any significant changes to pistil length, and overexpression of these genes leads to reduced ovule number (Cucinotta et al., 2018). Ultimately, research has shown that cytokinin promotes placenta length and ovule number, while further research may be needed to clarify the role of this hormone in regulating ovule density.

Brassinosteroids have also been shown to positively regulate ovule number, placenta length, and ovule density (Huang et al., 2013). Reduced brassinosteroid levels in the *det2* mutant and insensitivity to brassinosteroids in the *bri1-1* and *bin2-1* mutants lead to a significant reduction in gynoecium size and ovule number (Chory et al., 1991; Noguchi et al., 1999; Li and Nam, 2002; Huang et al., 2013; Yu et al., 2020). Brassinosteroid signaling results in the stabilization of the transcription factor BZR1, and the gain-of-function mutant *bzr1-1D* has significantly increased ovule number, placenta length, and ovule density due to the increased activity of BZR1 (Wang et al., 2002; Huang et al., 2013; Yu et al., 2020). BZR1 was shown to regulate transcriptional levels of transcription factors such as ANT or APETALA 2 (AP2) which are known ovule initiation regulators (Huang et al., 2013). In the shoot apical meristem, a comparison of BZR1 and bzr1-1D protein localization showed that the stabilized bzr1-1D protein is expressed in the boundary tissues, while the native BZR1 protein is degraded in these regions. The boundary expressed bzr1-1D protein was shown to cause repression of *CUC3* (Gendron et al., 2012). This research collectively suggests that brassinosteroids promote ovule initiation by increasing overall placenta length while also promoting the early steps of ovule initiation.

In contrast to the other phytohormones, gibberellins negatively regulate ovule initiation in Arabidopsis (Gomez et al., 2018; Barro-Trastoy et al., 2020). Loss of

GIBBERELLIN-INSENSITIVE DWARF 1 (GID1) receptor that senses GA leads to increased ovule numbers (Griffiths et al., 2006; Gomez et al., 2018). DELLA proteins function to negatively regulate GA signaling (Sun, 2010), and loss of DELLA proteins leads to shorter gynoecia with reduced ovule number (Gomez et al., 2018). Hyper-stable DELLA proteins such as *gai-1* cause increased ovule number and ovule density (Gomez et al., 2018). Transcriptomic analysis suggests that GA may repress transcription of two transcription factors, UNFERTILIZED EMBRYO SAC 16 (UNE16) and REPRODUCTIVE MERISTEM 22 (REM22), which were shown to regulate ovule number (Gomez et al., 2018). Ultimately, this data suggests that GA functions to negatively regulate ovule number and density in Arabidopsis.

In addition to the phytohormone signaling pathways, several other developmental transcription factors also regulate the initiation of ovule primordia in Arabidopsis. The AP2-like transcription factor AINTEGUMENTA (ANT) regulates organ initiation and promotes cellular divisions during plant development, and the role of ANT is particularly apparent during ovule initiation and development (Klucher et al., 1996; Krizek, 1999). Loss of function *ant* mutants have reduced ovule number without significant changes in gynoecium length, and this indicates that *ant* mutants have decreased ovule density. When the *ant* mutation is combined with mutations in AINTEGUMENTA-like paralogs or other gynoecium-regulating transcriptional co-regulators such as SUESS (SUE) or LEUNIG (LEU), the gynoecia show partially formed septal tissues that fail to make ovule primordia (Liu et al., 2000; Azhakanandam et al., 2008; Krizek, 2015). The failure to initiate ovule primordia in these mutants suggests that ANT works together with other developmental

transcriptional regulators to promote the initiation of ovule primordia. While ANT has been shown to promote cell proliferation to control organ size (Krizek, 1999), the exact mechanisms by which ANT promotes ovule initiation and ovule spacing remain elusive.

Proper distribution and development of organ primordia also require organ boundary-specific transcription factors that allow for differential growth of boundary tissues relative to the organ primordia themselves. Three NAC-domain transcription factors, CUC1, CUC2, and CUC3, are expressed in various organ boundaries during above-ground organ initiation including during ovule initiation. Loss of *cuc3* leads to infrequent fusions between ovule primordia, and the *cuc1 cuc3* and *cuc2 cuc3* double mutants have significantly increased numbers of ovule primordia fusions relative to wild type or *cuc3* single mutants. In contrast, the *proSEEDSTICK:RNAi_CUC1 cuc2* mutant that has reduced expression of *CUC1* and *CUC2* in the placenta displays reduced ovule number and increased spacing between ovule primordia. This data suggests that expression of *CUC* genes in boundary tissues inhibits organ primordia fusion and promotes proper ovule spacing. Several mechanisms have been proposed to explain the regulation of ovule initiation by *CUC* genes. The *proSTK:RNAi_CUC1 cuc2* mutant displays altered expression of PIN1 during ovule initiation which may lead to altered auxin distributions. Exogenous application of CK restores PIN1 expression and ovule number in the *proSTK:RNAi_CUC1 cuc2* mutant, and *UGT85A3* is overexpressed in this mutant. This suggests that *CUC* genes may function to regulate auxin distribution via CK-mediated regulation of PIN1 expression, although further research would be required to determine whether this is the primary mechanism by which *CUC* genes regulate ovule spacing.

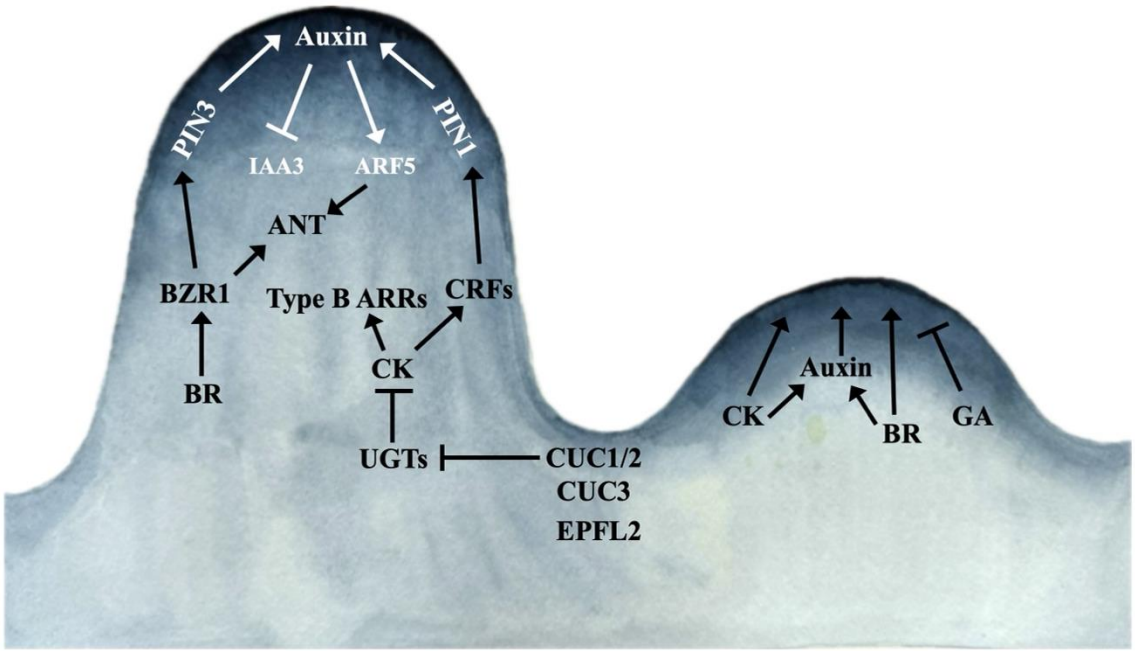

Figure 1.3. Model of gene regulatory networks controlling ovule initiation
This model highlights key genes and pathways regulating ovule initiation based on previous literature.

In addition to the individual roles of the known hormones and transcription factors controlling ovule initiation, there is an extensive amount of crosstalk between these regulators. *CUC1/2*, CK, and BR have all been suggested to promote the proper expression of PIN transporters during ovule initiation to mediate the formation of auxin maxima (Cucinotta et al., 2016; Cucinotta et al., 2018; Yu et al., 2020). The auxin-responsive *MP* has been shown to promote expression of *CUC1/2* and *ANT* during gynoecium development, and directly regulate *DRN* transcription during embryo development and meristem maintenance (Cole et al., 2009; Galbiati et al., 2013; Luo et al., 2018). The BR-responsive BZR1 transcription factor has been suggested to promote *ANT* expression during ovule initiation (Huang et al., 2013). Currently, it remains unclear whether GA signaling has any significant crosstalk with these known pathways during ovule initiation. Overall, the known positive regulators of ovule initiation in Arabidopsis display a significant amount of crosstalk that leads to proper expression of the auxin response and critical transcription factors.

Materials and Methods

Plant Materials and Growth Conditions

All research was performed using the Columbia ecotype of *Arabidopsis thaliana*. The *epfl4 (chl-2), epfl6 (chal-2), cuc2-3, cuc3-105, epfl1-1, epfl2-1,* and *bzr1-1D* mutants were described previously (Wang et al., 2002; Hibara et al., 2006; Abrash et al., 2011; Tameshige et al., 2016; Kosentka et al., 2019). The higher order mutants *epfl1 epfl2*, *epfl4 epfl6,* and *er-105 erl1-2 erl2-1* were generated earlier (Shpak et al., 2004; Kosentka et al.,

2019). When the *cuc3-105* mutation was outcrossed into *epfl2-1* backgrounds, the *epfl2-1* mutation was genotyped according to (Kosentka et al., 2019). The *cuc2-3* and *cuc3-105* mutations were identified based on genotyping using three-primer PCR. For genotyping of *cuc2-3*, the primers CUC2 GT F (5'-GCACGCACGCATACTCAGATAGA-3') and CUC2 GT R (5'- CCAGTAACCAGCCTCAGTTGCTC-3') were used to amplify the 931bp wild type fragment, and CUC2 GT R and SAIL LB (5'-TAGCATCTGAATTTCATAACCAA-3') were used to amplify an approximately 550 bp fragment of the mutant allele. For genotyping of *cuc3-105*, the primers CUC3 GT F (5'-GATGATGCTTGCGGTGGAAGATG-3') and CUC3 GT R (5'-GACATCCACACCACACGTACAGG-3') were used to amplify the 1062bp wild type fragment, and CUC3 GT R and GABI-Kat LB (5'-ATATTGACCATCATACTCATTGC-3') were used to amplify an approximately 400 bp fragment of the mutant allele. Double *cuc2-3 cuc3-105* mutants were identified based on cotyledon fusions and confirmed by genotyping. During a cross with *epfl1-1 epfl2-1*, a homozygous *bzr1-1D* mutant was identified based on the increased size of leaves and flower organs, delayed flowering, and bending of the inflorescence stem. During crosses, double *epf1-1 epfl2-1* mutant can be identified based on shorter petal phenotype and confirmed by genotyping (Kosentka et al., 2019).

Plants were grown on 1x Murashige and Skoog's (MS) solid media supplemented with 1% (w/v) sucrose until 5-7 days post-germination, when they were moved to the soil. The soil mixture contained a 1:1 ratio of Lambert LM-Org soil to Palmetto Fine-Medium A-2 vermiculite supplemented 75 mg/100g of soil Miracle-Gro and 0.25 g/100g of soil

Osmocoat 15-9-12 (Scotts). Plants were grown at 20^0 C under long-day conditions of 18 hours of light and 6 hours of darkness.

Generation of Transgenic Plants

Plasmids containing *proEPFL1:EPFL1:EPFL1term* (pPZK411) and *proEPFL2:EPFL2:EPFL2term* (pPZK412) in the binary vector pPZP222 and *proEPFL1:GUS-GFP:35sTer*m (pPZK401) and *proEPFL2:GUS-GFP:35sTerm* (pPZK402) in the binary vector pKGWFS7 were described previously (Kosentka et al., 2019). To generate *proEPFL1:EPFL2:EPFL1term* (pAMO101), overlapping PCR was used to fuse the 2.05 kb promoter of *EPFL1* with the transcribed region of *EPFL2* followed by the 0.95 kb *EPFL1* terminator. The fragment was inserted into pPZP222 between BamHI and KpnI sites. To generate *proEPFL2:EPFL1:EPFL2term* (pAMO100), overlapping PCR was used to fuse the transcribed region of *EPFL1* with the 1.1 kb *EPFL2* terminator. The fragment was inserted into pPZP222 between BamHI and KpnI sites. The 2.6 kb *EPFL2* promoter was then inserted between HindIII and BamHI sites of the vector. To generate *proEPFL1:EPFL6:EPFL1term* (pAMO105), overlapping PCR was used to fuse the 2.05 kb promoter of *EPFL1* with the transcribed region of *EPFL6* followed by the 0.95 kb *EPFL1* terminator. The fragment was inserted into pPZP222 between BamHI and KpnI sites. To generate *proEPFL2:EPFL6:EPFL2term* (pMIG101), overlapping PCR was used to fuse the transcribed region of *EPFL6* with the 1,1 kb *EPFL2* terminator. The fragment was inserted into pPZP222 between BamHI and KpnI sites. The 2.6 kb *EPFL2* promoter was then inserted between HindIII and BamHI sites of the vector. To generate

proEPFL2:H2B-eGFP:EPFL2term (pAMO124), *H2B-eGFP* was fused with the 1.1 kb *EPFL2* terminator using overlapping PCR. This fragment was inserted into pPZP222 between BamHI and KpnI sites. Then the 2.6 kb *EPFL2* promoter was inserted into the plasmid between HindIII and BamHI sites. The template for amplifying the H2B-EGFP sequence was a plasmid from the Z. Nimchuk lab (UNC Chapel Hill, USA). To generate the *proDRN:H2B-eGFP:DRNterm* construct (pAMO102b), *H2B-eGFP* was fused to the 1.38 kb *DRN* terminator using overlapping PCR and inserted into the binary vector pPZP222 between BamHI and SalI sites. Then, the 4.86 kb *DRN* promoter was inserted using the BamHI site. To generate a red endoplasmic reticulum localized DRN reporter *proDRN:er-mCherry:DRNterm* (pAMO119), the 4.86 kb *DRN* promoter was inserted into pPZP222 between BamHI and SalI sites. Next, *er-mCherry* was fused with the 1.38 kb *DRN* terminator using overlapping PCR and inserted into the plasmid using SalI. The *er-mCherry* sequence was amplified using pAN456 (Nelson et al., 2007).

In the obtained transgenic line carrying *proPIN1:PIN1-mGFP4:PIN1term* (Benkova et al., 2003), the insert was genetically linked with the *EPFL2* gene, and we were not able to outcross this marker into the *epfl1 epfl2* mutant. Using DNA from the transgenic plants, we reamplified *proPIN1:PIN1-mGFP4:PIN1term* and inserted it into pPZP222 between BamHI and KpnI sites creating plasmid pAMO103.

To generate the proERL1:H2B-eGFP:35Sterm construct (pESH751), H2B-eGFP was amplified and inserted into pESH245 using SalI and BamHI restriction sites. To generate the proERL2:H2B-eGFP:35Sterm construct (pESH752), *H2B-eGFP* was amplified and inserted into pESH246 using SalI and PstI restriction sites. pESH245 and

pESH246 vectors have been described previously (Shpak et al., 2004). They contain the *GUS* gene under the control of either *ERL1* or *ERL2* promoter in the pPZP222 backbone.

The inserted sequences in pAMO100, pAMO101, pAMO102b, pAMO103, pAMO105, pMIG101, pESH751, and pESH752 plasmids were confirmed by Sanger sequencing. The full sequence of pAMO119 and pAMO124 plasmids was determined by Oxford Nanopore Technology at Plasmidsaurus. Plasmids were transformed into an *Agrobacterium tumefaciens* strain GV3101/pMP90 by electroporation and introduced into Arabidopsis plants by the simplified floral dip method (Clough and Bent, 1998). pPZK411, pPZK412, pAMO100, pAMO101, pAMO105 and pMIG101 were introduced into the *epfl1 epfl2* mutant. pAMO102b was introduced into *epfl1 epfl2* and the wild type. pPZK401, pPZK402, and pAMO124 were introduced into the wild type. The *proCUC3:er-CFP* transgenic plants were previously described (Goncalves et al., 2015). This marker was outcrossed into the *epfl1 epfl2* mutant. pAMO119 was introduced into the wild type and *epfl1 epfl2* plants both containing *proCUC3:er-CFP*. pAMO 103 was at first introduced into the *epfl1 epfl2* mutant. Later, this marker was outcrossed from the mutant into the wild type using one stable transgenic line. pESH751 and pESH752 were introduced into *Landsberg erecta* ecotype that has a point mutation $K_{750} \rightarrow I_{750}$ in the *ERECTA* gene (*er-1* allele) (Torii et al., 1996). In T1 and T2, all transgenic plants described above, except pPZK401 and pPZK402, were selected using 100 mg/L and 60 mg/L gentamycin, respectively. Transgenic plants expressing pPZK401 and pPZK402 were selected using 25 mg/L kanamycin. Multiple homozygous T3 lines were generated for each construct.

The pGreenIIM proDR5v2:ntdTomato/proDR5:n3GFP and pGreenIIM proRPS5A:mDII-ntdTomato/proRPS5A:DII-n3Venus plasmids were described previously (Liao et al., 2015) and obtained from AddGene (plasmids #61628 and #61629, respectively). They were transformed into the *epfl1 epfl2* mutant. Transgenic plants were selected using MS plates with 0.1 mg/L methotrexate, and multiple homozygous T3 lines were generated. proDR5v2:ntdTomato/proDR5:n3GFP or proRPS5A:mDII-ntdTomato/proRPS5A:DII-n3Venus markers were outcrossed from one selected *epfl1 epfl2* line into the wild type.

Wild-type seeds expressing pGREENII proARF5:SV40-3x eGFP (CS67076) were obtained from the ABRC stock center and outcrossed into the *epfl1 epfl2* mutant. The *AtML1pro:ER-FLAG* construct (Uchida et al., 2012) was outcrossed from the *er-105* mutant into *epfl1 epfl2*. *proWUS:H2B-eGFP* marker (Zhang et al., 2021) was outcrossed from the wild type into *epfl1 epfl2*.

Microscopy

Inflorescence clusters containing flowers up to stage 12 were harvested from the primary inflorescences after a plant made 10-15 flowers. They were placed in 90% ethanol 10% acetic acid solution to rock overnight and then gradually rehydrated by replacing the solution with 90% ethanol, 70% ethanol, 50% ethanol, 20% ethanol, and water with 20 minutes of rocking in between each step. Afterward, the samples were placed in 0.5 M NaOH solution and incubated at 37^0 C for 15 to 20 minutes to make them transparent, then rinsed with water several times to remove residual NaOH before Differential Interference

Contrast (DIC) microscopy. To measure ovule density, stage 10 flowers were identified based on developmental markers such as the presence of all ovule primordia in a finger-like shape prior to integument initiation and the early differentiation of the style (Smyth et al., 1990; Schneitz et al., 1995; Yu et al., 2020).

Aniline blue staining follows the above tissue-clearing protocol described above. After the final rinsing step, the sample is placed in 0.1% (w/v) aniline blue solution in 50mM potassium phosphate pH 7.5 buffer for 30 minutes to one hour in a protocol adapted from (Lu et al., 2011). The samples were then rinsed with potassium phosphate buffer and imaged using a Nikon Eclipse 80i epifluorescence microscope with a 12-megapixel cooled color camera and a UV-2A filter (Nikon). Ovules in the process of meiosis II were identified by the presence of two strong callose bands stained by aniline blue as previously described (Cao et al., 2018). Ovules that were fully straightened out on the slide and in focus were imaged. Ovule height was measured using ImageJ by drawing a line selection from the middle of the base of the funiculus to the central tip of the nucellus on calibrated images.

For confocal microscopy, inflorescence clusters containing flowers up to stage 12 were harvested and fixed in 4% paraformaldehyde under a vacuum for up to 2 hours. Samples were then rinsed with 1x Phosphate-buffered saline (PBS) pH7.4 twice before placing them in ClearSee solution consisting of 25% (w/v) urea, 15% (w/v) sodium deoxycholate, and 10% (w/v) xylitol as previously described (Kurihara et al., 2015). Microcentrifuge tubes with samples were wrapped with foil to prevent photobleaching and rocked for 1 to 2 days with a daily change of ClearSee solution. Leaving samples in the

solution longer than 2 days will lead to the loss of the signal. The day before imaging, samples were placed in a staining solution containing 0.1% (v/v) SCRI Renaissance 2200 (SR2200) dye, 1% (v/v) DMSO, 0.05% (v/v) Triton-X100, 5% (v/v) glycerol in ClearSee solution and left to rock overnight (Musielak et al., 2015). Before imaging, the samples were rinsed with fresh ClearSee. Water instead of ClearSee was used as a mounting medium to prevent contamination of the microscope water immersion lens. Slight dissection was used to separate and expose stage 8 through stage 10 flowers. Confocal microscopy was performed using a Leica SP8 White Light Laser Confocal microscope. Samples were imaged using a 40x water immersion lens at 1024 x 512 pixel size with a zoom factor between 1.0x to 1.5x. Bidirectional scanning was used with a scan speed between 200 and 600 Hz, and line averaging was used with a line average of 3. Z-stacks were generated with a Z-step size of no greater than 0.5 microns. The SR2200 dye was excited with a 405 nm solid state UV laser and imaged using a 420-450 nm emission window. CFP was excited with a 456 nm argon laser and imaged using either a 460-500 nm emission window or, if GFP was also expressed in the sample, with a 460-480 nm emission window. GFP was excited with a 488 nm argon laser and imaged using a 500-520 nm emission window. Red fluorescent proteins such as mCherry or tdTomato were excited with a white light laser at 556 nm and imaged using a 605-625 nm emission window. Sequential line scanning was used to image multiple channels at once. Hybrid detectors were used when available, while PMT detectors were occasionally used when necessary. Laser power, gain, and emission filters were modified depending on the brightness of the signal and the number of fluorophores present in the sample. Confocal z-

stacks were processed into 2D images using FIJI software. For each channel, background subtraction and contrast enhancement were used if necessary to remove background and enhance signal-to-background ratios. For longitudinal cross sections of ovule initiation, the slices of the z-stack, which represent the center of the ovule primordia, were identified. Next, a Z-projection with frame averaging was created using 3 to 5 slices around the center of ovule primordia to create a smoother image while not exceeding the width of an individual cell. Finally, images were cropped to the desired size in microns, and image size in pixels was readjusted so that all images in an individual figure had the same dimensions in both pixels and microns.

Chemical Treatments of Inflorescences

To study the effect of gibberellins and auxin on ovule initiation, inflorescence clusters were briefly dipped into a water solution that contained 0.01% Tween-20, 0.05% DMSO one of the following: 25 mM gibberellic acid (GA), 4 mM paclobutrazol (PAC), 10 mM N-1-naphthylphthalamic acid (NPA) or 50 mM 2,4-Dichlorophenoxyacetic acid (2,4-D). The mock solution contained 0.01% Tween-20 and 0.05% DMSO. Dipping was done five days in a row once a day at the same time each day. Inflorescence clusters were collected on day six, and ovule initiation was studied using DIC microscopy. To study the effect of cytokinins on ovule initiation, inflorescence clusters were dipped into a water solution that contained 0.01% Silwet L-77, 0.1% DMSO and 1mM 6-benzylaminopurine (BAP). The mock solution contained 0.01% Silwet L-77 and 0.1% DMSO. Inflorescence clusters were dipped three days in a row and collected on day four.

Results

EPFL1 and *EPFL2* regulate ovule density in a partially redundant manner

Previous research demonstrated a role for *EPFL2* in the positive regulation of ovule density and control of ovule spacing (Kawamoto et al., 2020). To investigate whether other *EPFL* genes contribute to ovule initiation, we screened higher order *epfl* mutant combinations. Measurements of ovule number and placenta length for stage 10 flowers, when most ovules are formed (Yu et al., 2020), were taken, and ovule density was obtained by dividing ovule number by placenta length. As expected, the *epfl2* single mutant showed significantly reduced ovule density (Fig. 1.4A and B). While the ovule density of *epfl1* was not reduced, the *epfl1 epfl2* double mutant (also referred to as *epfl1,2* in figures) had a significant decrease in ovule number and density relative to *epfl2* without altering placenta length (Fig. 1.4A and B, Fig. 1.5 and 1.6). The reduction in ovule density leads to broader boundary regions separating ovule primordia in *epfl1 epfl2* (Fig. 1.4A). This data suggests that *EPFL1* and *EPFL2* synergistically promote ovule initiation. The simultaneous loss of *EPFL4* and *EPFL6* did not affect ovule density or placental length (Fig. 1.5). The quadruple *epfl1 epfl2 epfl4 epfl6* (*epfl1,2,4,6*) mutant had a significant decrease in the placenta length but no change in the ovule density relative to *epfl1 epfl2* (Fig. 1.5). This data indicates that EPFL4 and EPFL6 are not required for regulation of ovule density, and all four ligands synergistically promote gynoecium elongation during early flower development. We did not detect a significant decrease in the ovule density in *er erl1 erl2*

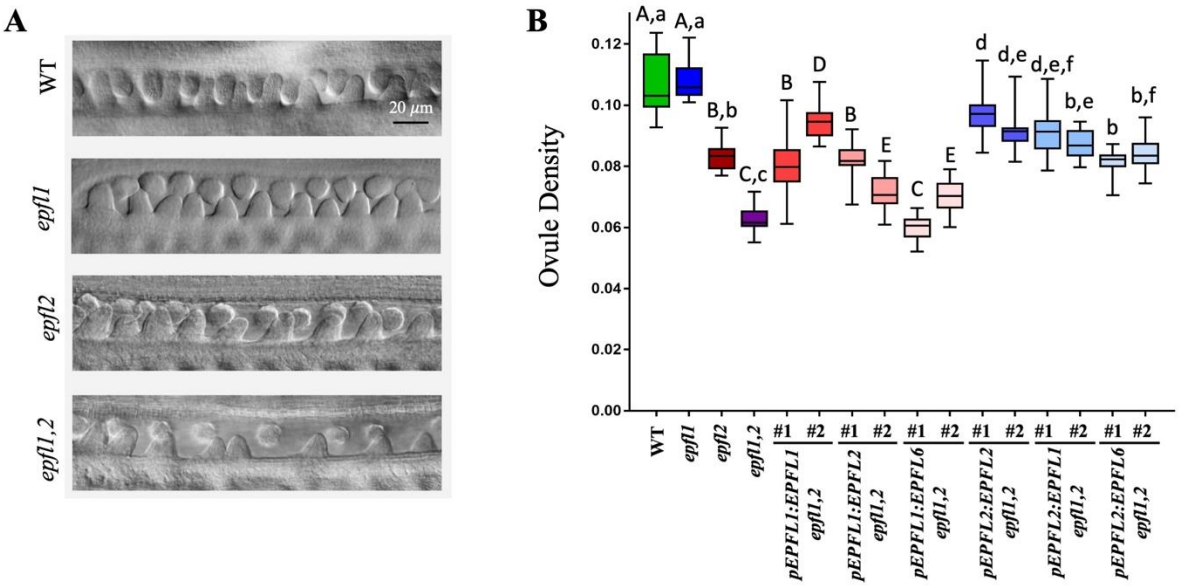

Figure 1.4. EPFL1 and EPFL2 positively regulate ovule density in a partially redundant manner

A. DIC images of stage 10 gynoecium demonstrate differences in ovule density. B. Ovule density in WT, *epfl* mutants, and transgenic plants expressing indicated constructs in the *epfl1 epfl2* (called *epfl1,2*) background. Two independent transgenic lines (labeled #1 and #2) were analyzed for each construct. N=20. Data is represented using box–whisker plots: the whiskers represent maximum and minimum values, and the boxes represent the upper quartile, exclusive median, and lower quartile. Constructs expressing EPFL ligands using EPFL1 promoter (upper case letters) and EPFL2 promoter (lower case letters) were compared separately to wild type and mutants using one-way ANOVA with Tukey post-hoc test (P value<0.01).

versus *epfl1 epfl2* (Fig. 1.5) suggesting that, out of all EPFLs, EPFL1 and EPFL2 are the only positive regulators of ovule initiation.

To test whether mutations in *EPFL1* and *EPFL2* are directly responsible for changes in ovule density, *proEPFL1:EPFL1* and *proEPFL2:EPFL2* were introduced into *epfl1 epfl2* and two independent transgenic lines were analyzed (Fig. 1.4B and Fig. 1.6). Both constructs contain terminator regions of the corresponding genes (Kosentka et al., 2019). The *proEPFL1:EPFL1* construct fully rescued the *epfl1* phenotype. The *epfl1 epfl2* plants expressing this construct were indistinguishable from *epfl2* plants. *proEPFL2:EPFL2* partially rescued *epfl1 epfl2* mutant. Ovule number and density were slightly reduced in plants carrying the *proEPFL2:EPFL2* construct compared to either the wild type or *epfl1*, suggesting that some regulatory elements might be missing in our construct. To address whether *EPFL1*, *EPFL2*, and the more distantly related *EPFL6* are functionally redundant on the protein level, the promoter of *EPFL1* was used to drive the expression of EPFL2 and EPFL6, and the promoter of *EPFL2* was used to drive the expression of EPFL1 and EPFL6 in the *epfl1 epfl2* mutant. The coding sequences included introns. Expression of EPFL2 under the *EPFL1* promoter was able to fully restore ovule density in one line, while another line was less effective. At the same time, EPFL6 under the *EPFL1* promoter did not rescue in one line while it was partially effective in another line (Fig. 1.4B). EPFL1 and EPFL6 expressed under the *EPFL2* promoter led to an increase in ovule density in all observed lines, although the effects were not as strong as when EPFL2 was expressed under its own promoter (Fig. 1.4B and Fig. 1.6). Overall, this suggests that EPFL1, EPFL2, and EPFL6 proteins can all function as ligands of ERf

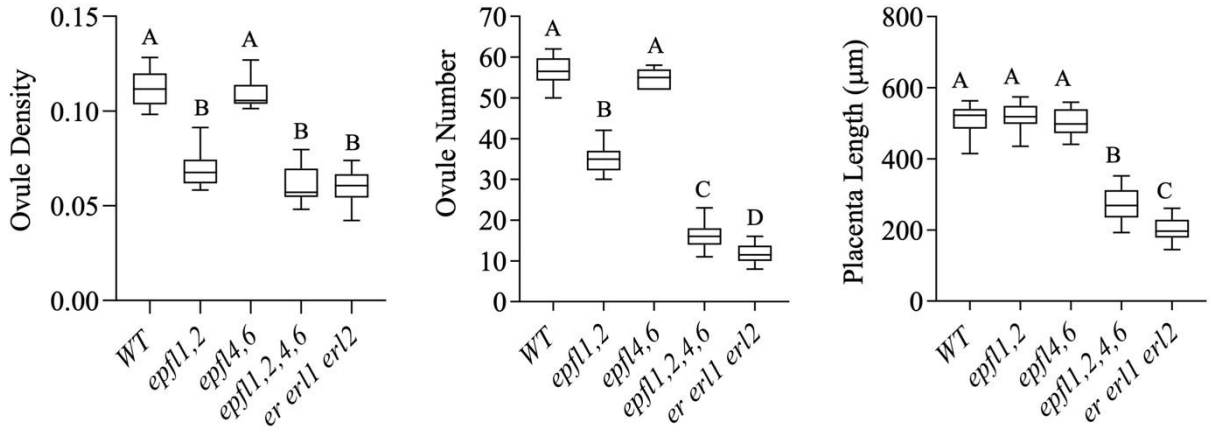

Figure 1.5. EPFL1, EPFL2, EPFL4, and EPFL6 synergistically regulate gynoecium elongation

Ovule density, ovule number, and placenta length of the stage 10 gynoecia of indicated genotypes. N=20 Data is represented using box–whisker plots: the whiskers represent maximum and minimum values, and the boxes represent the upper quartile, exclusive median, and lower quartile. A one-way ANOVA using Tukey's test with multiple comparisons was used to determine significance with a P-value < 0.01.

receptors during ovule initiation to some degree despite differences in protein sequences, while the *EPFL2* promoter has the strongest effect on regulating ovule density.

In Arabidopsis, ovule initiation occurs asynchronously, with new primordia arising in the boundaries of previously formed ones as the placenta elongates (Yu et al., 2020). To investigate whether *EPFL1* and *EPFL2* regulate the initiation of early or late primordia, ovule density was measured throughout the floral stage 9 (Fig. 1.7A). Overall, we observed stronger defects in ovule initiation in the apical half of the placenta (Fig. 1.7A). Quantification of ovule number as a function of placenta length demonstrated that ovule initiation in *epfl1 epfl2* is significantly reduced starting from the first wave of ovules (Fig. 1.7B). This suggests that decreased ovule formation in the mutant is caused by decreased ability of the placenta to form ovules and not due to changes in placenta elongation or formation of abnormal boundaries between the first wave of ovules.

In summary, EPFL1 and EPFL2 synergistically promote the ability of the placenta to form ovules, and these ligands likely function through all three ERf receptors during this process. The EPFL1, EPFL2, and EPFL6 proteins can be successfully interchanged to some degree, while the *EPFL2* promoter has the strongest effect on regulating ovule density.

EPFL1 and EPFL2 promote ovule outgrowth

Ovule development in Arabidopsis has been thoroughly described previously (Schneitz et al., 1995; Vijayan et al., 2021). Ovules initiate as finger-like protrusions. Later, inner and outer integuments develop, and three distinct regions form along a proximal-distal axis: the funiculus, the chalaza, and the nucellus. We noticed that *epfl1 epfl2* ovules

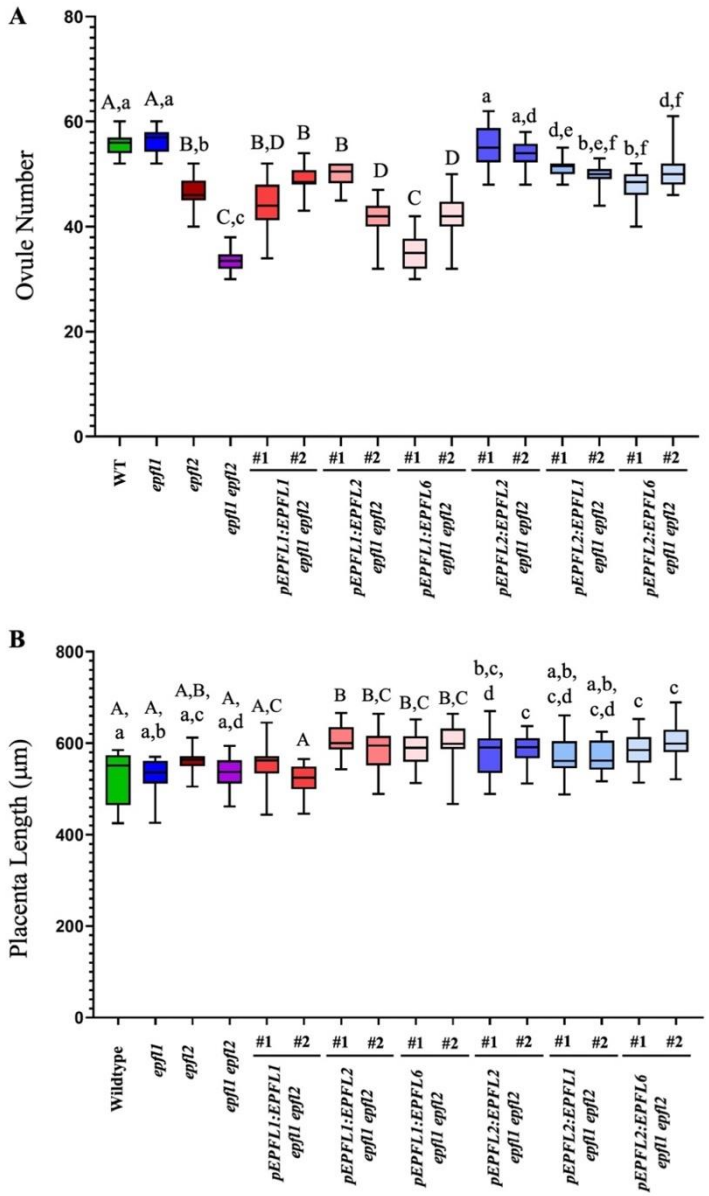

Figure 1.6. EPFL1 and EPFL2 promote ovule initiation by positively regulating ovule number

Ovule number (A) and placenta length (B) in WT, epfl mutants, and transgenic plants expressing indicated constructs in the *epfl1 epfl2* background. Two independent transgenic lines (labeled #1 and #2) were analyzed for each construct. N=20, Data is represented using box–whisker plots: the whiskers represent maximum and minimum values, and the boxes represent the upper quartile, exclusive median, and lower quartile. Constructs expressing EPFL ligands using *EPFL1* promoter (upper case letters) and *EPFL2* promoter (lower case letters) were compared separately to wt and mutants using one-way ANOVA with Tukey post-hoc test (P value<0.01).

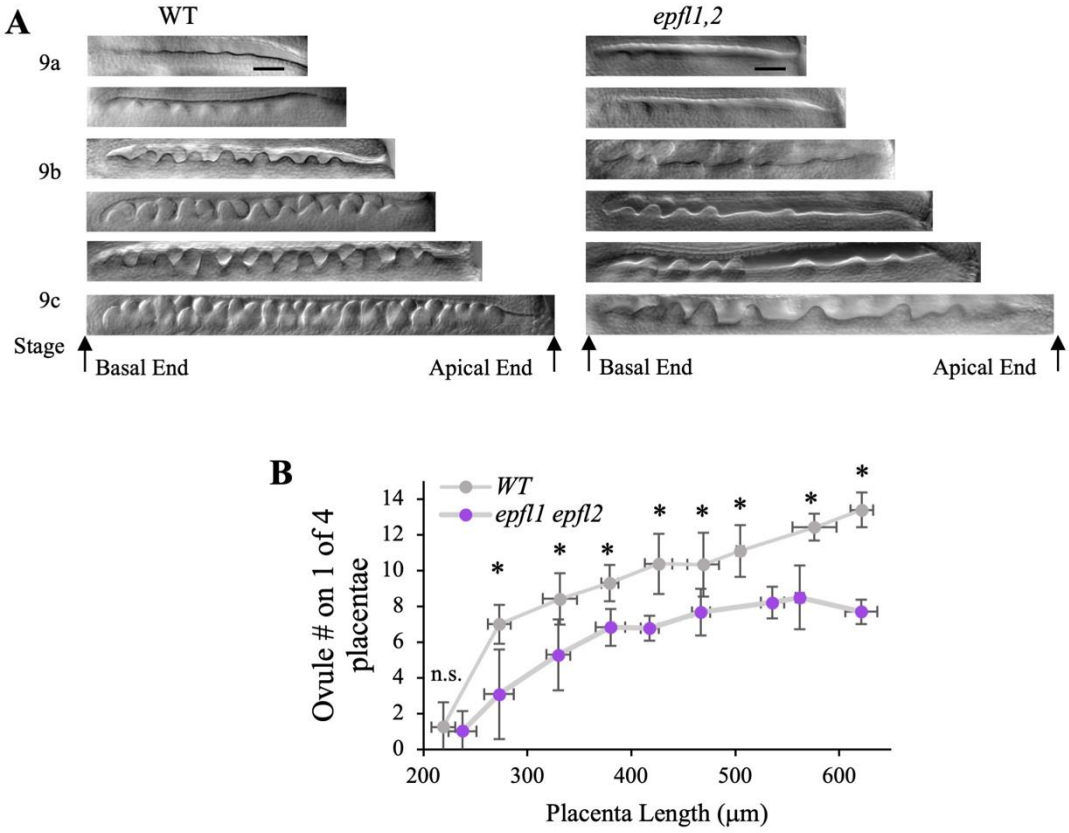

Figure 1.7. EPFL1/2 regulate ovule density at all stages of ovule initiation

A. DIC images of ovule initiation from stages 9a to 9c in wild type (WT) and *epfl1 epfl2* mutant. All images are to scale and the scalebar is 20 microns. B. Measurements of ovule number as a function of placenta length for WT and *epfl1 epfl2* stage 9a through stage 10. Measurements were separated into 50 mm placenta length bins from 200 to 650 mm. Each data point is an average of 10 or more measurements. n.s.= no statistically significant difference. Values were compared using an unpaired two-tailed Student's t-test $p<0.05$

grow slower than wild type. To obtain quantitative data, the height of ovules was measured during meiosis of the megaspore mother cell (MMC) when callose is deposited into the cell wall between megaspores. Callose was stained with fluorescent dye aniline blue. We observed that *epfl1 epfl2* ovules were approximately 1.6 times shorter compared to wild type during megasporogenesis (Fig. 1.8A and B). This change in shape was mostly due to the extremely short funiculus in the mutant. The *epfl1* single mutant formed ovules of a regular size while *epfl2* formed ovules shorter than the wild type but longer compared to *epfl1 epfl2*. These results suggest that EPFL1 and EPFL2 regulate ovule growth synergistically, with EPFL2 playing a more prominent role.

To quantify changes in ovule growth at an earlier stage, confocal cross sections of wild-type and *epfl1 epfl2* ovules were obtained at stage 2-I when a characteristic enlarged MMC forms (Fig. 1.8C). Already at this stage, *epfl1 epfl2* ovules were approximately 1.5 times shorter compared to wild type (Fig. 1.8D). We quantified number and length of L1 cells using 2-D images of ovules. There was no statistically significant difference in the cell length but the number of cells was reduced approximately 1.4 times in *epfl1 epfl2* (Fig. 1.8D). In the wild type, the transcription factor WUSCHEL (WUS) is expressed in the L1 layer at the top of the ovule starting from stage 1-II (Yu et al., 2020; Vijayan et al., 2021). Analysis of *proWUS:H2B-GFP* expression shows that *epfl1 epfl2* ovules are smaller than wild type at stage 1-II when *WUS* expression consistently appears. (Fig 1.8E, the third row from the top). At stage 2-I, *proWUS:H2B-GFP* demarcates the nucellus. Comparison of the wild type and *epfl1 epfl2* ovules at this stage suggests that while nucellus is developing in the mutant, the funiculus is severely reduced (Fig 1.8E, the fourth row from the top).

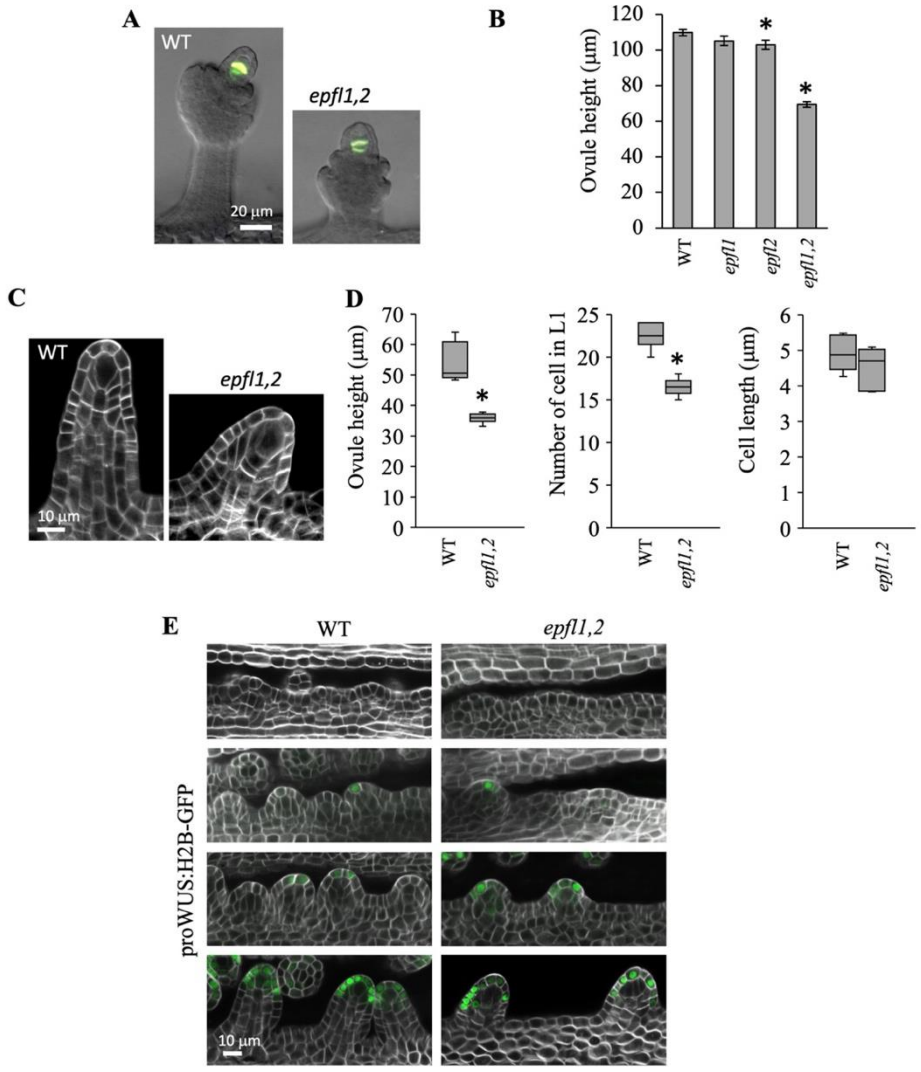

Figure 1.8. EPFL1 and EPFL2 promote early ovule growth

A. Epifluorescence and DIC overlay images of aniline blue stained ovules undergoing meiosis. B The mean height of ovules undergoing meiosis. n=10. Error bars=SE C. Representative confocal images of stage 2-I ovules with a characteristic enlarged megaspore mother cell. The cell walls were stained with SR2200. D. Ovule height (n=6), the number of L1 cells (n=6), and the length of L1 cells (15-24 cells/ovule in 6 ovules) were measured using cross-sections of six stage 2-I ovules. Data is represented using box–whisker plots: the whiskers represent maximum and minimum values, and the boxes represent the upper quartile, exclusive median, and lower quartile. B and D. Values that are significantly different from wt based on an unpaired two-tailed Student's t-test ($P<0.01$) are indicated by asterisks. E. Representative confocal images of *proWUS:H2B-GFP* expression in ovules from stages 9a to 10. The cell walls were stained with SR2200. All images are under the same magnification in individual panels A, C, and E.

Overall, these results indicate that EPFL1 and EPFL2 regulate ovule outgrowth by promoting cell proliferation and they are critical for funiculus elongation.

EPFL1 and *EPFL2* show cell-type specific expression during ovule initiation

To understand the role of ERf/EPFL signaling during ovule development, we asked which cells produce the EPFL ligands to induce signaling. We observed that *EPFL1* is expressed broadly in the placenta before ovule initiation (Fig. 1.9A) but with the onset of initiation, it is repressed in the subepidermal cell layer (Fig. 1.9B). Later, *EPFL1* expression is reduced at tip of the ovule and in the boundaries (Fig. 1.9C and E). During integument initiation, *EPFL1* expression gets further restricted to the basal side of the ovule (Fig. 1.9D). Previously, *EPFL2* expression was detected in the boundaries after ovules have initiated (Kawamoto et al., 2020). Our analysis indicted that *EPFL2* is very weakly expressed throughout the placenta before ovule initiation (Fig. 1.9F). During initiation, EPFL2 is upregulated, and its expression is restricted to boundaries between initiating ovules (Fig. 1.9G) and the base of ovules (Fig. 1.9H). *EPFL2* expression does not surround ovule at its base as *EPFL1* does but appears higher on the apical side of each ovule (Fig. 1.9I and J). In summary, our data suggest that *EPFL1* and *EPFL2* have unique expression patterns but their expression overlaps at the base of the forming ovules where they promote cell proliferation.

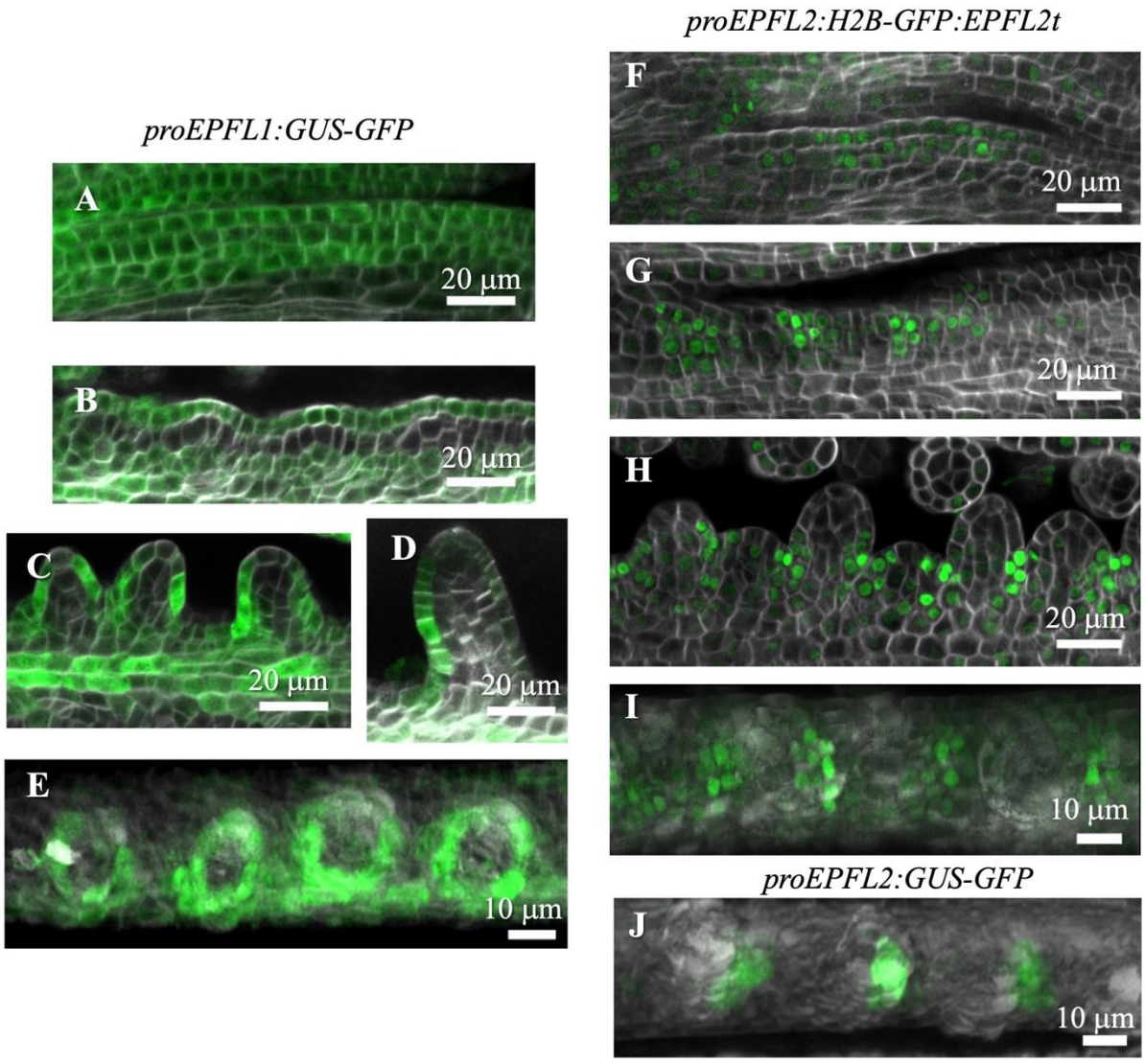

Figure 1.9. Expression patterns of *EPFL1* and *EPFL2* during early ovule development

Confocal images of the placenta at different stages of development in plants transformed with either *proEPFL1:GUS-GFP, proEPFL2:H2B-GFP: EPFL2term* or *proEPFL2:GUS-GFP* (green). The cell walls were stained with SR2200 (white). A-D and F-H. Cross sections of *EPFL1* and *EPFL2* expression in ovules of different stages viewed from the side. E, I and J. Confocal z-projections were used to show the expression of *EPFL1* and *EPFL2* in ovules from the top view.

All three ER family receptors promote ovule initiation

Previous research exploring the role of ERf receptors in regulation of seed density studied siliques at maturity (Kawamoto et al., 2020). Seed density at maturity depends on spacing of ovules during initiation and the subsequent elongation of the carpel valves. To gain deeper insight into the role of receptors in ovule initiation, we analyzed flowers at stage 10, shortly after ovules are initiated. Measurements of ovule number and placenta length in *er* flowers showed a slight reduction in placenta length but no changes in ovule density (Fig. 1.10A and B). Out of double *erf* mutants only *erl1 erl2* had a small but statistically significant decrease in ovule density (Fig. 1.10A and B). When all three receptors are disrupted the ovule density is reduced to the *epfl1 epfl2* levels (Fig. 1.10A and B). This analysis suggested that all three receptors promote ovule initiation, with ERL1 and ERL2 playing slightly more prominent roles. ER is more important for the control of the placenta elongation, but again all three receptors control this process (Fig. 1.10A and B and Fig. 1.5).

Previously, it was shown that *ER* and *ERL2* are expressed broadly in the placenta (Kawamoto et al., 2020). *ERL1* appeared only after ovules were formed which is inconsistent with our observation that it plays a significant role in ovule initiation. Expression of *ERL1* and *ERL2* is downregulated by active ERf signaling (Pillitteri et al., 2007). For another project, we created transgenic lines expressing *proERL1:H2B-GFP* and *proERL2:H2B-GFP* in the *Landsberg* erecta ecotype. This ecotype contains a knockout mutation in ER; thus, we used these lines to test the expression of *ERL1* and *ERL2* in the absence of ER. This experiment confirmed that *ERL2* is expressed weakly and broadly

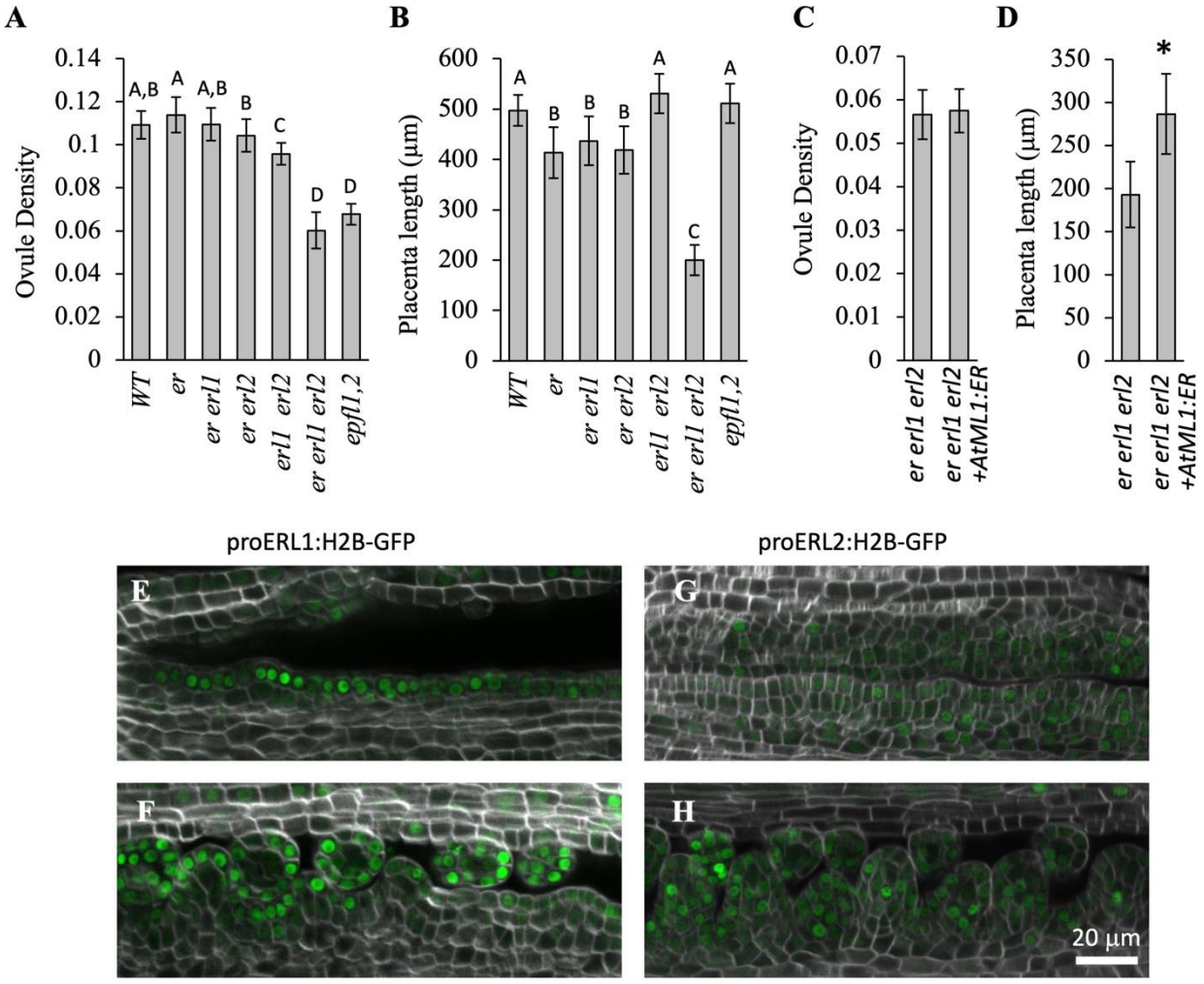

Figure 1.10. ERf receptors redundantly regulate ovule initiation

A-D. Mean ovule density and placenta length in stage 10 gynoecia of indicated genotypes. N=20 A one-way ANOVA using Tukey's test with multiple comparisons was used to determine significance with a P-value < 0.01. E-H Representative confocal images of the placenta in *Landsberg erecta* plants transformed with either *proERL1:H2B-GFP* or *proERL2:H2B-GFP* (green). The cell walls were stained with SR2200 (white). All images are under the same magnification.

through the placenta (Fig. 1.10G and H). It also detected expression of *ERL1* in the L1 layer of the placenta during ovule initiation supporting the role of ERL1 in that process (Fig.2.7E and F). Because the *er erl2* mutant initiates ovule as efficiently as the wild type, we hypothesized that the expression of receptors in the L1 layer might be sufficient for ovule initiation. To test this hypothesis, we analyzed ovule initiation in *er erl1 erl2* plants that express ER under the epidermis-specific AtML1 promoter (Sessions et al., 1999; Uchida et al., 2012). We observed that expression of ER in the epidermis can partially rescue the placenta elongation, but it has no effect on ovule density (Fig. 1.10C and D), which suggests that broader expression of ERf receptors is necessary to promote ovule initiation. It is possible that in the *er erl2* mutant *ERL1* is expressed outside of epidermis. Alternatively, the *ERL1* promoter that we used in this study is missing cis-elements that are necessary for broader expression. Another possibility is that a very small amount of ERL1 receptors in the internal layers, which we cannot detect by microscopy, is sufficient for the regulation of ovule initiation.

Decreased ovule initiation in *epfl1 epfl2* is not likely due to altered responses to auxin, cytokinin, or gibberellin

Multiple plant hormones have been implicated in the regulation of ovule number. Auxin is essential for ovule initiation, with auxin maxima being established at the tip of the ovule early in its formation (Galbiati et al., 2013). The inability to transport auxin or sense it leads to a dramatic reduction in ovule number (Benkova et al., 2003; Bencivenga et al., 2012; Cucinotta et al., 2021). In Arabidopsis, cytokinins and brassinosteroids

increase ovule number while gibberellins decrease it (Barro-Trastoy et al., 2020; Cucinotta et al., 2016; Gomez et al., 2018; Yu et al., 2020). To understand the cause of low ovule number in the *epfl1 epfl2* mutant, we tested whether its hormone metabolism is altered. Analysis of *pDR5rev::GFP* expression suggested that auxin is present in ovules starting from flower stage 9c, ovule stage 1-II (Galbiati et al., 2013). Here, we used a more sensitive auxin reporter proDR5v2:ntdTomato that has a $(TGTCGG)_9$ binding site with a higher affinity for ARFs compared to $(TGTCTC)_9$ binding site in the DR5rev (Liao et al., 2015). Analysis of proDR5v2:ntdTomato expression indicated that discrete auxin maxima appear in the epidermis during stage 9a when ovules are barely noticeable (Fig. 1.11A, the second row). The auxin maxima first appear at the basal end of the placenta, consistent with the primacy of ovule initiation at that end. In the wild type, auxin accumulates in 2-3 cells at the tip of the ovule. The *epfl1 epfl2* mutant is also able to accumulate auxin on top of the ovule but the peaks are broader (Fig. 1.11A, compare the bottom row of the wild type and the mutant). This result is consistent with our previous work that demonstrated a negative effect of ERf signaling on auxin signaling in the L1 layer of the SAM (Chen et al., 2013; DeGennaro et al., 2022). Next, we used the *proRPS5A:DII-n3Venus/proRPS5A:mDII-ntdTomato* reporter known as R2D2 that is independent of signaling downstream of the auxin receptors. Because auxin directly causes the auxin dependent proteolytic turnover of any protein harboring the DII degron sequence, this reporter indicates auxin accumulation through an absence of n3Venus fluorescence (Liao et al., 2015). Cells in which the reporter is expressed are marked by red ntdTomato fluorescence expressed from the RPS5A

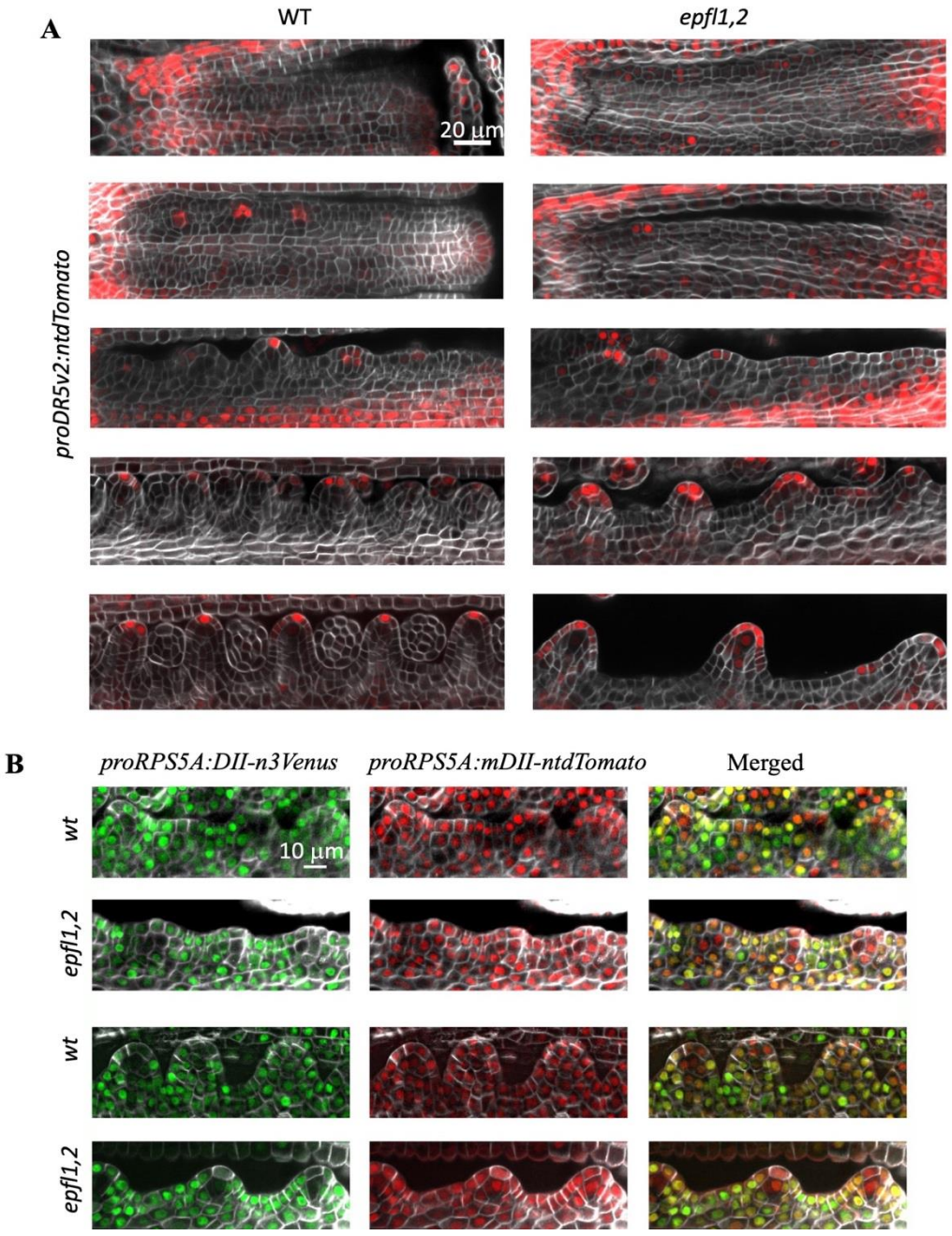

Figure 1.11. Auxin is able to accumulate into maxima during ovule initiation in the *epfl1 epfl2* mutant

Representative confocal images of the placenta at stages 8, 9a, 9b, 9c and 10 of flower development in plants transformed with (A) *proDR5v2:ntdTomato* (red) or stages 9b and 10 of flower development in plants transformed with (B) *proRPS5A:DII-n3Venus* (green)/*proRPS5A:mDII-ntdTomato* (red) . The cell walls were stained with SR2200 (white). All images in a panel are under the same magnification.

(Fig. 1.11B) (Liao et al., 2015). This experiment confirmed that auxin forms a peak at the top of an ovule in both the wild type and the *epfl1 epfl2* mutant (Fig. 1.11B).

PIN1 is an auxin efflux carrier that is important for formation of auxin maxima in ovules (Benkova et al., 2003; Bencivenga et al., 2012). As described previously, it is expressed in the placenta epidermis before ovule initiation (Galbiati et al., 2013). During ovule initiation, its expression in the epidermis is upregulated at the center of the ovule and decreased in the boundaries (Fig. 1.12A). PIN1 expression is absent in the subepidermal layer of the placenta and present in the deeper layers (Fig. 1.12B). Over time, PIN1 expression in the deeper layers is restricted to the forming vasculature (Fig. 1.12C). PIN1 is polarly localized in the plasma membrane to enable auxin transport to the ovule tip (Fig. 1.12D). A comparison of PIN1 expression in the wild type and the *epfl1 epfl2* mutant did not identify any differences in its pattern of expression or polar localization (Fig. 1.12).

Previously, a treatment of *er erl1 erl2* seedlings with N-1-naphthylphthalamic acid (NPA), an inhibitor of polar auxin transport, or with synthetic auxin 2,4-Dichlorophenoxyacetic acid (2,4D) partially rescued leaf initiation because, in both cases, it increased accumulation of auxin in the L1 layer (DeGennaro et al., 2022). Here, a treatment of flowers with NPA reduced ovule initiation in both the wild type and the *epfl1 epfl2* mutant (Fig. 1.13A), while 2,4 D did not alter ovule initiation in either genotype (Fig. 1.13B). This result highlights differences in auxin homeostasis between the shoot apical meristem and the placenta, but most importantly it indicates the similarity of auxin responses in the wild type and the *epfl1 epfl2* mutant. In the presence of high auxin concentrations, AUX//IAA proteins are degraded which relieves repression of transcription

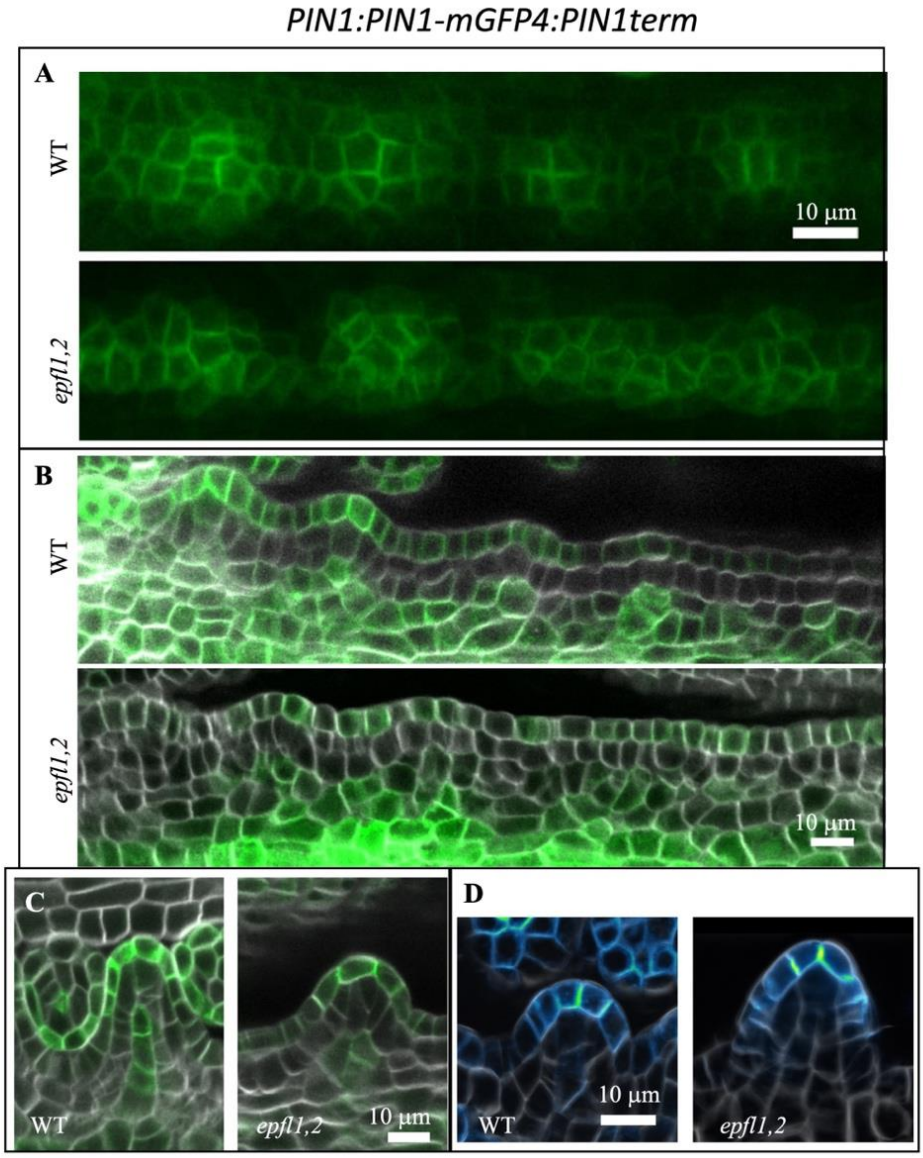

Figure 1.12. The efflux transporter of auxin PIN1 is expressed similarly in the wild type and *epfl1 epfl2* mutant

Representative confocal images of *PIN1:PIN1-mGFP4:PIN1term* expression (green in A, B and C, "Green Fire Blue" Look Up Table (LUT) from FIJI. In D). The cell walls were stained with SR2200 (white). All images in a panel are under the same magnification. A. The top view of the placenta at stage 9a. B. The side view of the placenta at stage 9a. C and D The side view of ovules at stages 1-I. In C, PIN1 is visible not only in the epidermis but also in forming vasculature. In D polar PIN1 localization is visible at the tip of forming

factors such as MP. Previous research showed that *pMP:MP-GFP* is expressed throughout the placenta before ovule initiation (Galbiati et al., 2013). After ovules initiate, MP expression is suppressed at the tip of the ovule and expressed mostly in the boundaries (Galbiati et al., 2013). Our analysis of *proARF5:SV40-3xeGFP* expression indicated that starting from early stage 9a MP is being restricted to boundaries of ovules and is expressed similarly in the wild type and the *epfl1 epfl2* mutant (Fig. 1.14). Altogether, this data points towards similar auxin distribution and responses during ovule initiation in the wild type and the *epfl1 epfl2* mutant.

As previously shown, the exogenous application of the synthetic cytokinin 6-benzylaminopurine (BAP) led to increased gynoecium size and ovule number in wild-type plants (Galbiati et al., 2013; Cucinotta et al., 2014). Treatment of both wild type and *epfl1 epfl2* mutants with 1 mM BAP led to a significant increase in ovule number and placenta length without significant changes in ovule density (Fig. 1.15A). This suggests that cytokinin promotes proliferation of the placenta tissue which allows for the initiation of more ovules, while cytokinin may not play as strong of a role in regulating the spacing of ovule primordia along the length of the placenta. The *epfl1 epfl2* mutant is still responsive to cytokinin in a similar manner to wild type, and the ovule density phenotype of the *epfl1 epfl2* mutant is not restored after BAP treatment (Fig. 1.15A). This suggests that the *epfl1 epfl2* mutant does not have an impaired ability to respond to cytokinin during ovule initiation.

In contrast, gibberellins (GA) are phytohormones known to inhibit ovule number and ovule density (Gomez et al., 2018; Barro-Trastoy et al., 2020). As expected, the

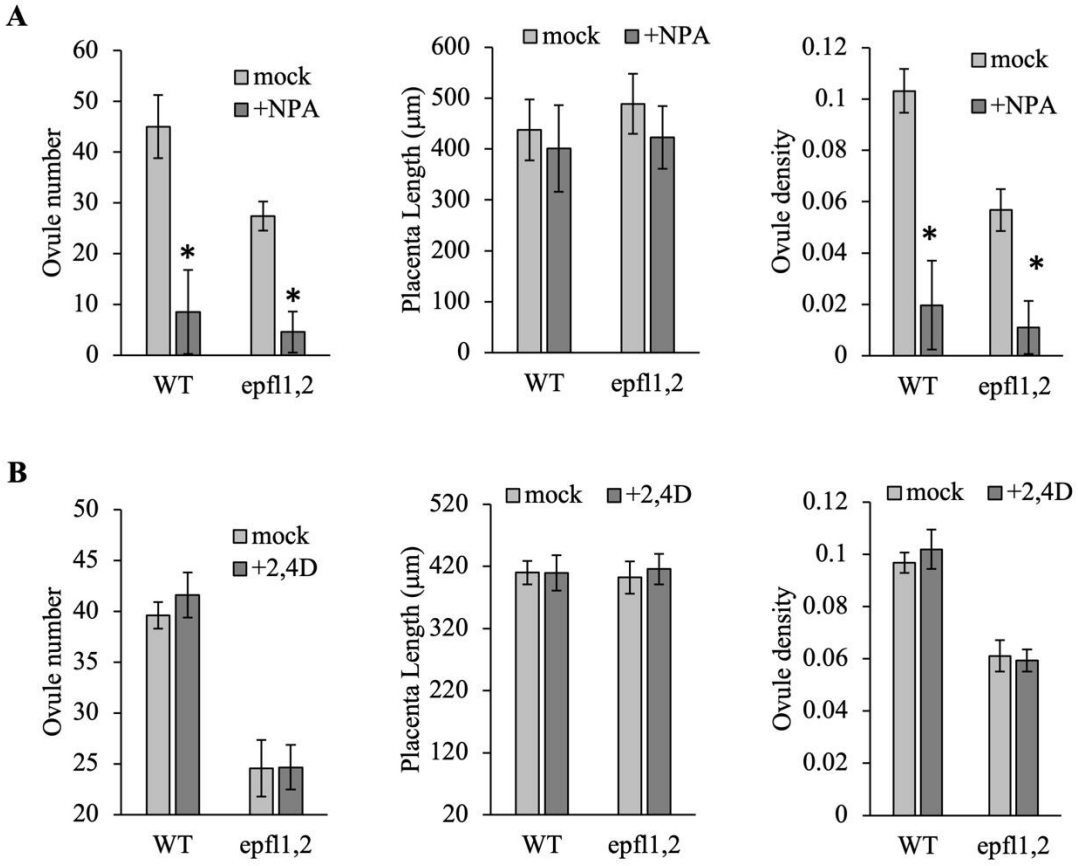

Figure 1.13. Inhibition of auxin transport severely reduces ovule density, while exogenous auxin does not affect either placenta length or ovule initiation

Ovule number, placenta length, and ovule density of the stage 10 gynoecia in the wild type and *epfl1 epfl2* mutant. Inflorescence clusters were treated with (A) 10 mM N-1-naphthylphthalamic acid (NPA) or (B) 50 mM 2,4-Dichlorophenoxyacetic acid (2,4-D). Data are mean ± S.D. n=20. Values that are significantly different from the wild type based on an unpaired two-tailed Student's t-test ($P<0.01$) are indicated by asterisks.

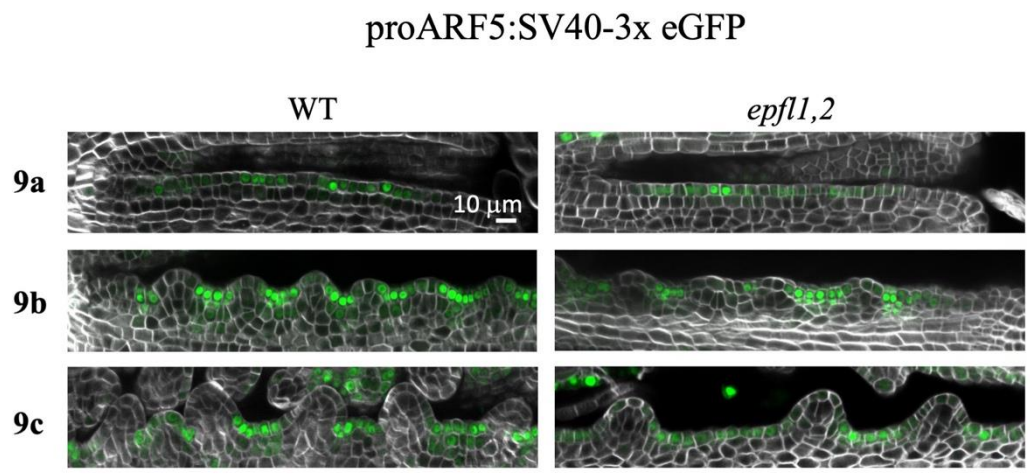

Figure 1.14. Expression of MP/ARF5 in wild type and *epfl1 epfl2*

Representative confocal images of the wild type and *epfl1 epfl2* placenta at different stages of development in plants transformed with proARF5:SV40-3x eGFP (green). The cell walls were stained with SR2200 (white). All images in a panel are under the same magnification.

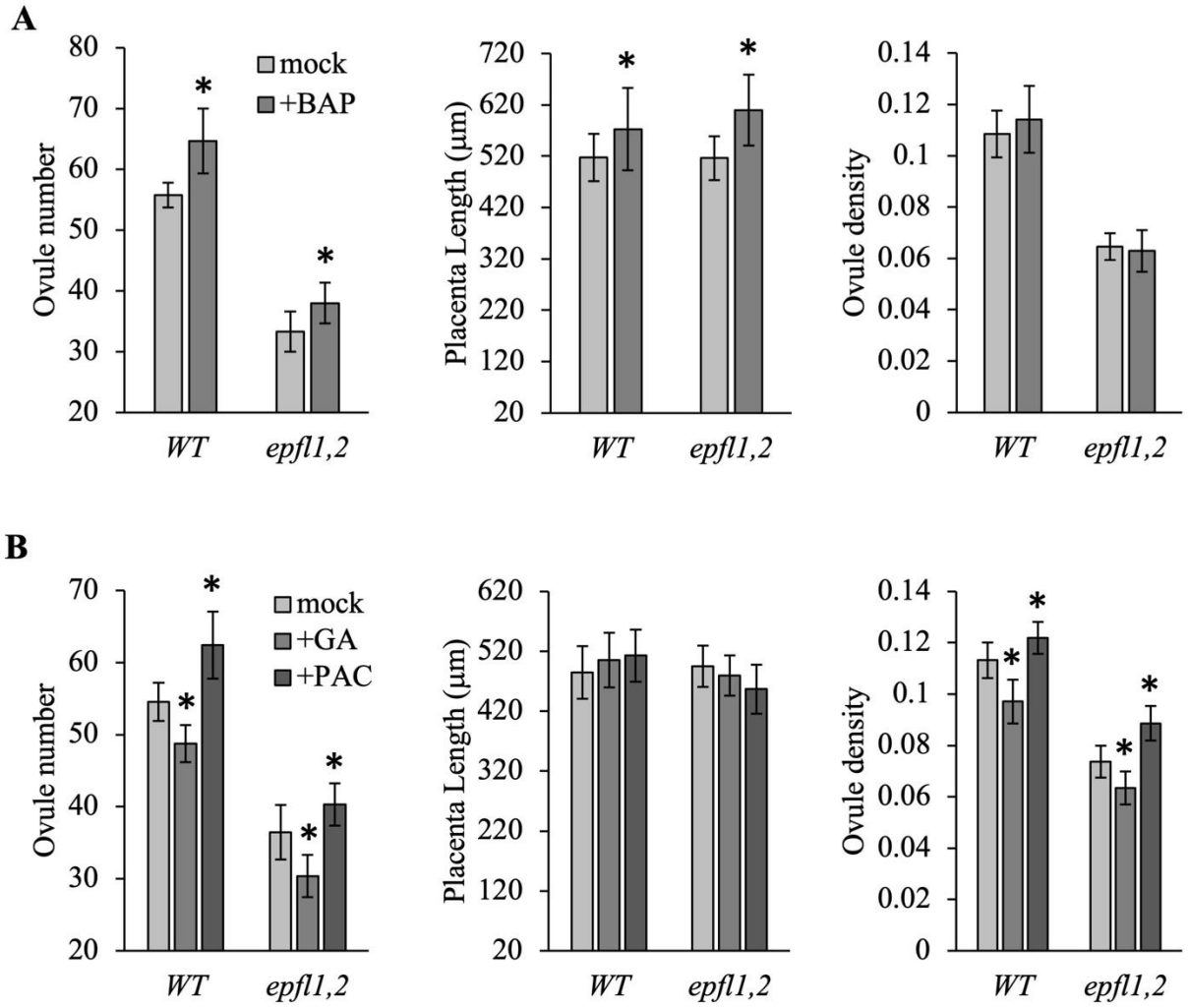

Figure 1.15. Exogenous cytokinins promote placenta elongation while exogenous gibberellins inhibit ovule density

Ovule number, placenta length, and ovule density of the stage 10 gynoecia in the wild type and *epfl1 epfl2* mutant. Inflorescence clusters were treated with (A) 1mM 6-benzylaminopurine (BAP), (B) 25 mM gibberellic acid (GA) or 4 mM paclobutrazol (PAC). Data are mean ± S.D. n=20. Values that are significantly different from the wild type based on an unpaired two-tailed Student's t-test ($P<0.01$) are indicated by asterisks.

application of GA to wild-type inflorescences caused a decrease in ovule number and ovule density without significantly affecting placenta length, while the application of a gibberellin biosynthesis inhibitor paclobutrazol (PAC) caused increased ovule number and density without significantly affecting placenta length (Fig. 1.15B). The *epfl1 epfl2* mutant showed a similar response to both GA and PAC when compared to wild-type plants (Fig. 1.15B), and this suggests that the altered ovule number and density of the *epfl1 epfl2* mutant is not caused by altered GA signaling or biosynthesis. In conclusion, *epfl1 epfl2* mutants do not show obvious defects in cytokinin or GA related pathways during ovule initiation.

The transcription factor BZR1 has been shown to play a role in regulating ovule number and placenta length, and this transcription factor functions as a positive effector of brassinosteroid (BR) signaling (Wang et al., 2002). The *bzr1-1D* mutant protein is resistant to degradation in the absence of BR signaling, and this leads to hyperactivity of the BZR1 transcription factor (Wang et al., 2002; Huang et al., 2013; Yu et al., 2020). In wild type plants, the *bzr1-1D* mutation leads to increased placenta length, ovule number, and ovule density (Fig. 1.16A-D). This suggests that BZR1 can promote both placenta elongation and ovule initiation. In contrast, the introduction of the *bzr1-1D* mutation into the *epfl1 epfl2* mutant background leads to severe decrease in ovule number and density, despite an increase in placenta length (Fig. 1.16A-D). Ultimately, these results suggest that BZR1 functions to promote ovule initiation in wild type plants, but increased BZR1 activity has a significant negative impact on ovule density of the *epfl1 epfl2* mutant.

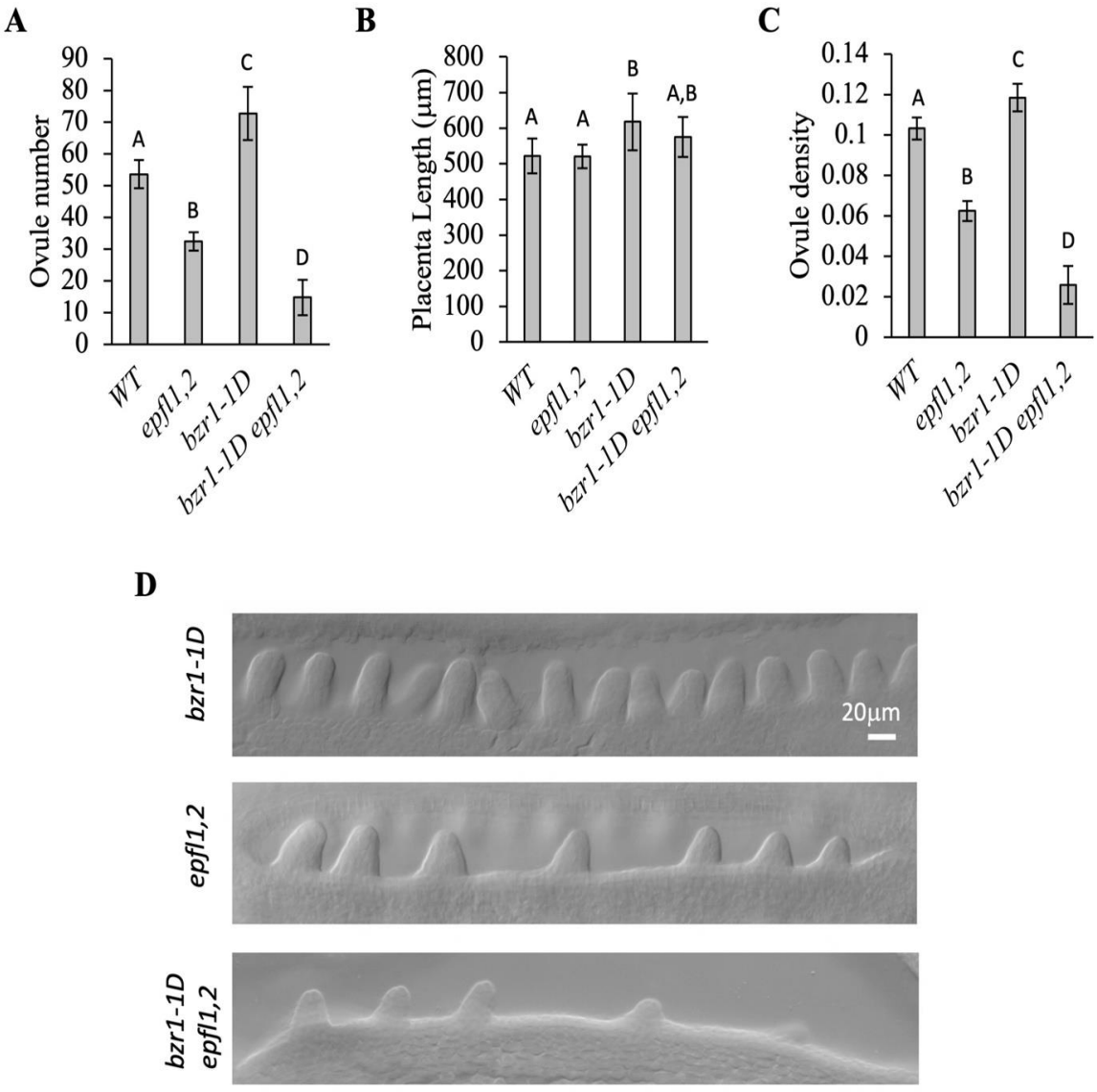

Figure 1.16. The *bzr1-1D* mutation inhibits ovule initiation in the *epfl1 epfl2* background

A-C. Mean ovule number, placenta length, and ovule density in stage 10 gynoecia of indicated genotypes. N=20 A one-way ANOVA using Tukey's test with multiple comparisons was used to determine significance with a P-value < 0.01. D. DIC images of stage 10 gynoecia demonstrate differences in ovule initiation in indicated genotypes. All images are under the same magnification.

Synergistic regulation of ovule initiation by *CUC2, CUC3, EPFL1,* and *EPFL2*

CUP-SHAPED COTYLEDON (CUC) transcription factors regulate ovule spacing (Galbiati et al., 2013; Goncalves et al., 2015). We examined genetic interactions between *EPFL1, EPFL2, CUC2,* and *CUC3 b*ecause these two CUC proteins are expressed in the boundaries of initiating ovules in a pattern similar to *EPFL2* (Goncalves et al., 2015). Relative to the wild type, the ovule density is not changed in single *cuc2* or *cuc3* mutants and is only slightly increased in the *cuc2 cuc3* double mutant (Fig. 1.17). As described previously (Goncalves et al., 2015) we observed irregular ovule spacing and ovule fusions in *cuc2 cuc3*. The addition of *cuc2* mutation to *epfl1 epfl2* or to *epfl1 epfl2 cuc3* did not alter ovule density of those mutants (Fig. 1.17A). While the addition of *cuc3* to *epfl2* did not change ovule density, the *cuc3 epfl1 epfl2* mutant had a significantly reduced ovule density relative to *epfl1 epfl2* (Fig. 1.17A and B), indicating a synergistic interaction between *CUC3*,*EPFL1* and *EPFL2* and the importance of *CUC3* for ovule initiation. While ovule density of the *epfl1 epfl2 cuc2 cuc3* mutant was not statically different compared to *epfl1 epfl2 cuc3*, the ovules looked dramatically different. Individual ovules became more recognizable during later stages of development, and the phenotype was variable (Fig. 1.17B and C). In addition, they are very broad and short without a clearly defined funiculus (Fig. 1.17D). This indicates that EPFL1, EPFL2 CUC2, and CUC3 synergistically regulate morphology of ovules. All four genes are especially important for elongation of funiculus. This data suggests that *EPFL1, EPFL2, CUC2, and CUC3* have both unique and common downstream targets during ovule initiation.

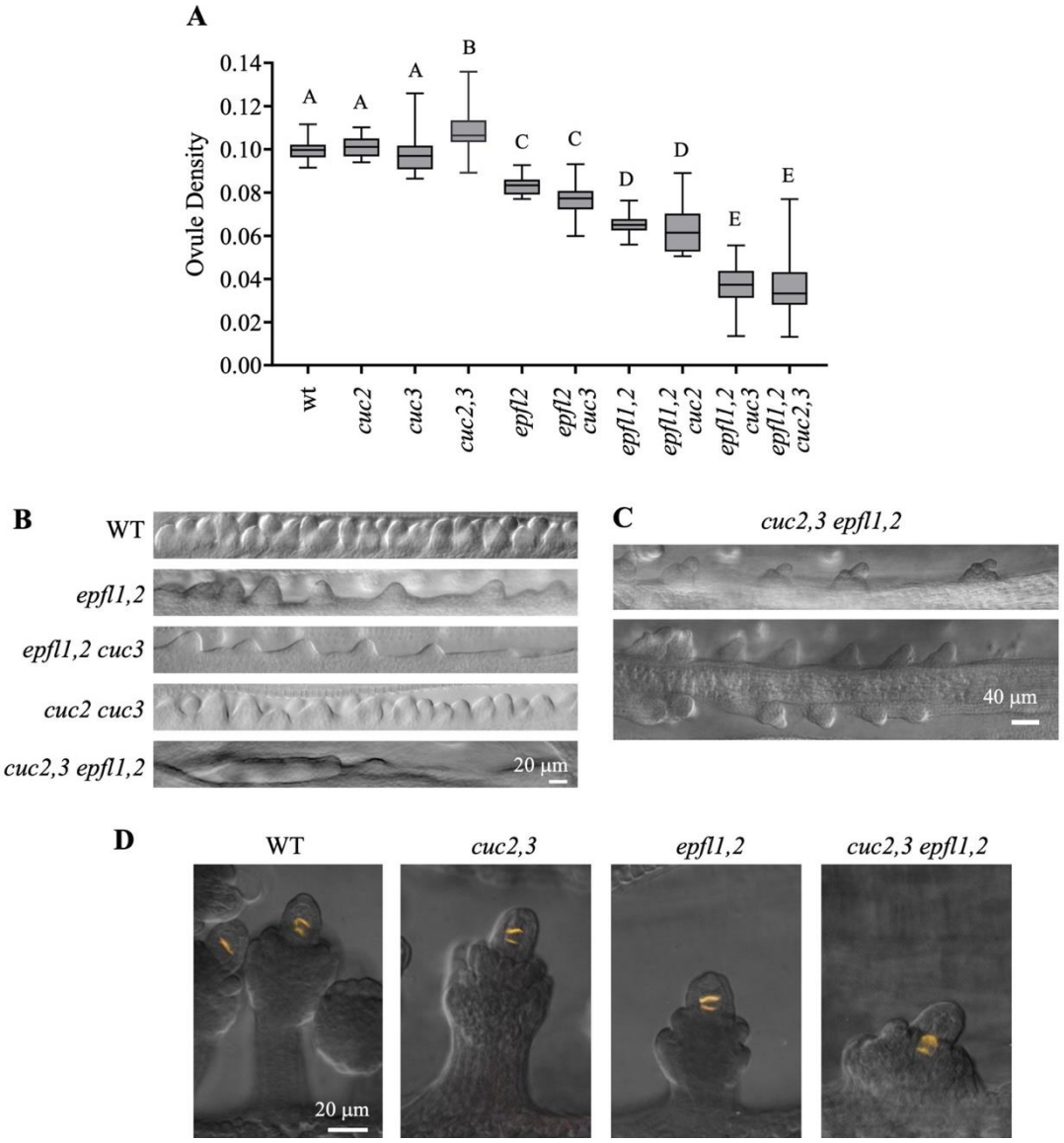

Figure 1.17. EPFL1 EPFL2 and CUC2,3 regulate ovule initiation and growth synergistically

A. Ovule density measurements of the wild type and indicated mutants. N=10 Data is represented using box–whisker plots: the whiskers represent maximum and minimum values, and the boxes represent the upper quartile, exclusive median, and lower quartile. A one-way ANOVA using Tukey's test with multiple comparisons was used to determine significance with a P-value < 0.01. B. DIC images of stage 10 gynoecia demonstrate differences in ovule initiation in indicated genotypes. C. DIC images of stage 11 gynoecia indicate that ovules can sometimes initiate in the *cuc2,3 epfl1 epfl2* mutant over time. D. Epifluorescence and DIC overlay images of aniline blue stained ovules undergoing meiosis demonstrate altered morphology of ovules in indicated mutants. B-D Images in the same panel are under the same magnification.

CUC2 and *EPFL2* are expressed between ovules and at the base of ovules (Fig. 1.18A and B). They are excluded from the forming nucellus. While it has been reported previously that CUC2 inhibits *EPFL2* expression (Li et al., 2020b), we did not observe significant changes in the expression of *EPFL2* in *cuc2 cuc3* mutant (Fig. 1.18A). However, we cannot exclude a possibility that all three *CUC* genes regulate *EPFL2* expression and the presence of CUC1 is sufficient to control *EPFL2* expression. We did not detect changes in *CUC2* expression in the *epfl1 epfl2* mutant (Fig. 1.18B). *CUC3* was expressed more broadly in the *epfl1 epfl2* mutant which is partly due to more broad boundaries between ovules in the mutant and partly due to slower inhibition of its expression in initiating ovule (Fig, 1.20A through D).

DORNROSCHEN (DRN) is a transcription factor known to be expressed in shoot meristems as well as the apex of cotyledon and ovule primordia (Chandler et al., 2008; Kawamoto et al., 2020). During ovule initiation, DRN is expressed in placenta tissues during early gynoecium formation and is later restricted to the apex of forming ovule primordia (Kirch et al., 2003; Kawamoto et al., 2020). Previous research identified altered patterning of DRN expression along the placenta of the *epfl2* single mutant during ovule initiation, where the number of L1 cells between each DRN maxima became more variable in the mutant relative to the wild type (Kawamoto et al., 2020). To investigate DRN expression in the *epfl1 epfl2* mutant, *proDRN:H2B-GFP:DRNterm* was transformed into both the wild type and the *epfl1 epfl2* mutant. In the wild type, *DRN* expression is concentrated into peaks along the placenta during early stage 9a with repression in boundary regions even before ovule primordia protrude from the placenta. (Fig. 1.19).

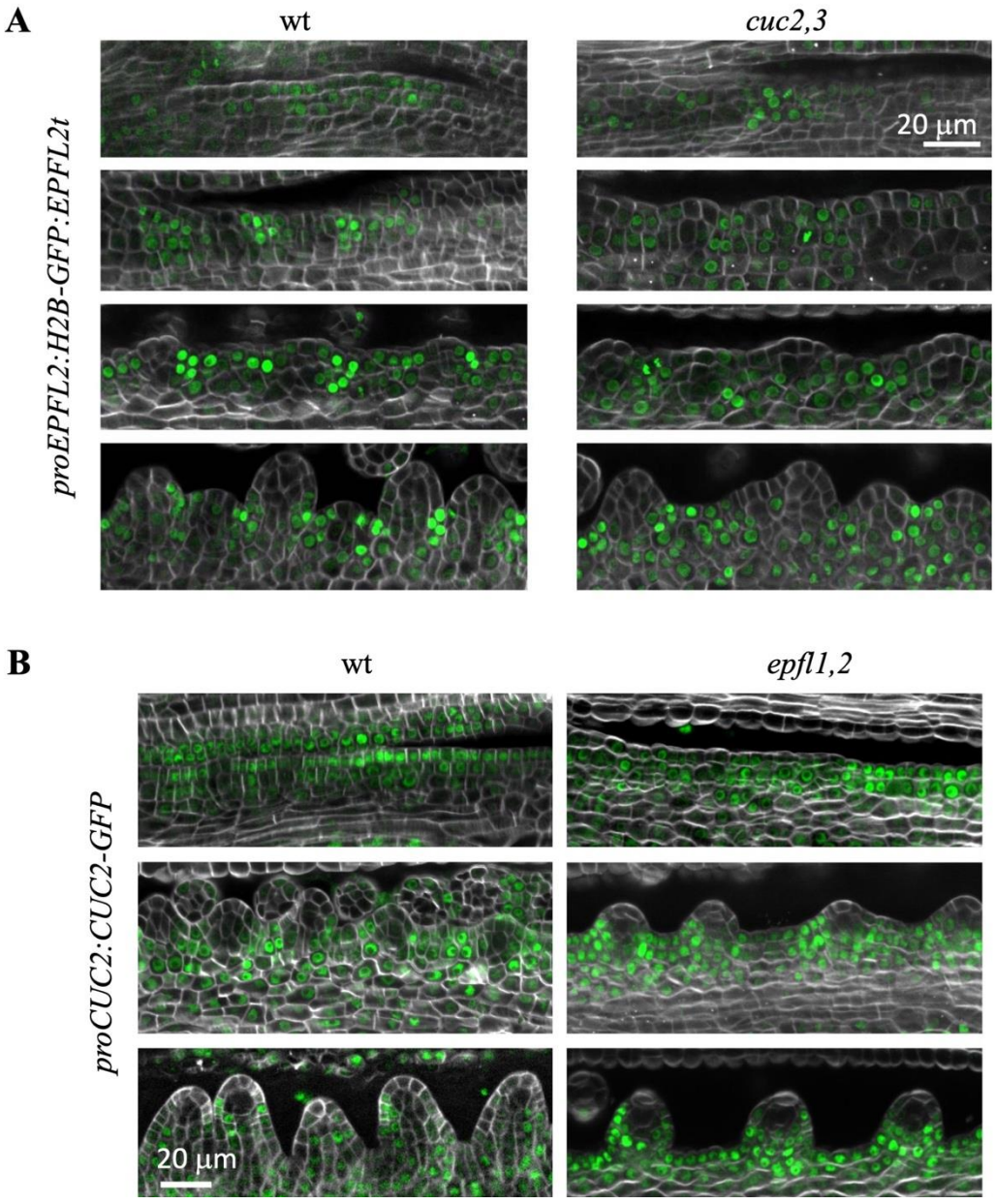

Figure 1.18. Expression of EPFL2 and CUC2 is not altered in *cuc2 cuc3* and *epfl1 epfl2* mutants, respectively

Representative confocal images of the placenta at different stages of development in plants transformed with *proEPFL2:H2B-GFP:EPFL2term* (A) or proCUC2:CUC2-GFP (B) (green). The cell walls were stained with SR2200 (white). All images in a panel are under the same magnification.

While *DRN* is repressed in boundary cells, new *DRN* peaks form along the placenta as it elongates throughout stage 9 when sufficient space is available. Once ovule primordia are established, *DRN* expression remains concentrated in L1 of the apex of the ovule (Fig. 1.19). In the *epfl1 epfl2* mutant during early stages of ovule initiation, DRN expression is not efficiently concentrated into concise regions designating sites of ovule primordia initiation, and expression is instead broadly distributed along L1 of the placenta (Fig. 1.19). Expression of DRN in the *epfl1 epfl2* mutant remains more broadly distributed than in the wild type until after ovules have fully initiated at stage 10 of flower development (Fig. 1.19).

Co-expression of *proDRN:er-mCherry:DRNterm* along with the boundary specific *proCUC3:er-CFP* reporter demonstrates that *DRN* expression is efficiently repressed in boundary cells of wild type during ovule initiation (Fig. 1.20). On the other hand, separation of *DRN* and *CUC3* expression during early stages of ovule initiation is less distinct in the *epfl1 epfl2* mutant (Figure 1.20). Overall, this indicates that EPFL1/2 may play a role in the patterning of ovule founder cells and boundary cells along the placenta.

Discussion

The placenta of Arabidopsis is tissue derived from the carpel margin meristem that is comprised of cells competent of producing ovule primordia. Ovule initiation is a process that involves coordinated differentiation and growth along the elongating placenta. While there are many mutations that lead to reduced ovule number, this is often accompanied by reduced placenta length and subsequent reduction in space for ovule initiation. *EPFL2* is

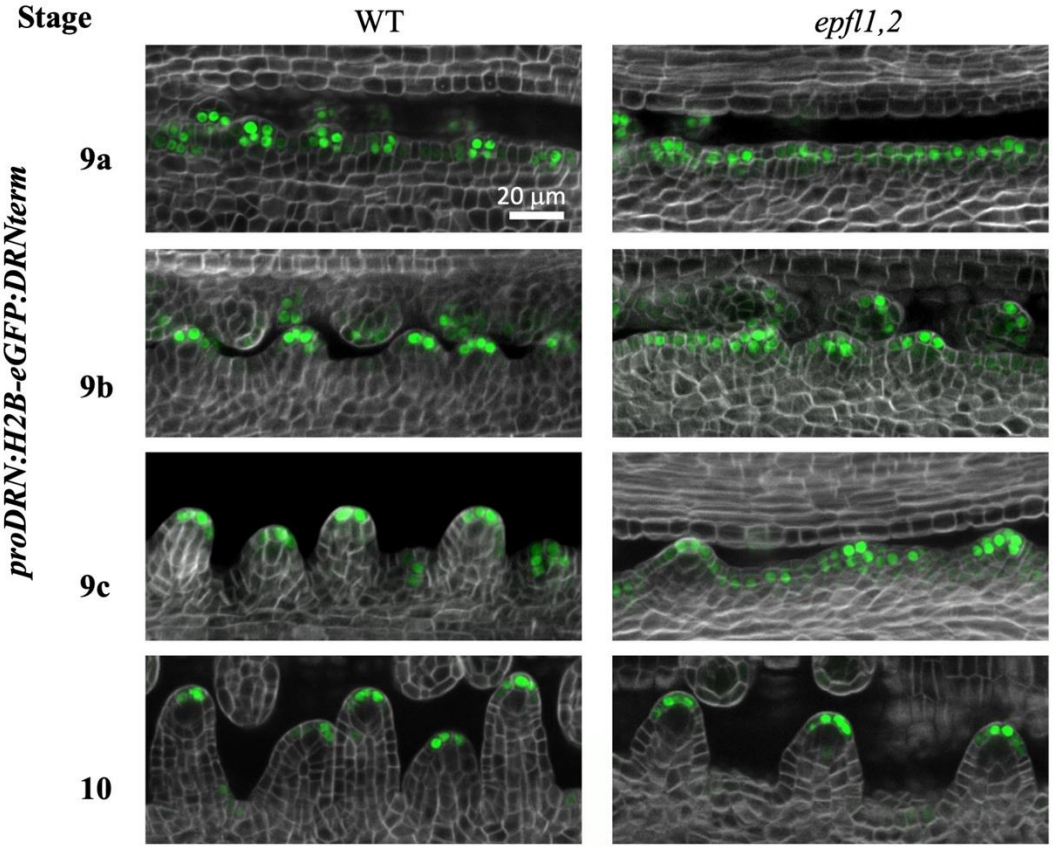

Figure 1.19. Expanded expression of *DRN* in *epfl1 epfl2* compared to the wild type.

Representative confocal microscopy images of proDRN:H2B-GFP:DRNterm (green) during ovule initiation in wild type and *epfl1 epfl2* mutants from stage 9a to stage 10. The cell walls were stained with SR2200 dye (white).

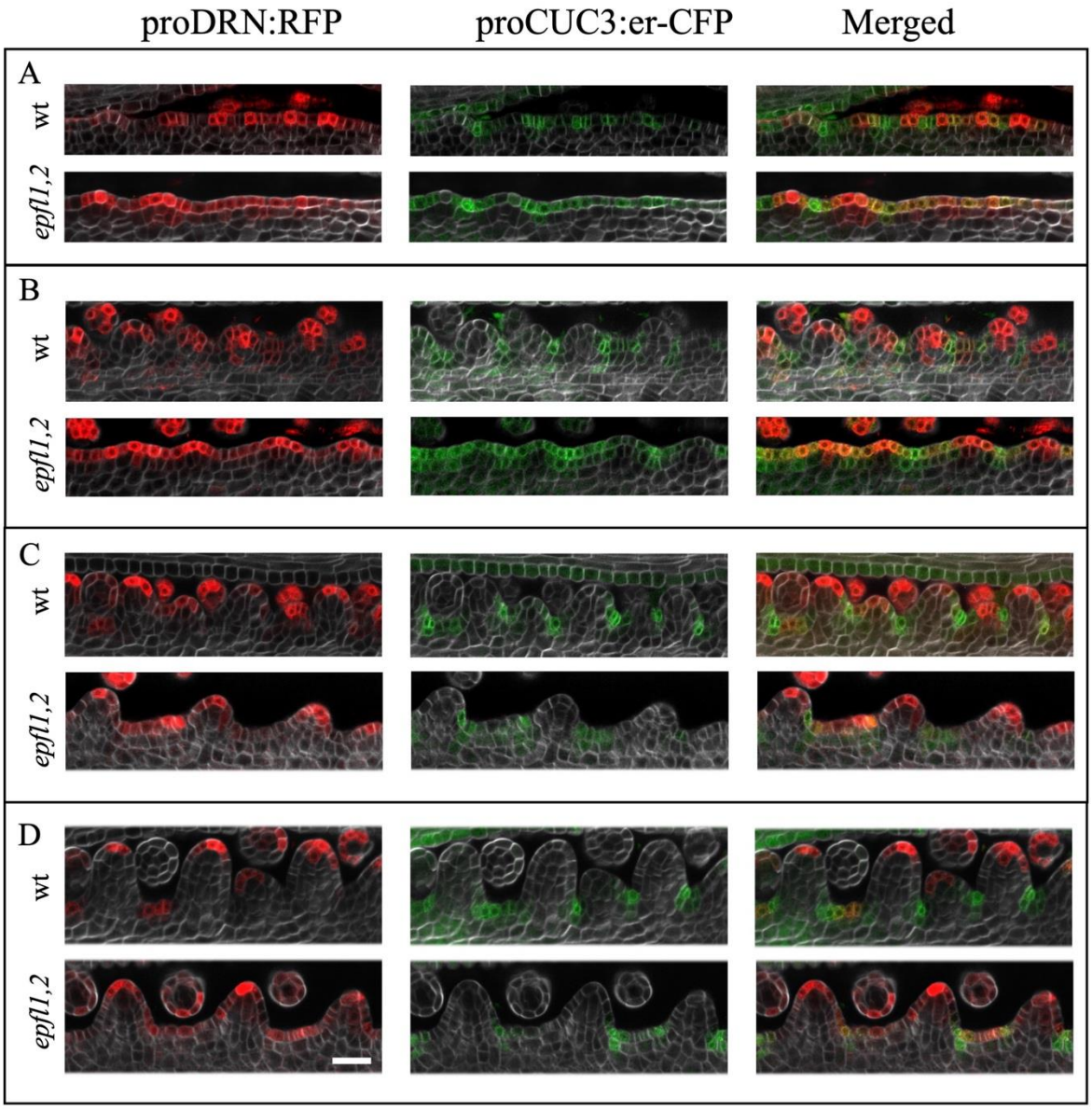

Figure 1.20. Expression of DRN and CUC3 in wild type and *epfl1 epfl2* mutants

Representative confocal images of the wild type and *epfl1 epfl2* placenta at different stages of development in plants co-transformed with proDRN:RFP (red) and proCUC3:er-CFP (green). The cell walls were stained with SR2200 (white). All images in this figure are under the same magnification and the scale bar is 20 microns.

expressed in the boundaries between ovule primordia during initiation, and the *epfl2* mutants display reduced ovule density (Kawamoto et al., 2020). Further loss of the paralog *EPFL1* leads to a more significant reduction in ovule density. The decreased density of the *epfl1 epfl2* mutant is due to a reduced number of ovules and increased spacing among ovules with little change to placenta length. The *er erl1 erl2* triple mutant ovule density is comparable to that of the *epfl1 epfl2* mutant, while *erf* double mutants do not have as severe reductions in ovule density. This suggests that all three receptors play a role in regulating ovule density and that EPFL1 and EPFL2 are the main EPFL ligands regulating ovule density. The inability of the *epfl1 epfl2* mutant to maintain proper spacing and initiation of ovule primordia indicates that this signaling pathway may regulate early steps of cell differentiation and/or proliferation during organ primordia initiation.

The *epfl1 epfl2* mutant ovules are significantly shorter than wild-type ovules at any given stage. The *epfl1 epfl2* mutant ovules have reduced cell number in L1 with little change in average cell length, and the area of reduced proliferation occurs at the base of the ovule below the nucellus where *WUS* is expressed at stage 1-II of ovule development. These results suggest that the base of the ovule, or funiculus, fails to proliferate during early ovule development in the *epfl1 epfl2* mutant. In addition, the *cuc2 cuc3 epfl1 epfl2* mutant shows even further reduction in ovule outgrowth. *CUC2*, *CUC3*, *EPFL1* and *EPFL2* all show some expression at the base of ovule primordia where proliferation occurs. This data suggest that *CUC* genes also play a role in ovule primordia growth. The mechanisms underlying this reduced ovule primordia proliferation are unclear, although

some other ovule initiation regulators such as *ANT* are also known to promote cell proliferation and organ size (Mizukami and Fischer, 2000). The *epfl1 epfl2* mutant shows altered expression of genes such as *CUC3* and *DRN* during early ovule initiation and development, and it is possible that many other genes share these altered expression patterns. Some of these changes in gene expression patterns may influence the growth of ovule primordia in the *epfl1 epfl2* mutant, although further research is required to identify these genes and characterize their effect on ovule growth.

CUC genes are NAC domain transcription factors that have been shown to be expressed in boundary tissues of above ground organs (Hibara et al., 2006). These transcription factors have been well characterized to inhibit organ fusion, and they also regulate other processes such as leaf tooth outgrowth and axillary branching (Hibara et al., 2006; Hasson et al., 2011; Goncalves et al., 2015; Cucinotta et al., 2018). *CUC* genes show boundary expression during ovule initiation, and the expression of *CUC3* appears similar to the expression of *EPFL2* during this process (Fig. 2.5 and Fig. 2.16). In addition, certain *cuc* single and double mutants display ovule fusions, which are also occasionally seen in the *epfl2* mutant (Goncalves et al., 2015; Kawamoto et al., 2020). These observations prompted us to investigate the genetic interactions between *EPFL1, EPFL2* and *CUC* genes to determine whether these separate genes function in a linear pathway. Mutations in *cuc2*, *cuc3*, or *cuc2 cuc3* did not reduce ovule density in the wild type, while the *epfl1 epfl2* mutant shows significantly reduced ovule density. When the *cuc3* mutation is introduced to the *epfl1 epfl2* mutant, a strong synergistic reduction in ovule density occurs. The underlying mechanism of this synergistic interaction between CUC3 and EPFL1/2 requires

further investigation. Our analysis of expression patterns with fluorescent reporters determined that *EPFL2* is still expressed in the boundary between ovule primordia in *cuc* mutants, and this suggests that CUC transcription factors are not essential for expression of *EPFL2* in the boundaries between ovule primordia. The expression of *CUC2* and *CUC3* reporters in the *epfl1 epfl2* mutant show expanded boundary tissue expressing these reporters, and CUC3 sometimes appears to show ectopic expression in ovule primordia, but it is unclear whether the expansion of CUC expression is due to the altered phenotype or due to direct regulation of CUC expression. Further research to identify downstream targets of both *EPFL* and *CUC* genes during ovule initiation may help explain these observed genetic interactions.

While the three *CUC* genes do have overlapping functions, research has shown that these transcription factors are not completely redundant. For instance, the *cuc2 cuc3* mutant has increased ovule fusions with little change to ovule density, while the *cuc1 cuc2* mutant has been reported to have decreased ovule density along with gynoecium defects (Galbiati et al., 2013; Goncalves et al., 2015). In addition, the expression of *CUC3* is not identical to that of *CUC1* and *CUC2*, particularly due to the lack of expression of CUC3 in internal tissues. Our research demonstrated that *CUC3* had similar expression patterns to *EPFL2*, and the *cuc3* mutation had the strongest interaction with *epfl1 epfl2* mutants. Further research should be conducted to determine the cause of this co-expression pattern and genetic interaction to understand the roles that CUC3 and EPFL2 play during ovule initiation. The promoters of *CUC3* and *EPFL2* may contain regulatory elements that explain their co-expression, and the identification of transcription factors that allow for

these specific expression patterns may help elucidate the overall pathways regulating ovule patterning. In addition, further research is needed to determine the targets of the CUC3 transcription factor during ovule initiation, while also determining how these targets impact ovule initiation in the wild type and the *epfl1 epfl2* mutant. Overall, the coexpression of EPFL2 and CUC3 and the synergistic interaction of *cuc3* and *epfl1 epfl2* warrants further research into the mechanisms underlying these observations. Determining the downstream targets of both CUC3 transcriptional regulation and EPFL1/2 signaling will be critical in understanding this interaction.

The phytohormones auxin, cytokinin, and brassinosteroids are known to positively promote ovule initiation, while gibberellins inhibit ovule initiation (Bartrina et al., 2011; Huang et al., 2013; Cucinotta et al., 2016; Cucinotta et al., 2018; Gomez et al., 2018; Yu et al., 2020; Zu et al., 2022). Exogenous chemical treatments used in this study indicate that the *epfl1 epfl2* mutant responds to cytokinin and gibberellins similarly to wild-type plants. While exogenous auxin doesn't affect ovule initiation with conditions used, the inhibition of polar auxin transport caused drastic inhibition of ovule initiation and reduced density in both the wild type and the *epfl1 epfl2* mutant. Furthermore, auxin-related reporters such as DR5v2, PIN1-GFP, and R2D2 failed to show obvious changes of expression in the mutant ovule primordia relative to the wild type. MP was expressed only in boundaries of ovule primordia where auxin is depleted, while DR5v2, R2D2 and PIN1-GFP expression all suggest that auxin is concentrated at the tip of ovule primordia. Therefore, questions remain as to which ARFs are responsible for signaling at the apex of ovule primordia during initiation and what function MP has in the boundary tissues

between ovule primordia. It is possible that MP expression in the boundary allows these cells to respond to auxin accumulation during the initiation of new ovule primordia as the placenta elongates. Ultimately, this suggests that the *epfl1 epfl2* mutant may suffer from defects that are somewhat independent of these phytohormone signaling pathways including auxin, cytokinin, and gibberellins, as the mutant still apparently responds to these hormones normally, although further research is needed to solidify this hypothesis.

Brassinosteroid signaling in Arabidopsis leads to the activation of transcription factors such as BZR1/2 and BES1. BR signaling in Arabidopsis is often investigated using the *bzr1-1D* dominant mutation. This point mutation in BZR1 leads to hyper-stability of the transcription factor (Wang et al., 2002). Both our research and previously published date have shown that the *bzr1-1D* mutation leads to increased ovule number, placenta length, and ovule density in the wild type (Huang et al., 2013; Zu et al., 2022). Unexpectedly, this mutation significantly reduces ovule number and density in the *epfl1 epfl2* mutant despite still increasing placenta length. Previous research has shown that BZR1 protein is degraded in the peripheral regions of the inflorescence meristem where CUC3 expressed due to the absence of brassinosteroid signaling, but the *bzr1-1D* mutation leads to stability of the protein in these regions and subsequent ectopic expression in boundary tissues (Gendron et al., 2012). Furthermore, this ectopic expression of BZR1 protein led to repression of *CUC* genes such as *CUC3* during inflorescence development. Given the synergy between *cuc3* and the *epfl1 epfl2* mutant, one could anticipate that the synergistic interaction between *bzr1-1D* and *epfl1 epfl2* could be due to ectopic repression of *CUC3* in boundary tissues. This could potentially explain why both the *cuc3* or *bzr1-1D*

mutations have similar severe negative impacts upon the *epfl1 epfl2* mutant ovule density. Further research is needed to determine BZR1 expression pattern during ovule initiation, as well as the effects of increased BZR1 activity on expression of *CUC3*. Previous research has also suggested that BZR1 can regulate expression of known ovule transcriptional regulators such as ANT, AP2, and HLL, as well as regulation of the auxin response, so it is also possible that other unknown mechanisms exist that could explain the synergistic interaction seen between *epfl1 epfl2* and *bzr1-1D* (Huang et al., 2013). Further research will be needed to fully characterize the role of BZR1 in regulating ovule spacing in the context of the *epfl1 epfl2* mutant.

Previous research indicated that the AP2-like transcription factors DRN and its paralog DRNL are differentially regulated by EPFL-ERf signaling during vegetative meristem maintenance (Uzair et al., 2024). Additional evidence suggested that *DRN* expression patterning is altered in the *epfl2* mutant during ovule initiation, as the number of cells between *DRN* maxima showed larger variation in the mutant relative to the wild type (Kawamoto et al., 2020). While the role of DRN during ovule initiation is unknown, DRN and DRNL have been shown to regulate patterning of cotyledon primordia during embryogenesis where the *drn drnl* double mutant sometimes has one cotyledon, three cotyledons, or fused cup-shaped cotyledons, and this suggests that these genes may be involved in above-ground organ initiation (Chandler et al., 2008). These observations prompted the investigation of *DRN* expression in the more severe *epfl1 epfl2* mutant during ovule initiation. While *DRN* expression is efficiently concentrated into concise peaks at the site of ovule primordia initiation in the wild type, the expression of *DRN* is expanded and

diffuse at this same stage of development in the *epfl1 epfl2* mutant. This altered expression of DRN during early ovule initiation may indicate that there are defects in differentiation of placenta cells during ovule initiation in the *epfl1 epfl2* mutant that may explain the altered ovule spacing. Further research is required to establish whether *DRN* expression has any impact on ovule initiation, and this may be achieved by phenotypic analysis of loss of function and gain of function mutations in *DRN.*

The promoter of *DRN* has been shown to contain five auxin response elements, and these regulatory elements are required for expression of *DRN* at the apex of cotyledon primordia (Cole et al., 2009). In contrast, the loss of all five auxin response elements does not alter the expression of *DRN* within the embryonic meristem (Cole et al., 2009). The carpel margin meristem is composed of cells expressing stem cell markers such as *SHOOTMERISTEMLESS,* and the placenta tissues must undergo differentiation to generate ovules and boundaries (Kamiuchi et al., 2014). Therefore, the expression of *DRN* during ovule initiation may involve both meristematic regulatory elements and auxin responsive regulatory elements. In addition, MP was shown to directly repress *DRN* expression in the boundary of the inflorescence meristem, and *MP* shows boundary-specific expression during ovule initiation (Galbiati et al., 2013; Luo et al., 2018). This may suggest that MP could function as a repressor of *DRN* in the boundary between ovules in the absence of auxin. Therefore, analysis of a *DRN* promoter-reporter that is missing all five auxin response elements may allow to distinguish between meristematic expression and auxin responsive expression, and this may allow for further understanding of how *EPFL* genes regulate *DRN* expression pattern.

Several possibilities remain regarding why the *epfl1 epfl2* mutant fails to initiate ovule primordia despite available placenta tissue. It is possible that EPFL signaling functions to restrict certain transcription factors to tissue-specific domains in response to developmental cues to regulate cell differentiation along the placenta. For instance, expression of EPFL2 in the boundary of a recently initiated ovule may send cues to neighboring placenta cells that dictate where the next ovule will form. This could be possible if EPFL signaling functions to repress expression of certain developmental transcription factors in the placenta cells that must transition to either boundary identity or organ founder-cell identity. An alternative possibility is that *EPFL* genes regulate organ primordia outgrowth during early organ initiation. In this case, developmental cues would be present, and differentiation would begin to occur, but the mutant would be somewhat incapable of performing the necessary cell proliferation associated with organ initiation leading to failed organ outgrowth.

In conclusion, EPFL1 and EPFL2 function during ovule initiation to promote both proper spacing of ovules as well as proper growth of ovules. The *epfl1 epfl2* mutant shows a synergistic interaction with *cuc3* and *bzr1-1D* during this process, but further research is required to understand the mechanism of these interactions. The *epfl1 epfl2* mutant does not appear to have severe defects with auxin transport or signaling based on the reporters used, and the *epfl1 epfl2* mutant responds to cytokinin and gibberellin normally. *DRN* expression is more diffuse along L1 in the *epfl1 epfl2* mutant relative to the wild type during early ovule initiation, but the mechanism of this regulation and its importance during development require further investigation.

Chapter 2

Generation of an Inducible EPFL2 Construct Driven by the EPFL2 Promoter

Introduction

The EPFL peptide ligands are secretory peptides that show specific expression patterns in specific developmental contexts (Uchida et al., 2012; Tameshige et al., 2016; Kosentka et al., 2019). To induce the EPFL//ERf signaling cascade, previous research has used purified mature peptides that are exogenously applied to the entire tissue to induce a signaling response (Uchida et al., 2012; Kawamoto et al., 2020; Zhang et al., 2021; Uzair et al., 2024). While this method has been shown to successfully elicit the signaling response, it is more difficult in dense tissues such as the stage 9 gynoecium where peptide penetration may be insufficient to reach the placenta. In addition, the mature peptide would be applied evenly across all tissues, while promoter reporters of *EPFL* genes suggest that their expression is tissue specific. Furthermore, little is known about post-translational regulation of EPFL1/2, such as the processing of the full protein into the mature peptide by proteases which might contribute to restriction of EPFL signaling to selected set of cells. To address these issues, a construct was made to induce the expression of EPFL2 protein in its endogenous domain of expression following dexamethasone treatment.

The dexamethasone inducible system involves the use of the rat glucocorticoid receptor (GR) fused to a mutant version of the lac repressor $LacI^{His17}$ with high DNA binding affinity (Lh) and the Gal4 activation domain (G4) (Samalova et al., 2005). This synthetic transcription factor, known as GR-LhG4, is sequestered into the cytosol in the absence of the dexamethasone ligand (Samalova et al., 2005). Binding of dexamethasone to the rat glucocorticoid receptor leads to nuclear localization of GR-LhG4 (Samalova et al., 2005). The second component of the inducible system involves a synthetic bidirectional

promoter consisting of six repeats of the Lac operon flanked by minimal CaMV 35S promoters and translational enhancers driving expression of the genes of interest. Upon nuclear localization of GR-LhG4, the $LacI^{His17}$ domain binds to the repeats of the lac operon, and the Gal4 activation domain is able to initiate transcription of the genes of interest (Samalova et al., 2005). By using the promoter of a gene of interest to drive expression of GR-LhG4, this inducible system can be specifically localized to a subset of tissues or cells. Ultimately, this inducible system allows for tissue specific induction of genes in a timely manner which can be useful when attempting to observe downstream effects of a gene.

Materials and Methods

Plant Materials and Growth Conditions

The Columbia ecotype of *Arabidopsis thaliana* was used as the wild type. The *epfl1 epfl2* and *epfl1 epfl2 epfl4 epfl6* mutants in the Columbia ecotype have been previously described (Kosentka et al., 2019). Seedlings were grown on modified Murashige and Skoog medium plates supplemented with 1% (w/v) sucrose. Plates were stratified for two days at 4°C and then moved to the growth room with the following conditions: 18 h light/6 h dark cycle and 21°C.

The following research has been published (Uzair et al., 2024). “The following construct was generated to generate dexamethasone-inducible EPFL2 that is induced only in cells with EPFL2 promoter activity (Fig. 2.1). The 2.58 kb promoter of EPFL2 was

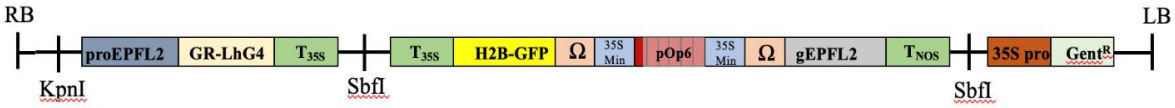

proEPFL2 – 2.58 kb EPFL2 promoter
GR-LhG4 – a fusion between the rat glucocorticoid receptor (GR), a high-affinity DNA-binding lac repressor LacI His17 (Lh), and the Gal4 II activation domain (G4).
T35S – 35S terminator
H2B-GFP – GFP fused with histone H2B
Ω - omega translational enhancer
35S Min - 35s minimal promoter
pOp6 – 6 repeats of the lac operon
gEPFL2 – coding sequence of EPFL2 with introns
T_{NOS} – Nos terminator
35S pro – 35S promoter
GentR – gentamycin resistance gene
LB and RB – left and right borders of insert

Figure 2.1. The structure of T-DNA insert in the pAMO113 vector

This diagram shows the design of dexamethasone-inducible EPFL2 that is expressed specifically in its endogenous domain. The backbone of the construct is from pPZP222.

amplified using pPZK412 (Kosentka et al., 2019) and fused with GR-LhG4:T35S amplified from pBIN-LhGR-N (Fig 2.1) (Samalova et al., 2005) via overlapping PCR. This DNA fragment was introduced into the binary vector pPZP222 between KpnI and SbfI sites, and the plasmid was named pAMO112. The next step involved 8 PCR reactions. PCR1 amplified H2B-GFP:35S terminator (T_{35S}). PCR2 amplified the omega translational enhancer (Ω) and 35s minimal promoter (35S Min) using plasmid pH-TOP (Samalova et al., 2005) as a template. PCR1 and PCR2 products were overlapped to generate PCR3 fragment. PCR4 used pH-TOP as a template to generate a fragment containing pPOP6 followed by 35S Min and Ω. PCR5 amplified the EPFL2 coding sequence with introns using the pPZK412 vector as a template. PCR6 amplified the NOS terminator (T_{NOS}) using pBIN-LhGR-N as a template. PCR7 was an overlapping PCR that fused DNA fragments created by PCR4, PCR5, and PCR6. Finally, PCR8 was overlapping PCR that fused PCR3 and PCR7 DNA fragments. It generated a DNA fragment containing T_{35s}:H2B-GFP: Ω:35SMin:pOp6:35SMin: Ω:gEPFL2: T_{NOS}. The DNA segment generated by PCR8 was inserted in the SbfI site of pAMO112. Orientation was confirmed via restriction digest and Sanger sequencing. The sequencing identified additional SbfI sites between two T35s. The final construct was named pAMO113 and contained: proEPFL2:GR-LhG4:T_{35S}___T_{35S}:H2B-GFP:Ω:35sMin_pOp6_35sMin:Ω:gEPFL2:T_{NOS}.

The generated constructs were transformed into an Agrobacterium tumefaciens strain GV3101/pMP90 by electroporation and introduced into the wild type (Columbia ecotype), *epfl1 epfl2* and *epfl1/+ epfl2 epfl4 epfl6* plants by the floral dip method.

To induce EPFL2, *epfl1/+ epfl2 epfl4 epfl6,* mutant harboring the T-DNA from pAMO113 was grown on modified Murashige and Skoog medium (MS-0) plates for five days (3DPG). Then 15 seedlings per biological replicate were transferred to 2 ml of liquid MS-0 containing 10 µM Dex or an equivalent amount of DMSO (mock treatment). The 50 mM stock solution of Dex was prepared using DMSO. 24 well culture plates with the samples were kept on a rocker in the growth room for seven hours, and then seedlings were preserved in liquid nitrogen.

Due to the infertility of the *epfl1 epfl2 epfl4 epfl6* mutant, we isolated it from the progeny of *epfl1/+ epfl2 epfl4 epfl6* plants. A small piece of root was cut from a seedling and placed into the PCR mix. PCR was performed using the Phire Plant Direct PCR Master Mix kit (Thermo Fisher Scientific). The rest of the seedling was preserved in 4% paraformaldehyde for microscopy. A three-primer PCR reaction with EPFL1.74, EPFL1.436.rev, and 3dspm was performed to genotype for *epfl1* (Kosentka et al., 2019). The mutant band was approximately 200bp, and the wild-type band 387bp."

Microscopy

For confocal microscopy, inflorescence clusters containing flowers up to stage 12 were harvested and fixed in 4% paraformaldehyde under a vacuum for up to 2 hours. Samples were then rinsed with 1x Phosphate-buffered saline (PBS) pH7.4 twice before placing them in ClearSee solution consisting of 25% (w/v) urea, 15% (w/v) sodium deoxycholate, and 10% (w/v) xylitol as previously described (Kurihara et al., 2015). Microcentrifuge tubes with samples were wrapped with foil to prevent photobleaching and

rocked for 1 to 2 days with a daily change of ClearSee solution. Leaving samples in the solution longer than 2 days will lead to the loss of the signal. The day before imaging, samples were placed in a staining solution containing 0.1% (v/v) SCRI Renaissance 2200 (SR2200) dye, 1% (v/v) DMSO, 0.05% (v/v) Triton-X100, 5% (v/v) glycerol in ClearSee solution and left to rock overnight (Musielak et al., 2015). Before imaging, the samples were rinsed with fresh ClearSee. Water instead of ClearSee was used as a mounting medium to prevent contamination of the microscope water immersion lens. Light dissection was used to separate and expose stage 8 through stage 10 flowers. Confocal microscopy was performed using a Leica SP8 White Light Laser Confocal microscope. Samples were imaged using a 40x water immersion lens at 1024 x 512 pixel size with a zoom factor between 1.0x to 1.5x. Bidirectional scanning was used with a scan speed between 200 and 600 Hz, and line averaging was used with a line average of 3. Z-stacks were generated with a Z-step size of no greater than 0.5 microns. The SR2200 dye was excited with a 405 nm solid state UV laser and imaged using a 420-450 nm emission window. CFP was excited with a 456 nm argon laser and imaged using either a 460-500 nm emission window or, if GFP was also expressed in the sample, with a 460-480 nm emission window. GFP was excited with a 488 nm argon laser and imaged using a 500-520 nm emission window. Red fluorescent proteins such as mCherry or tdTomato were excited with a white light laser at 556 nm and imaged using a 605-625 nm emission window. Sequential line scanning was used to image multiple channels at once. Hybrid detectors were used when available, while PMT detectors were occasionally used when necessary. Laser power, gain, and emission filters were modified depending on the

brightness of the signal and the number of fluorophores present in the sample. Confocal z-stacks were processed into 2D images using FIJI software. For each channel, background subtraction and contrast enhancement were used if necessary to remove background and enhance signal-to-background ratios. For longitudinal cross sections of ovule initiation, the slices of the z-stack, which represent the center of the ovule primordia, were identified. Next, a Z-projection with frame averaging was created using 3 to 5 slices around the center of ovule primordia to create a smoother image while not exceeding the width of an individual cell. Finally, images were cropped to the desired size in microns, and image size in pixels was readjusted so that all images in an individual figure had the same dimensions in both pixels and microns.

Results

The following research on the effect of inducible EPFL2 during meristem development is published by Uzair et al., 2024. "A previous experiment was conducted to use transcriptomics after EPFL4 peptide treatment of the seedling to identify downstream targets of EPFL signaling (Uzair et al., 2024). Several genes such as *CLAVATA3 (CLV3)*, Mei2-like genes *TEL2*, *MCT1* and *MCT2*, and *WUSCHEL (WUS)* were identified as genes that were downregulated by EPFL4 peptide treatment (Uzair et al., 2024). EPFL4 is expressed throughout the peripheral zone of the shoot apical meristem (SAM) near the central zone, while EPFL2 is expressed in the boundaries between SAM and forming primordia (Kosentka et al., 2019). To test whether EPFL2 can alter the expression of genes previously identified by transcriptomics when only expressed in the boundary of the SAM,

we created *epfl1 epfl2 epfl4 epfl6* transgenic plants with inducible *EPFL2* expression (*epfl,2,4,6*^{T}). We used the pOp/LhGR system that allows tissue-specific expression of a gene of choice in response to dexamethasone (DEX) (Samalova et al., 2005). The construct was created in such a way that in response to DEX, expression of EPFL2 and H2B-GFP is induced in tissues where the *EPFL2* promoter is active (Fig. 2.1) Before induction, we did not detect H2B-GFP (Fig. 2.2A). After seven hours of induction, H2B-GFP was clearly detected in the boundary zone of the SAM in 3 day old seedlings (Fig. 2.2A). Interestingly, RT-qPCR indicated that both H2B-GFP and EPFL2 are expressed in transgenic plants without induction (Fig. 2.2B). After induction their expression increases only slightly. This suggested that our construct leads to a leaky and broad expression at very low levels. This expression does not noticeably alter the phenotype of the *epfl1 epfl2 epfl4 epfl6* mutant based on the enlarged meristem size observed in the transgenic plants (Fig 2.2). In response to DEX, H2B-GFP expression and presumably EPFL2 was strongly activated in cells where the *EPFL2* promoter functions. However, because this happened in very few cells out of many, RT-qPCR could not detect this change. Expression of *CLV3*, *MCT1*, *MCT2*, and *TEL2* genes in transgenic seedlings without induction (*epfl1,2,4,6*^{T}-mock) was increased in a manner similar to their expression in untransformed *epfl1 epfl2 epfl4 epfl6* (Uzair et al., 2024). When DEX induced EPFL2 expression for seven hours in the boundary of the SAM, expression of *CLV3*, *MCT1*, and *MCT2* was decreased (Fig. 2.2C). *TEL2* expression was not significantly altered by *EPFL2* induction. *TEL2* might be a specific target of EPFL4 and EPFL6. Induction of *EPFL2* in the boundary did not significantly lower *WUS* expression. It is possible that very low and broad expression of *EPFL2* reduced

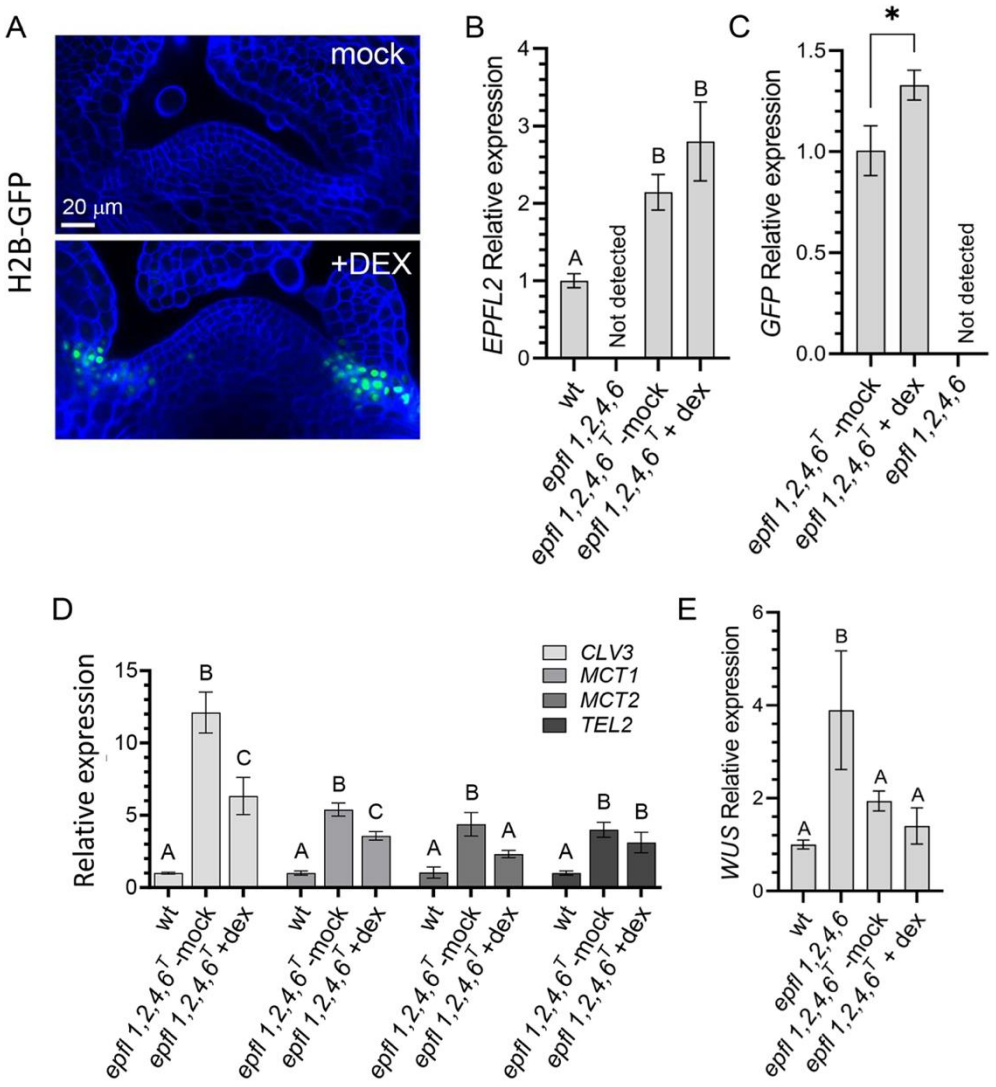

Figure 2.2. Induction of EPFL2 in the SAM boundary leads to decreased expression of *CLV3*, *MCT1* and *MCT2*

(A) Confocal images of 3DPG *epfl1,2,4,6*^{T} seedlings following mock treatment or DEX treatment for 7 h. The seedlings express H2B-GFP (green) under the *EPFL2* promoter in response to DEX. Both images were acquired with the same magnification, and the same settings were used for confocal microscopy. The cell walls were stained with SR2200 (blue). Images are representative of ten seedlings. (B-E) RT-qPCR analysis of (B) *EPFL2*; (C) *H2B-GFP*; (D) *CLV3*, *MCT1*, *MCT2* and *TEL2*; and (E) *WUS* expression in (B,D,E) 3DPG wild-type (wt) seedlings, (B,C,E) 3DPG *epfl1,2,4,*6 seedlings and (B-E) 3DPG *epfl1,2,4,6*^{T} seedlings expressing inducible EPFL2 and H2B-GFP under the *EPFL2* promoter, with either mock treatment or DEX treatment as indicated. Data are presented as the mean±s.d. of *n*=3. Statistical differences were detected using a one-way ANOVA followed by a Tukey post-hoc test with $P<0.05$; letters denote statistically significant differences, with no statistically significant difference between groups marked by the same letter. *$P<0.05$ in C.

the expression of *WUS* in *epfl1,2,4,6*^{T}-mock to levels that are only slightly above the wild-type levels. In summary, this experiment confirmed that *CLV3, MCT1,* and *MCT2* are endogenous targets of EPFL2."

To determine whether the inducible EPFL2 construct could function during ovule initiation, the construct was transformed into the *epfl1 epfl2* mutant. After a stable transformant line was obtained, the *epfl1 epfl2* mutant containing inducible EPFL2 was crossed with the *epfl1 epfl2* mutant containing *proDRN:er-mCherry:DRNterm* and *proCUC3:er-CFP* that was previously generated (see Fig. 1.20). The *epfl1 epfl2* mutant containing all three constructs was then treated with either mock solution (0.1% v/v DMSO, 0.01% v/v Silwet L-77) or a 10 micromolar DEX solution with the same concentration of DMSO and Silwet L-77 by dipping the inflorescences in the solution every 2 hours from 10 am to 4 pm on day 1 before collecting inflorescences on day 2 for confocal imaging. Microscopic analysis revealed that this treatment method does indeed induce H2B-GFP and presumably EPFL2 in the boundaries between ovules between stage 9a and 9b (Fig. 2.3). In addition, no GFP signal was detected in mock treated samples at the same stages of development (Fig. 2.3). While several methods were attempted to quantify differences in the patterning of DRN and CUC3 expression after induction of EPFL2, such as colocalization analysis using Peason's correlation coefficient, large variation in the patterning and image quality rendered these attempts unsuccessful. Nonetheless, this research confirms that the inducible EPFL2 construct functions during both seedling development and flower development, and future research will be needed to determine how

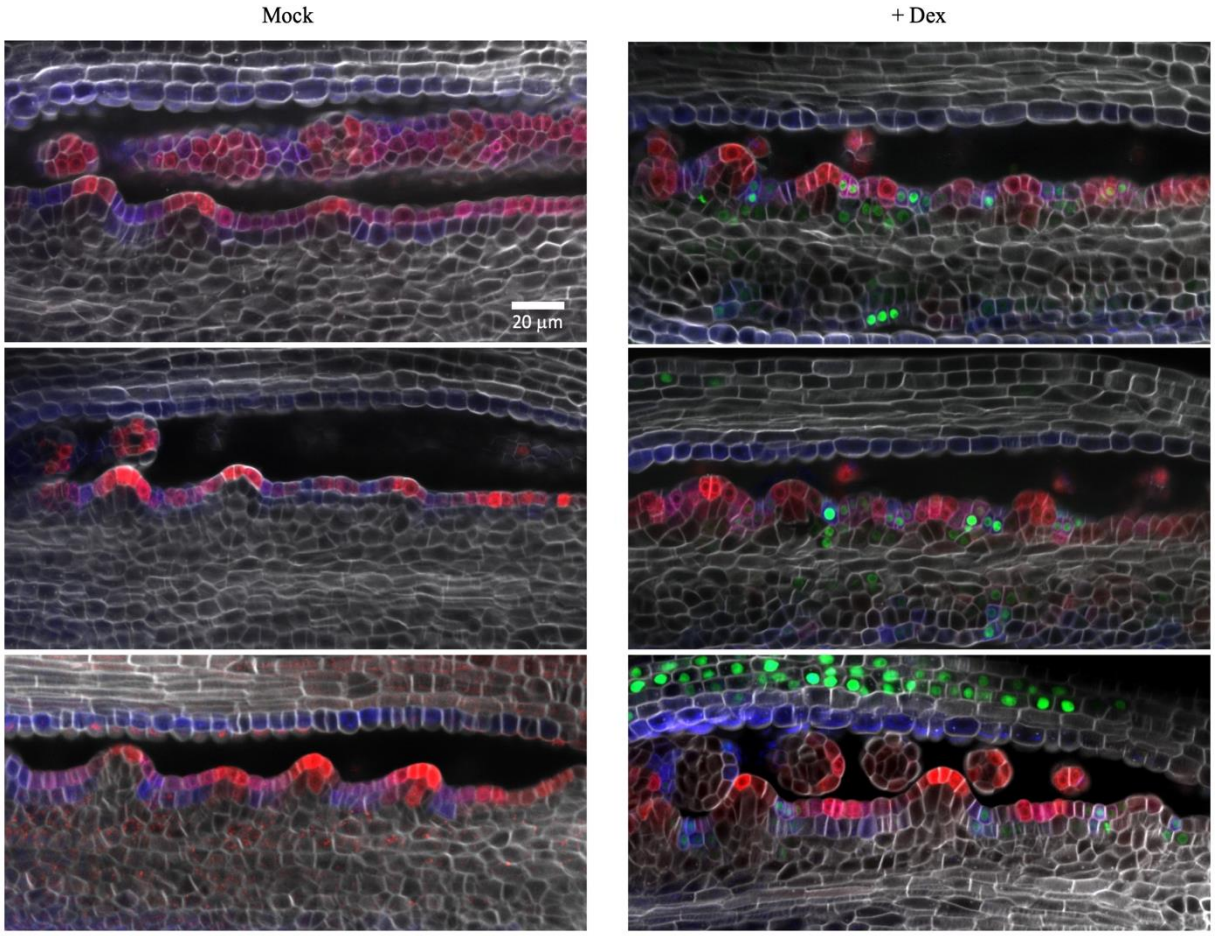

Figure 2.3. Induction of H2B-GFP/EPFL2 in the *epfl1 epfl2* mutant containing DRN and CUC3 reporters during ovule initiation

Confocal images of stage 9a to 9b placentae of the *epfl1 epfl2* mutant containing proDRN:er-mCherry:DRNterm (red), proCUC3:er-CFP (blue), and inducible H2B-GFP/EPFL2 (green) after treatment with either mock solution (left 3 panels) or 10 μM Dex solution (right 3 panels). The cell walls were stained with SR22000 (white).

to appropriately utilize this construct to further understand EPFL2 function during ovule initiation.

Discussion

ERf-EPFL signaling has been shown to regulate meristem maintenance through genetic analysis of mutants and activation of peptide signaling in mutants (Chen et al., 2013; Uchida et al., 2013; Kosentka et al., 2019; Uzair et al., 2024). Loss of ERf signaling leads to increased levels of WUS and CLV3 mRNA relative to wild type, and this suggests that this signaling may repress transcription of these meristematic regulator genes (Zhang et al., 2021; Uzair et al., 2024). Overexpression of WUS and CLV3 could lead to the enlarged meristems seen in higher order *epfl1 epfl2 epfl4 epfl6* mutant seedlings. EPFL4 peptide application to the seedling of the *epfl1 epfl2 epfl4 epfl6 clv3* mutant leads to repression of WUS and CLV3, but expression analysis suggests that EPFL4 is only expressed in the peripheral region of the meristem (Kosentka et al., 2019; Uzair et al., 2024). The use of inducible EPFL2 allows for one to observe downstream changes caused by ERf signaling only in the tissues that would normally express EPFL2. This construct successfully showed that EPFL2 was capable of repressing *CLV3, MCT1,* and *MCT2* genes in seedlings when induced in its endogenous domain, and this further supports the notion that these genes are downstream targets of endogenous EPFL signaling in the shoot apical meristem.

EPFL signaling is a process that involves many steps, and this allows for various levels of regulation. Many of these potential regulatory steps are not fully understood. For

instance, the specific timing and localization of expression of EPFLs has been observed to some degree, but further research is required to understand the importance of this specificity in a developmental context. In addition, EPFL proteins undergo processing by proteases to become the mature peptide (Engineer et al., 2014; Fanourakis et al., 2020), but the proteases that regulate EPFL1/2 signaling have yet to be identified and their importance in signaling is unclear. Finally, it is unclear what other transcriptional, translational, and post-translation regulatory steps may be important. Previous studies attempting to elicit EPF/EPFL signaling responses often use purified mature peptides that are applied to the entire organ or organism (Abrash et al., 2011; Kawamoto et al., 2020; Uzair et al., 2024). While this technique was proven to be effective during stomata differentiation and meristem maintenance, this technique poses several issues with regards to flower development and ovule initiation. One issue is the large amount of purified protein required to treat a sufficient number of flowers at a given stage. Another issue is the inability to ensure full penetration of the peptide into enclosed areas such as the gynoecium. Finally, this method leads to a ubiquitous distribution of the mature peptide, while the endogenous *EPFL2* gene shows very specific timing and localization of expression. Furthermore, while application of EPFL4 peptide to the *epfl1 epfl2 epfl4 epfl6 clv3* quintuple mutant did lead to the anticipated responses (Uzair et al., 2024), one may question whether some signaling may be caused by ectopic application of the peptide and may not reflect native signaling responses.

The use of dexamethasone-inducible EPFL2 driven by the EPFL2 promoter allows to avoid these issues and observe a signaling response that is more comparable to

endogenous signaling. Nonetheless, some issues with this system remain. While no H2B-GFP is seen in samples that have not been exposed to DEX, quantitative RT-PCR shows leaky expression of GFP and EPFL2 in the absence of DEX treatment. This leakiness did not alter phenotypes associated with EPFL2, but it is still unclear whether this leakiness may have an impact on downstream targets. While the source of the leaky expression is unclear, it may be caused by basal levels of transcription of H2B-GFP and EPFL2 driven by the minimal 35S promoters even in the absence of the GR-LhG4 protein. To prevent this leakiness, further research would need to be conducted to identify minimal promoters that have no basal transcriptional activity in the absence of nuclear GR-LhG4 protein while still promoting strong induction when the GR-LhG4 protein is present in the nucleus. Furthermore, the use of the floral dip method prevents constitutive activation of the construct and leads to pulses of induction corresponding to each treatment. Further research is needed to identify treatment methods that lead to constitutive DEX-induced activation of the construct in tissues such as flowers without causing significant stress or tissue death.

While transcriptomic analysis of tissues with and without induction of signaling has potential to identify many unknown targets of the signaling pathway, isolation of sufficient quantities of the relevant tissues while avoiding inclusion of nonrelevant tissues proves difficult with regards to the stage 9 gynoecium of Arabidopsis. The use of this construct in conjunction with fluorescent reporters could potentially allow for spatiotemporal visualization of gene expression changes caused by EPFL2 signaling once candidate gene targets are identified. However, further refining of the methods of treatment and quantification are required. Furthermore, the use of reporter proteins such as H2B-

GFP, er-mCherry, and er-CFP leads one to question the lifetime of these proteins and how well their fluorescence reflects active transcriptional changes. For instance, if a cell expressing *DRN* had made a sufficient amount of er-mCherry, and then induction of EPFL2 repressed DRN promoter activity in this cell, how long would it take for the fluorescence levels of er-mCherry to be altered? This issue could be fixed by fusing the fluorescent protein to the target protein to observe the lifetime of the target protein rather than the reporter protein. This would show a more realistic representation of how EPFL signaling affects the expression of the target gene.

In the case of the DRN/CUC3 reporter system, colocalization analysis may be used to determine the amount of overlap between DRN and CUC3 expression and whether that amount changes following induction of EPFL2 (Bolte and Cordelieres, 2006). First, one must establish that colocalization analysis can distinguish between the wild type and *epfl1 epfl2* mutant expression patterns of DRN/CUC3. Based on preliminary observations, one would expect more overlap of DRN/CUC3 in the *epfl1 epfl2* mutant relative to wild type, and this would yield a higher Pearson's correlation coefficient than wild type (Bolte and Cordelieres, 2006). Attempts to apply this method with a limited sample size showed large variation amongst samples. This could be caused by variations in image quality, tissue fixation, clearing, or even natural variation. Further research is needed to make sure all images are as comparable as possible, and a larger sample size is likely needed to deal with variation. In conclusion, this construct provides an efficient method for tissue specific induction of EPFL2, and this construct may be useful for future experiments attempting to further understand the functions of EPFL2 signaling.

Chapter 3

Conclusions

The ERf signaling pathway has been shown to play important roles in various developmental processes in plants (Shpak, 2013). While the downstream effects of this signaling cascade have been well studied during the process of stomata development, other developmental processes regulated by ERf signaling are not as thoroughly characterized. This research has aimed to elucidate how EPFL1 and EPFL2 signaling through ERf receptors promotes ovule initiation, proper ovule spacing, and ovule primordia elongation. The *epfl1 epfl2* mutant has significantly reduced ovule density, and this reduction in ovule density is comparable to the *er erl1 erl2* receptor mutant. This data suggests that EPFL1 and EPFL2 are the primary ligands of ERf receptors during the process of ovule initiation. In addition to the reduced ovule density, the *epfl1 epfl2* mutant shows reduced cell proliferation during ovule primordia elongation. The auxin reporters DR5v2, R2D2, and PIN1-GFP were not significantly altered in the *epfl1 epfl2* mutant, and this suggests that auxin transport, auxin signaling, and the auxin response are functioning normally during ovule initiation in the *epfl1 epfl2* mutant. In addition, the *epfl1 epfl2* mutant responds to cytokinin and gibberellin biosynthesis inhibitors in a similar manner as wild type but this does not restore the ovule density phenotype. This suggests that the *epfl1 epfl2* mutant ovule density phenotype is not associated with decreased cytokinin or increased gibberellins. A synergistic genetic interaction was observed when *bzr1-1D* was crossed with the *epfl1 epfl2* mutant. While the *bzr1-1D* mutant has increased ovule number and density in the wild-type background, this mutation causes a severe decrease in ovule number and density in the *epfl1 epfl2* mutant background. Loss of the boundary specific transcription factor CUC3 in the *epfl1 epfl2* mutant background causes a similar decrease

in ovule number and density. It is possible that stabilization of BZR1 in boundary tissues leads to repression of CUC3, and this would explain the similar genetic interactions seen in *cuc3 epfl1 epfl2* and *bzr1-1D epfl1 epfl2*. Finally, the AP2-like transcription factor DRN was observed to have expanded expression during ovule initiation in the *epfl1 epfl2* mutant. While DRN shows concise localization to the L1 layer at the tip of ovule primordia and absence in boundary tissues during early ovule initiation in wild type, DRN expression is not effectively repressed in the boundary regions between ovule primordia in the *epfl1 epfl2* mutant. Visualization of a dual CUC3/DRN reporter system in the *epfl1 epfl2* mutant suggests that the *epfl1 epfl2* mutant may have defects in the early differentiation steps during ovule initiation that separate primordia cells from the boundary cells, as DRN and CUC3 expression domains show more overlap in the *epfl1 epfl2* mutant relative to wild type.

Using loss of function mutations in *epfl* and *erf* genes has allowed for the identification of multiple developmental processes regulated by ERf signaling (Shpak, 2013). While these approaches are successful in identifying and characterizing phenotypes and changes in gene expression, this does not always allow for one to elucidate which downstream changes are directly caused by the loss of the signaling cascade. The application or induction of EPF/EPFL peptides has previously been used to successfully illicit downstream changes in gene expression and phenotype, and this method has also allowed for the identification of novel downstream target genes (Uchida et al., 2012; Uzair et al., 2024). Application of peptide or ubiquitous induction may lead to ectopic activation of the EPFL signaling cascade which may lead to results that are not relevant to the native

process. In addition, ectopic expression of *EPFL2* driven by the *DRN* promoter has a negative impact on ovule density, and this suggests that the localized expression of *EPFL2* is important for its function (Kawamoto et al., 2020). To address these issues, a construct was created to induce *EPFL2* expression only in cells that express the *EPFL2* promoter following dexamethasone treatment. This construct was successfully used to demonstrate that *EPFL2* can repress expression of the known target *CLV3* when only induced in the boundary around the shoot apical meristem, and this further supports that *CLV3* is a downstream target of ERf signaling (Uzair et al., 2024). Furthermore, this construct is functional during flower development, and this allows for tissue specific induction of *EPFL2* in dense tissues that would be difficult to treat with exogenous peptides. Overall, this construct will be useful in further research by providing a controlled method to induce EPFL-ERf signaling during various developmental processes.

References

Abrash, E.B., Davies, K.A., and Bergmann, D.C. (2011). Generation of signaling specificity in Arabidopsis by spatially restricted buffering of ligand-receptor interactions. Plant Cell **23,** 2864-2879.

Alonso, J.M., Stepanova, A.N., Leisse, T.J., Kim, C.J., Chen, H., Shinn, P., Stevenson, D.K., Zimmerman, J., Barajas, P., Cheuk, R., Gadrinab, C., Heller, C., Jeske, A., Koesema, E., Meyers, C.C., Parker, H., Prednis, L., Ansari, Y., Choy, N., Deen, H., Geralt, M., Hazari, N., Hom, E., Karnes, M., Mulholland, C., Ndubaku, R., Schmidt, I., Guzman, P., Aguilar-Henonin, L., Schmid, M., Weigel, D., Carter, D.E., Marchand, T., Risseeuw, E., Brogden, D., Zeko, A., Crosby, W.L., Berry, C.C., and Ecker, J.R. (2003). Genome-wide insertional mutagenesis of Arabidopsis thaliana. Science **301,** 653-657.

Ashikari, M., Sakakibara, H., Lin, S., Yamamoto, T., Takashi, T., Nishimura, A., Angeles, E.R., Qian, Q., Kitano, H., and Matsuoka, M. (2005). Cytokinin oxidase regulates rice grain production. Science **309,** 741-745.

Azhakanandam, S., Nole-Wilson, S., Bao, F., and Franks, R.G. (2008). SEUSS and AINTEGUMENTA mediate patterning and ovule initiation during gynoecium medial domain development. Plant Physiol **146,** 1165-1181.

Barro-Trastoy, D., Carrera, E., Banos, J., Palau-Rodriguez, J., Ruiz-Rivero, O., Tornero, P., Alonso, J.M., Lopez-Diaz, I., Gomez, M.D., and Perez-Amador, M.A. (2020). Regulation of ovule initiation by gibberellins and brassinosteroids in tomato and Arabidopsis: two plant species, two molecular mechanisms. Plant J **102,** 1026-1041.

Bartrina, I., Otto, E., Strnad, M., Werner, T., and Schmulling, T. (2011). Cytokinin regulates the activity of reproductive meristems, flower organ size, ovule formation, and thus seed yield in Arabidopsis thaliana. Plant Cell **23,** 69-80.

Becker, A. (2020). A molecular update on the origin of the carpel. Curr Opin Plant Biol **53,** 15-22.

Bencivenga, S., Simonini, S., Benkova, E., and Colombo, L. (2012). The transcription factors BEL1 and SPL are required for cytokinin and auxin signaling during ovule development in Arabidopsis. Plant Cell **24,** 2886-2897.

Benkova, E., Michniewicz, M., Sauer, M., Teichmann, T., Seifertova, D., Jurgens, G., and Friml, J. (2003). Local, efflux-dependent auxin gradients as a common module for plant organ formation. Cell **115,** 591-602.

Bergmann, D.C., Lukowitz, W., and Somerville, C.R. (2004). Stomatal development and pattern controlled by a MAPKK kinase. Science **304,** 1494-1497.

Bolte, S., and Cordelieres, F.P. (2006). A guided tour into subcellular colocalization analysis in light microscopy. J Microsc **224,** 213-232.

Bowman, J.L., Smyth, D.R., and Meyerowitz, E.M. (1989). Genes directing flower development in Arabidopsis. Plant Cell **1,** 37-52.

Bowman, J.L., Drews, G.N., and Meyerowitz, E.M. (1991). Expression of the Arabidopsis floral homeotic gene AGAMOUS is restricted to specific cell types late in flower development. Plant Cell **3,** 749-758.

Caine, R.S., Chater, C.C., Kamisugi, Y., Cuming, A.C., Beerling, D.J., Gray, J.E., and Fleming, A.J. (2016). An ancestral stomatal patterning module revealed in the non-vascular land plant Physcomitrella patens. Development **143,** 3306-3314.

Cao, L., Wang, S., Venglat, P., Zhao, L., Cheng, Y., Ye, S., Qin, Y., Datla, R., Zhou, Y., and Wang, H. (2018). Arabidopsis ICK/KRP cyclin-dependent kinase inhibitors function to ensure the formation of one megaspore mother cell and one functional megaspore per ovule. PLoS Genet **14,** e1007230.

Cao, X., Yang, H., Shang, C., Ma, S., Liu, L., and Cheng, J. (2019). The Roles of Auxin Biosynthesis YUCCA Gene Family in Plants. Int J Mol Sci **20**.

Chandler, J.W., Cole, M., and Werr, W. (2008). The role of DORNROESCHEN (DRN) and DRN-LIKE (DRNL) in Arabidopsis embryonic patterning. Plant Signal Behav **3,** 49-51.

Chen, M.K., Wilson, R.L., Palme, K., Ditengou, F.A., and Shpak, E.D. (2013). ERECTA family genes regulate auxin transport in the shoot apical meristem and forming leaf primordia. Plant Physiol **162,** 1978-1991.

Cheng, Y., Dai, X., and Zhao, Y. (2006). Auxin biosynthesis by the YUCCA flavin monooxygenases controls the formation of floral organs and vascular tissues in Arabidopsis. Genes Dev **20,** 1790-1799.

Chory, J., Nagpal, P., and Peto, C.A. (1991). Phenotypic and Genetic Analysis of det2, a New Mutant That Affects Light-Regulated Seedling Development in Arabidopsis. Plant Cell **3,** 445-459.

Clough, S.J., and Bent, A.F. (1998). Floral dip: a simplified method for Agrobacterium-mediated transformation of Arabidopsis thaliana. Plant J **16,** 735-743.

Cole, M., Chandler, J., Weijers, D., Jacobs, B., Comelli, P., and Werr, W. (2009). DORNROSCHEN is a direct target of the auxin response factor MONOPTEROS in the Arabidopsis embryo. Development **136,** 1643-1651.

Cucinotta, M., Colombo, L., and Roig-Villanova, I. (2014). Ovule development, a new model for lateral organ formation. Front Plant Sci **5,** 117.

Cucinotta, M., Manrique, S., Cuesta, C., Benkova, E., Novak, O., and Colombo, L. (2018). CUP-SHAPED COTYLEDON1 (CUC1) and CUC2 regulate cytokinin homeostasis to determine ovule number in Arabidopsis. J Exp Bot **69,** 5169-5176.

Cucinotta, M., Manrique, S., Guazzotti, A., Quadrelli, N.E., Mendes, M.A., Benkova, E., and Colombo, L. (2016). Cytokinin response factors integrate auxin and cytokinin pathways for female reproductive organ development. Development **143,** 4419-4424.

Cucinotta, M., Cavalleri, A., Guazzotti, A., Astori, C., Manrique, S., Bombarely, A., Oliveto, S., Biffo, S., Weijers, D., Kater, M.M., and Colombo, L. (2021). Alternative Splicing Generates a MONOPTEROS Isoform Required for Ovule Development. Curr Biol **31,** 892-899 e893.

DeGennaro, D., Urquidi Camacho, R.A., Zhang, L., and Shpak, E.D. (2022). Initiation of aboveground organ primordia depends on combined action of auxin, ERECTA family genes, and PINOID. Plant Physiol **190,** 794-812.

Engineer, C.B., Ghassemian, M., Anderson, J.C., Peck, S.C., Hu, H., and Schroeder, J.I. (2014). Carbonic anhydrases, EPF2 and a novel protease mediate CO2 control of stomatal development. Nature **513,** 246-250.

Fanourakis, D., Nikoloudakis, N., Pappi, P., Markakis, E., Doupis, G., Charova, S.N., Delis, C., and Tsaniklidis, G. (2020). The Role of Proteases in Determining Stomatal Development and Tuning Pore Aperture: A Review. Plants (Basel) **9**.

Ferrándiz, C.F., C.; Prunet, N.; Scutt, C.; Sundberg, E.; Trehin, C.; Vialette-Guiraud, A.;. (2010). Advances in Botanical Research.

Ferrari, C., Shivhare, D., Hansen, B.O., Pasha, A., Esteban, E., Provart, N.J., Kragler, F., Fernie, A., Tohge, T., and Mutwil, M. (2020). Expression Atlas of Selaginella moellendorffii Provides Insights into the Evolution of Vasculature, Secondary Metabolism, and Roots. Plant Cell **32,** 853-870.

Fujihara, R., Uchida, N., Tameshige, T., Kawamoto, N., Hotokezaka, Y., Higaki, T., Simon, R., Torii, K.U., Tasaka, M., and Aida, M. (2021). The boundary-expressed EPIDERMAL PATTERNING FACTOR-LIKE2 gene encoding a signaling peptide promotes cotyledon growth during Arabidopsis thaliana embryogenesis. Plant Biotechnol (Tokyo) **38,** 317-322.

Furumizu, C., and Aalen, R.B. (2023). Peptide signaling through leucine-rich repeat receptor kinases: insight into land plant evolution. New Phytol **238,** 977-982.

Galbiati, F., Sinha Roy, D., Simonini, S., Cucinotta, M., Ceccato, L., Cuesta, C., Simaskova, M., Benkova, E., Kamiuchi, Y., Aida, M., Weijers, D., Simon, R., Masiero, S., and Colombo, L. (2013). An integrative model of the control of ovule primordia formation. Plant J **76,** 446-455.

Gendron, J.M., Liu, J.S., Fan, M., Bai, M.Y., Wenkel, S., Springer, P.S., Barton, M.K., and Wang, Z.Y. (2012). Brassinosteroids regulate organ boundary formation in the shoot apical meristem of Arabidopsis. Proc Natl Acad Sci U S A **109,** 21152-21157.

Gomez, M.D., Barro-Trastoy, D., Escoms, E., Saura-Sanchez, M., Sanchez, I., Briones-Moreno, A., Vera-Sirera, F., Carrera, E., Ripoll, J.J., Yanofsky, M.F., Lopez-Diaz, I., Alonso, J.M., and Perez-Amador, M.A. (2018). Gibberellins negatively modulate ovule number in plants. Development **145**.

Goncalves, B., Hasson, A., Belcram, K., Cortizo, M., Morin, H., Nikovics, K., Vialette-Guiraud, A., Takeda, S., Aida, M., Laufs, P., and Arnaud, N. (2015). A conserved role for CUP-SHAPED COTYLEDON genes during ovule development. Plant J **83,** 732-742.

Griffiths, J., Murase, K., Rieu, I., Zentella, R., Zhang, Z.L., Powers, S.J., Gong, F., Phillips, A.L., Hedden, P., Sun, T.P., and Thomas, S.G. (2006). Genetic characterization and functional analysis of the GID1 gibberellin receptors in Arabidopsis. Plant Cell **18,** 3399-3414.

Guilfoyle, T.J., Ulmasov, T., and Hagen, G. (1998). The ARF family of transcription factors and their role in plant hormone-responsive transcription. Cell Mol Life Sci **54,** 619-627.

Hara, K., Kajita, R., Torii, K.U., Bergmann, D.C., and Kakimoto, T. (2007). The secretory peptide gene EPF1 enforces the stomatal one-cell-spacing rule. Genes Dev **21,** 1720-1725.

Hardtke, C.S., and Berleth, T. (1998). The Arabidopsis gene MONOPTEROS encodes a transcription factor mediating embryo axis formation and vascular development. EMBO J **17,** 1405-1411.

Hasson, A., Plessis, A., Blein, T., Adroher, B., Grigg, S., Tsiantis, M., Boudaoud, A., Damerval, C., and Laufs, P. (2011). Evolution and diverse roles of the CUP-SHAPED COTYLEDON genes in Arabidopsis leaf development. Plant Cell **23,** 54-68.

Heisler, M.G., Ohno, C., Das, P., Sieber, P., Reddy, G.V., Long, J.A., and Meyerowitz, E.M. (2005). Patterns of auxin transport and gene expression during primordium development revealed by live imaging of the Arabidopsis inflorescence meristem. Curr Biol **15,** 1899-1911.

Hibara, K., Karim, M.R., Takada, S., Taoka, K., Furutani, M., Aida, M., and Tasaka, M. (2006). Arabidopsis CUP-SHAPED COTYLEDON3 regulates postembryonic shoot meristem and organ boundary formation. Plant Cell **18,** 2946-2957.

Higuchi, M., Pischke, M.S., Mahonen, A.P., Miyawaki, K., Hashimoto, Y., Seki, M., Kobayashi, M., Shinozaki, K., Kato, T., Tabata, S., Helariutta, Y., Sussman, M.R., and Kakimoto, T. (2004). In planta functions of the Arabidopsis cytokinin receptor family. Proc Natl Acad Sci U S A **101,** 8821-8826.

Hou, B., Lim, E.K., Higgins, G.S., and Bowles, D.J. (2004). N-glucosylation of cytokinins by glycosyltransferases of Arabidopsis thaliana. J Biol Chem **279,** 47822-47832.

Hu, L.Q., Chang, J.H., Yu, S.X., Jiang, Y.T., Li, R.H., Zheng, J.X., Zhang, Y.J., Xue, H.W., and Lin, W.H. (2022). PIN3 positively regulates the late initiation of ovule primordia in Arabidopsis thaliana. PLoS Genet **18,** e1010077.

Huang, H.Y., Jiang, W.B., Hu, Y.W., Wu, P., Zhu, J.Y., Liang, W.Q., Wang, Z.Y., and Lin, W.H. (2013). BR signal influences Arabidopsis ovule and seed number through regulating related genes expression by BZR1. Mol Plant **6,** 456-469.

Hunt, L., Bailey, K.J., and Gray, J.E. (2010). The signalling peptide EPFL9 is a positive regulator of stomatal development. New Phytol **186,** 609-614.

Jewaria, P.K., Hara, T., Tanaka, H., Kondo, T., Betsuyaku, S., Sawa, S., Sakagami, Y., Aimoto, S., and Kakimoto, T. (2013). Differential effects of the peptides Stomagen, EPF1 and EPF2 on activation of MAP kinase MPK6 and the SPCH protein level. Plant Cell Physiol **54,** 1253-1262.

Kamiuchi, Y., Yamamoto, K., Furutani, M., Tasaka, M., and Aida, M. (2014). The CUC1 and CUC2 genes promote carpel margin meristem formation during Arabidopsis gynoecium development. Front Plant Sci **5,** 165.

Kawamoto, N., Del Carpio, D.P., Hofmann, A., Mizuta, Y., Kurihara, D., Higashiyama, T., Uchida, N., Torii, K.U., Colombo, L., Groth, G., and Simon, R. (2020). A Peptide Pair Coordinates Regular Ovule Initiation Patterns with Seed Number and Fruit Size. Curr Biol **30,** 4352-4361 e4354.

Kirch, T., Simon, R., Grunewald, M., and Werr, W. (2003). The DORNROSCHEN/ENHANCER OF SHOOT REGENERATION1 gene of Arabidopsis acts in the control of meristem ccll fate and lateral organ development. Plant Cell **15,** 694-705.

Klucher, K.M., Chow, H., Reiser, L., and Fischer, R.L. (1996). The AINTEGUMENTA gene of Arabidopsis required for ovule and female gametophyte development is related to the floral homeotic gene APETALA2. Plant Cell **8,** 137-153.

Kosentka, P.Z., Overholt, A., Maradiaga, R., Mitoubsi, O., and Shpak, E.D. (2019). EPFL Signals in the Boundary Region of the SAM Restrict Its Size and Promote Leaf Initiation. Plant Physiol **179,** 265-279.

Krizek, B.A. (1999). Ectopic expression of AINTEGUMENTA in Arabidopsis plants results in increased growth of floral organs. Dev Genet **25,** 224-236.

Krizek, B.A. (2015). AINTEGUMENTA-LIKE genes have partly overlapping functions with AINTEGUMENTA but make distinct contributions to Arabidopsis thaliana flower development. J Exp Bot **66,** 4537-4549.

Kuhlemeier, C., and Reinhardt, D. (2001). Auxin and phyllotaxis. Trends Plant Sci **6,** 187-189.

Kurihara, D., Mizuta, Y., Sato, Y., and Higashiyama, T. (2015). ClearSee: a rapid optical clearing reagent for whole-plant fluorescence imaging. Development **142,** 4168-4179.

Lampard, G.R., Wengier, D.L., and Bergmann, D.C. (2014). Manipulation of mitogen-activated protein kinase kinase signaling in the Arabidopsis stomatal lineage reveals motifs that contribute to protein localization and signaling specificity. Plant Cell **26,** 3358-3371.

Larsson, E., Roberts, C.J., Claes, A.R., Franks, R.G., and Sundberg, E. (2014). Polar auxin transport is essential for medial versus lateral tissue specification and vascular-mediated valve outgrowth in Arabidopsis gynoecia. Plant Physiol **166,** 1998-2012.

Lavy, M., and Estelle, M. (2016). Mechanisms of auxin signaling. Development **143,** 3226-3229.

Lee, J.S., Hnilova, M., Maes, M., Lin, Y.C., Putarjunan, A., Han, S.K., Avila, J., and Torii, K.U. (2015). Competitive binding of antagonistic peptides fine-tunes stomatal patterning. Nature **522,** 439-443.

Lee, J.S., Kuroha, T., Hnilova, M., Khatayevich, D., Kanaoka, M.M., McAbee, J.M., Sarikaya, M., Tamerler, C., and Torii, K.U. (2012). Direct interaction of ligand-receptor pairs specifying stomatal patterning. Genes Dev **26,** 126-136.

Li, J., and Nam, K.H. (2002). Regulation of brassinosteroid signaling by a GSK3/SHAGGY-like kinase. Science **295,** 1299-1301.

Li, T., Kang, X., Wei, L., Zhang, D., and Lin, H. (2020a). A gain-of-function mutation in Brassinosteroid-insensitive 2 alters Arabidopsis floral organ development by altering auxin levels. Plant Cell Rep **39,** 259-271.

Li, X., Zheng, Y., Xing, Q., Ardiansyah, R., Zhou, H., Ali, S., Jing, T., Tian, J., Song, X.S., Li, Y., and Muller-Xing, R. (2020b). Ectopic expression of the transcription factor CUC2 restricts growth by cell cycle inhibition in Arabidopsis leaves. Plant Signal Behav **15,** 1706024.

Liao, C.Y., Smet, W., Brunoud, G., Yoshida, S., Vernoux, T., and Weijers, D. (2015). Reporters for sensitive and quantitative measurement of auxin response. Nat Methods **12,** 207-210, 202 p following 210.

Liu, Z., Franks, R.G., and Klink, V.P. (2000). Regulation of gynoecium marginal tissue formation by LEUNIG and AINTEGUMENTA. Plant Cell **12,** 1879-1892.

Lu, Y., Chanroj, S., Zulkifli, L., Johnson, M.A., Uozumi, N., Cheung, A., and Sze, H. (2011). Pollen tubes lacking a pair of K+ transporters fail to target ovules in Arabidopsis. Plant Cell **23,** 81-93.

Luo, L., Zeng, J., Wu, H., Tian, Z., and Zhao, Z. (2018). A Molecular Framework for Auxin-Controlled Homeostasis of Shoot Stem Cells in Arabidopsis. Mol Plant **11,** 899-913.

Meng, X., Chen, X., Mang, H., Liu, C., Yu, X., Gao, X., Torii, K.U., He, P., and Shan, L. (2015). Differential Function of Arabidopsis SERK Family Receptor-like Kinases in Stomatal Patterning. Curr Biol **25,** 2361-2372.

Mizukami, Y., and Fischer, R.L. (2000). Plant organ size control: AINTEGUMENTA regulates growth and cell numbers during organogenesis. Proc Natl Acad Sci U S A **97,** 942-947.

Musielak, T.J., Schenkel, L., Kolb, M., Henschen, A., and Bayer, M. (2015). A simple and versatile cell wall staining protocol to study plant reproduction. Plant Reprod **28,** 161-169.

Nelson, B.K., Cai, X., and Nebenfuhr, A. (2007). A multicolored set of in vivo organelle markers for co-localization studies in Arabidopsis and other plants. Plant J **51,** 1126-1136.

Nemhauser, J.L., Feldman, L.J., and Zambryski, P.C. (2000). Auxin and ETTIN in Arabidopsis gynoecium morphogenesis. Development **127,** 3877-3888.

Noguchi, T., Fujioka, S., Choe, S., Takatsuto, S., Yoshida, S., Yuan, H., Feldmann, K.A., and Tax, F.E. (1999). Brassinosteroid-insensitive dwarf mutants of Arabidopsis accumulate brassinosteroids. Plant Physiol **121,** 743-752.

Ohki, S., Takeuchi, M., and Mori, M. (2011). The NMR structure of stomagen reveals the basis of stomatal density regulation by plant peptide hormones. Nat Commun **2,** 512.

Okada, K., Ueda, J., Komaki, M.K., Bell, C.J., and Shimura, Y. (1991). Requirement of the Auxin Polar Transport System in Early Stages of Arabidopsis Floral Bud Formation. Plant Cell **3,** 677-684.

Pillitteri, L.J., Bemis, S.M., Shpak, E.D., and Torii, K.U. (2007). Haploinsufficiency after successive loss of signaling reveals a role for ERECTA-family genes in Arabidopsis ovule development. Development **134,** 3099-3109.

Putarjunan, A., Ruble, J., Srivastava, A., Zhao, C., Rychel, A.L., Hofstetter, A.K., Tang, X., Zhu, J.K., Tama, F., Zheng, N., and Torii, K.U. (2019). Bipartite anchoring of SCREAM enforces stomatal initiation by coupling MAP kinases to SPEECHLESS. Nat Plants **5,** 742-754.

Robinson-Beers, K., Pruitt, R.E., and Gasser, C.S. (1992). Ovule Development in Wild-Type Arabidopsis and Two Female-Sterile Mutants. Plant Cell **4,** 1237-1249.

Samalova, M., Brzobohaty, B., and Moore, I. (2005). pOp6/LhGR: a stringently regulated and highly responsive dexamethasone-inducible gene expression system for tobacco. Plant J **41,** 919-935.

Schneitz, K., Hulskamp, M., and Pruitt, R.E. (1995). Wild-Type Ovule Development in Arabidopsis-Thaliana - a Light-Microscope Study of Cleared Whole-Mount Tissue. Plant J **7,** 731-749.

Sessions, A., Weigel, D., and Yanofsky, M.F. (1999). The Arabidopsis thaliana MERISTEM LAYER 1 promoter specifies epidermal expression in meristems and young primordia. Plant J **20,** 259-263.

Sessions, A., Nemhauser, J.L., McColl, A., Roe, J.L., Feldmann, K.A., and Zambryski, P.C. (1997). ETTIN patterns the Arabidopsis floral meristem and reproductive organs. Development **124,** 4481-4491.

Shimada, T., Sugano, S.S., and Hara-Nishimura, I. (2011). Positive and negative peptide signals control stomatal density. Cell Mol Life Sci **68,** 2081-2088.

Shiu, S.H., and Bleecker, A.B. (2001). Receptor-like kinases from Arabidopsis form a monophyletic gene family related to animal receptor kinases. Proc Natl Acad Sci U S A **98,** 10763-10768.

Shpak, E.D. (2013). Diverse roles of ERECTA family genes in plant development. J Integr Plant Biol **55,** 1238-1250.

Shpak, E.D., Berthiaume, C.T., Hill, E.J., and Torii, K.U. (2004). Synergistic interaction of three ERECTA-family receptor-like kinases controls Arabidopsis organ growth and flower development by promoting cell proliferation. Development **131,** 1491-1501.

Shpak, E.D., McAbee, J.M., Pillitteri, L.J., and Torii, K.U. (2005). Stomatal patterning and differentiation by synergistic interactions of receptor kinases. Science **309,** 290-293.

Skoog, F., and Miller, C.O. (1957). Chemical regulation of growth and organ formation in plant tissues cultured in vitro. Symp Soc Exp Biol **11,** 118-130.

Sluis, A., and Hake, S. (2015). Organogenesis in plants: initiation and elaboration of leaves. Trends Genet **31,** 300-306.

Smyth, D.R., Bowman, J.L., and Meyerowitz, E.M. (1990). Early flower development in Arabidopsis. Plant Cell **2,** 755-767.

Sun, T.P. (2010). Gibberellin-GID1-DELLA: a pivotal regulatory module for plant growth and development. Plant Physiol **154,** 567-570.

Tameshige, T., Okamoto, S., Lee, J.S., Aida, M., Tasaka, M., Torii, K.U., and Uchida, N. (2016). A Secreted Peptide and Its Receptors Shape the Auxin Response Pattern and Leaf Margin Morphogenesis. Curr Biol **26,** 2478-2485.

Tian, Q., Uhlir, N.J., and Reed, J.W. (2002). Arabidopsis SHY2/IAA3 inhibits auxin-regulated gene expression. Plant Cell **14,** 301-319.

Torii, K.U., Mitsukawa, N., Oosumi, T., Matsuura, Y., Yokoyama, R., Whittier, R.F., and Komeda, Y. (1996). The Arabidopsis ERECTA gene encodes a putative receptor protein kinase with extracellular leucine-rich repeats. Plant Cell **8,** 735-746.

Uchida, N., Shimada, M., and Tasaka, M. (2013). ERECTA-family receptor kinases regulate stem cell homeostasis via buffering its cytokinin responsiveness in the shoot apical meristem. Plant Cell Physiol **54,** 343-351.

Uchida, N., Lee, J.S., Horst, R.J., Lai, H.H., Kajita, R., Kakimoto, T., Tasaka, M., and Torii, K.U. (2012). Regulation of inflorescence architecture by intertissue layer ligand-receptor communication between endodermis and phloem. Proc Natl Acad Sci U S A **109,** 6337-6342.

Uzair, M., Urquidi Camacho, R.A., Liu, Z., Overholt, A.M., DeGennaro, D., Zhang, L., Herron, B.S., Hong, T., and Shpak, E.D. (2024). An updated model of shoot apical meristem regulation by ERECTA family and CLAVATA3 signaling pathways in Arabidopsis. Development **151**.

Vijayan, A., Tofanelli, R., Strauss, S., Cerrone, L., Wolny, A., Strohmeier, J., Kreshuk, A., Hamprecht, F.A., Smith, R.S., and Schneitz, K. (2021). A digital 3D reference atlas reveals cellular growth patterns shaping the Arabidopsis ovule. Elife **10**.

Wang, G., Ellendorff, U., Kemp, B., Mansfield, J.W., Forsyth, A., Mitchell, K., Bastas, K., Liu, C.M., Woods-Tor, A., Zipfel, C., de Wit, P.J., Jones, J.D., Tor, M., and Thomma, B.P. (2008). A genome-wide functional investigation into the roles of receptor-like proteins in Arabidopsis. Plant Physiol **147,** 503-517.

Wang, H., Ngwenyama, N., Liu, Y., Walker, J.C., and Zhang, S. (2007). Stomatal development and patterning are regulated by environmentally responsive mitogen-activated protein kinases in Arabidopsis. Plant Cell **19,** 63-73.

Wang, Z.Y., Nakano, T., Gendron, J., He, J., Chen, M., Vafeados, D., Yang, Y., Fujioka, S., Yoshida, S., Asami, T., and Chory, J. (2002). Nuclear-localized BZR1 mediates brassinosteroid-induced growth and feedback suppression of brassinosteroid biosynthesis. Dev Cell **2,** 505-513.

Werner, T., Motyka, V., Laucou, V., Smets, R., Van Onckelen, H., and Schmulling, T. (2003). Cytokinin-deficient transgenic Arabidopsis plants show multiple developmental alterations indicating opposite functions of cytokinins in the regulation of shoot and root meristem activity. Plant Cell **15,** 2532-2550.

Yu, S.X., Jiang, Y.T., and Lin, W.H. (2022). Ovule initiation: the essential step controlling offspring number in Arabidopsis. J Integr Plant Biol **64,** 1469-1486.

Yu, S.X., Zhou, L.W., Hu, L.Q., Jiang, Y.T., Zhang, Y.J., Feng, S.L., Jiao, Y., Xu, L., and Lin, W.H. (2020). Asynchrony of ovule primordia initiation in Arabidopsis. Development **147**.

Zhang, L., DeGennaro, D., Lin, G., Chai, J., and Shpak, E.D. (2021). ERECTA family signaling constrains CLAVATA3 and WUSCHEL to the center of the shoot apical meristem. Development **148**.

Zhao, Y., Christensen, S.K., Fankhauser, C., Cashman, J.R., Cohen, J.D., Weigel, D., and Chory, J. (2001). A role for flavin monooxygenase-like enzymes in auxin biosynthesis. Science **291,** 306-309.

Zu, S.H., Jiang, Y.T., Chang, J.H., Zhang, Y.J., Xue, H.W., and Lin, W.H. (2022). Interaction of brassinosteroid and cytokinin promotes ovule initiation and increases seed number per silique in Arabidopsis. J Integr Plant Biol **64,** 702-716.

Vita

Alex Overholt was born in Woodbury, New Jersey in 1993. He moved to Knoxville, Tennessee in 1995. He attended Bearden High School and graduated in 2012. He attended the University of Tennessee, Knoxville where he acquired a Bachelor of Science in the Biochemistry and Cellular & Molecular Biology department in 2018. He stayed at the University of Tennessee to pursue a doctorate degree specializing in plant development and molecular biology.